Deliverable 6.2
Conditioning of ashes of RSOW by geopolymer or cement-based encapsulation

Date 31.8.2023 Final

Dissemination level Public

Vojtěch Galek
Affiliation: Research Centre Řež
Address: Hlavní 130, Husinec – Řež, 250 69, Czech Republic

Email: vojtech.galek@cvrez.cz
Tel: +420 266172688

This project has received funding from the Euratom research and training programme 2019-2020 under grant agreement No 945098.

Project acronym PREDIS	Project title PRE-DISposal management of radioactive waste		Grant agreement No. 945098
Deliverable No. 6.2	Deliverable title Conditioning of ashes of RSOW by geopolymer or cement-based encapsulation		Version 1.0
Type Report	Dissemination level Public		Due date M36
Lead beneficiary CVRez			WP No. 6
Main author Vojtěch Galek, CVRez	Reviewed by Thierry Mennecart, WP6 leader, SCK CEN	Accepted by Maria Oksa, Coordinator, VTT	
Contributing author(s) Anna Sears (CVRez), Martin Vacek (CVRez), Pedro Perez-Cortes (CSIC), Inés Garcia-Lodeiro (CSIC), Francisca Puertas (CSIC), María Cruz Alonso (CSIC), E. Mossini (POLIMI), A. Santi (POLIMI), F. Galluccio (POLIMI), G. Magugliani (POLIMI), E. Macerata (POLIMI), M. Giola (POLIMI), M. Mariani (POLIMI), Tandré Oey (VTT), Gianni Vettese (UH), Hélène Nonnet (CEA), Claire Corkhill (USFD), Josh Radford (USFD), Sam Walling (USFD), Yu, Federonko (SIIEG), A. Rozko (SIIEG), B. Zlobenko (SIIEG)			Pages 95

Abstract

This Deliverable consists of contributions from all partners with their work on conditioning of ashes of RSOW by geopolymer or cement-based encapsulation.

Coordinator contact

Maria Oksa

VTT Technical Research Centre of Finland Ltd

Kivimiehentie 3, Espoo / P.O. Box 1000, 02044 VTT, Finland

E-mail: maria.oksa.@vtt.fi

Tel: +358 50 5365 844

Acknowledgement

This project has received funding from the Euratom research and training programme 2019-2020 under grant agreement No 945098.

TABLE OF CONTENTS

1 Introduction

This document describes the main contribution of all partners in Task 6.4 with the conditioning of ashes created during thermal treatment processes. The conditioning of these wastes was focused on geopolymer or cement-based encapsulation. These findings are differentiated by the waste type used (ashes) and different methods of encapsulation. Each partner has the means to use their most suited materials and matrices.

2 CVRez Contribution

2.1 Introduction

CVRez focused on incorporating their ashes from RSOW thermal treatment process (Molten Salt Oxidation) into the geopolymer matrix. In task 6.4 CVRez had several different commercial metakaolin based geopolymers for their disposal to see how each would react to this type of waste, and the contributor looked for the best options to incorporate this waste. Developing a new recipe for incorporating waste was also studied. The emphasis was made on the maximum waste loading and measuring the physical properties of the samples.

Waste from Molten Salt Oxidation was sent to other partners to see if other means of encapsulation would be more suitable and more stable in the case of leaching experiments.

2.2 Experiments

2.2.1 MSO waste

As the main generator of RSOW from the thermal treatment process of Molten Salt Oxidation CVRez was able to supply this waste to other partners. This waste needed to be removed from the storage tank and reconditioned for encapsulation. That means waste was pre-dried in the air, ground for smoother particles, and dried in the oven for 65 °C to get low moisture levels as the moisture could negatively affect the final product. Figure *1* shows the XRD analysis of the dried-up waste salt samples.

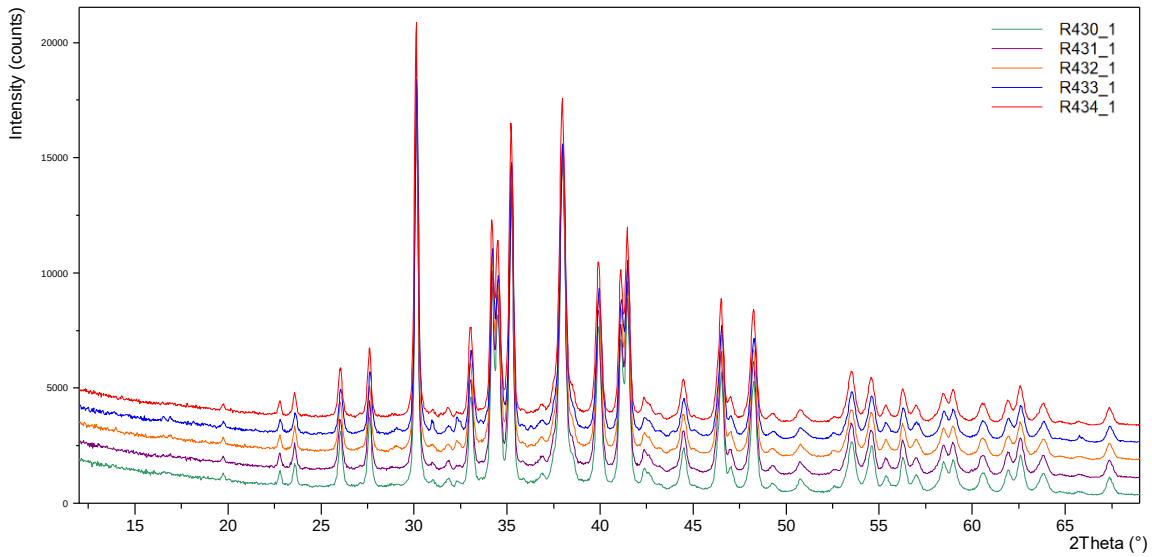

Figure 1. The XRD analysis of MSO waste salt samples.

Table 1 shows the weight % of the phase distributions in each sample with Natrite as the primary phase. The results show homogenous compositions throughout the bulk of the waste.

Table 1. The phase composition generated from XRD analysis of each sample by (w.%)

Phase		R430	R431	R432	R433	R434
Natrite	Na_2CO_3	96.41	96.52	95.07	94.12	96.25
Essenite	$CaFeAlSiO_6$	3.38	3.48	3.32	3.14	3.71
Thermonatrite	$Na_2CO_3 \cdot H_2O$	0.21	-	0.79	1.79	0.04
Trona	$Na_3H(CO_3)_2 \cdot 2H_2O$	-	-	0.81	0.95	-

The waste was very hygroscopic and contained Cs^+, Co^{2+} and Sr^{2+} tracers from thermally treated Ion Exchange Resins (IER).

The semiquantitative analysis of the MSO waste was also performed, and its results are shown in Table 2. The results are shown in weight % from each sample and show a minor constitution, but it can be assumed as background.

Table 2. The semiquantitative analysis of waste salt determined by w. %.

Ident		R430	R431	R432	R433	R434
Al_2O_3	*(%)*	7.48	6.23	7.29	3.8	6.38
CaO	*(%)*	0.137	0.161	0.142	0.134	0.148
Cl^-	*(%)*	0.066	0.072	0.064	0.073	0.076
Co_3O_4	*(%)*	0.029	0.038	0.031	0.026	0.036
Cr_2O_3	*(%)*	0.079	0.082	0.077	0.094	0.073
CuO	*(%)*	0.009	0.007			
Fe_2O_3	*(%)*	0.26	0.19	0.22	0.22	0.24
K_2O	*(%)*	1.647	1.67	1.663	1.744	1.585
MgO	*(%)*	0.223	0.269	0.255	0.261	0.252
MnO	*(%)*		0.01			
Na_2O	*(%)*	81.927	84.662	82.448	89.283	84.185
NiO	*(%)*	0.243	0.219	0.233	0.246	0.222
P_2O_5	*(%)*	0.009	0.009	0.013	0.009	0.01
SO_3	*(%)*	0.164	0.263	0.176	0.193	0.157
SeO_2	*(%)*		0.003			
SiO_2	*(%)*	7.494	5.959	7.193	3.763	6.434
SrO	*(%)*	0.034	0.034	0.034	0.035	0.031
TiO_2	*(%)*	0.15	0.082	0.12	0.077	0.13
ZnO	*(%)*	0.043	0.041	0.04	0.041	0.045

The humidity of the samples was also determined because this could affect the mechanical properties of the prepared geopolymer samples. As the Na_2CO_3 and its hydrates are highly

hygroscopic, the blooming effect and swelling take place, which causes cracks in the samples, which leads to stability loss. [1]

Table *3*. The moisture content in the measured samples (w.%)Table 3 shows the humidity of the analysed samples. Different compositions with Trona and Thermonatrite present can determine the changes in the sample R432.

Table 3. The moisture content in the measured samples (w.%)

Moisture	**R430**	**R431**	**R432**	**R433**	**R434**
Weight %	1.31	1.31	4.20	1.48	1.20

2.2.2 Used geopolymers

The work was carried out with commercial metakaolin based geopolymers from Czech company České Lupkové Závody a.s. This company offers three types of metakaolin based geopolymers: Baucis LNa, Baucis LBNa and Baucis LK. Each geopolymer has a similar composition and differs by alkaline activators. The recipe provided by the company is 60:40 (metakaolin:activator) with the addition of fire clay as filler which ranges from 75 to 125 w.%. For our work, we used our modified recipe with more metakaolin as filler, improving mechanical properties. Table 4 shows the average composition of the used metakaolin.

Table 4. The contents of metakaolin based geopolymers provided by České lupkové závody, a.s., components show in w.% [2]

Geopolymer	**Metakaolin**	**Activator**	**Al_2O_3**	**SiO_2**	**K_2O**	**Fe_2O_3**	**TiO_2**	**MgO**	**CaO**
Baucis LNa	Mefisto L05	Na_2SiO_3	40.10	54.10	0.80	1.10	1.80	0.18	0.13
Baucis LBNa	Mefisto LB05		37.50	54.10	1.10	3.50	1.30	0.25	0.28
Baucis LK	Mefisto L05	K_2SiO_3	40.10	54.10	0.80	1.10	1.80	0.18	0.13

The Mefisto L05 was analysed with XRD analysis to obtain a mineralogical composition. Figure 2 shows the results of the analysis. The samples contained the Al compounds such as Kaolinite, Mullite, Illite and Muscovite. Also, Anatase and Quartz were present with two different mineralogical polymorphs of $CaCO_3$: Calcite and Aragonite.

The first experiments were made to determine the right geopolymer for the MSO waste encapsulation from the mechanical strength point of view. The mixture was put into the 5x5x5 PP moulds and let to dry up in the air for one week in laboratory conditions. After the dry curing, the samples were taken out and left to dry in the laboratory. These samples were tested for mechanical strength to determine the best one for the MSO salt encapsulation.

When the geopolymer was chosen, the encapsulation began with the determination of the maximum loading of the waste. Firstly, the experiments were carried out similarly without waste loading, so they were left for one week to dry cure in the mould and then taken out and left to dry out in the laboratory conditions or in the laboratory oven to speed up drying. The maximum waste loading was determined to be 40 w.%, but after discussions with other partners, it was decided that samples would be cured in the sealed bag option. That means wrapping the mould with the mixture into the aluminium foil and put into a plastic bag to establish non-aerated conditions. After four weeks, the samples were taken out, weighted, and their mechanical strength was tested. The exact amount of MSO salt waste could be encapsulated with this curing type, as a higher amount of waste caused its blooming, instability, and non-solidified state.

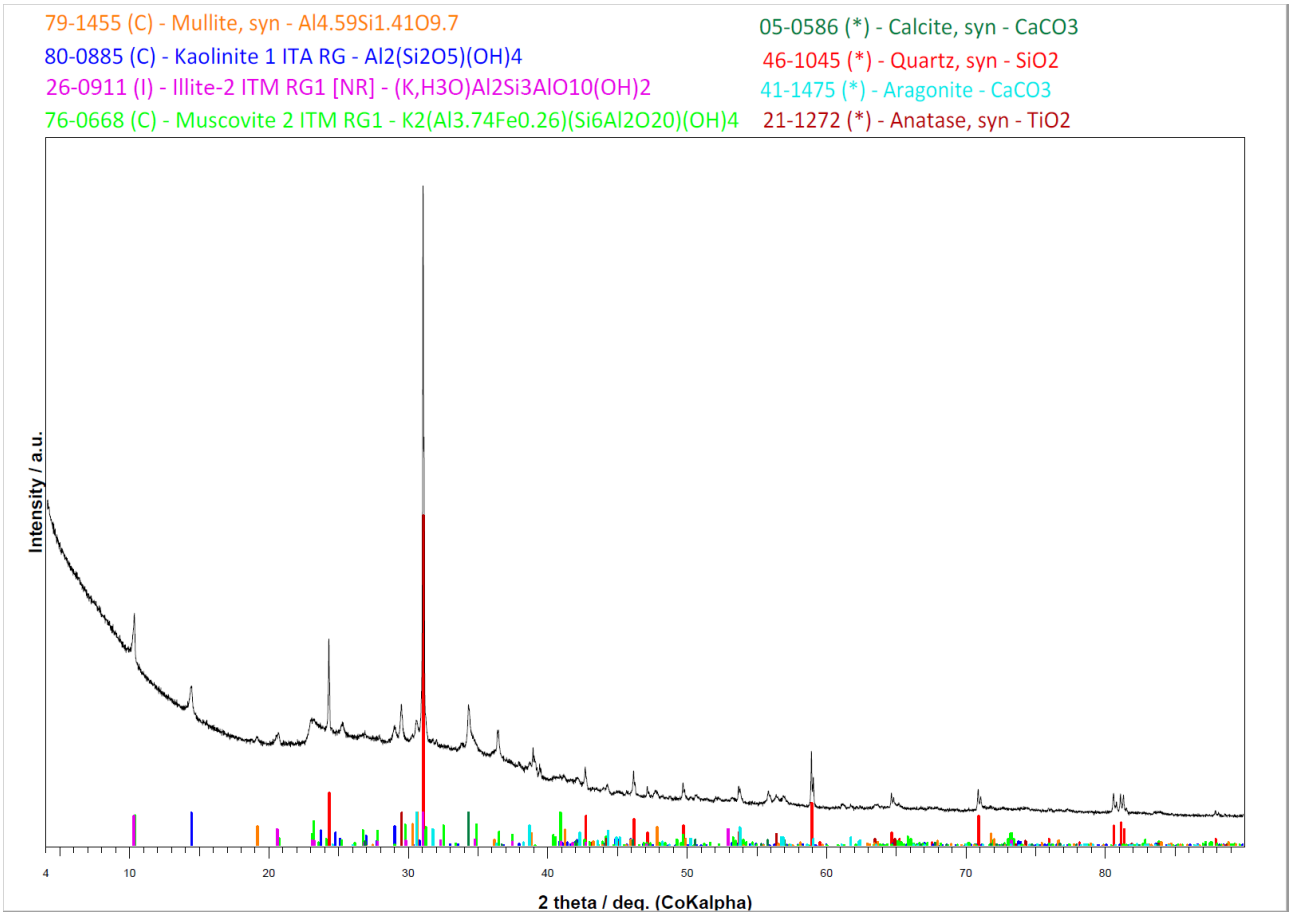

Figure 2: The XRD analysis of Mefisto L05.

After testing the statistics to get similar results, the last curing type was determined to see the curing of the samples in different conditions. This lets us see the samples' reaction in a higher moisture environment. The samples were prepared in the same procedure as before, but after curing in the mould for three days, they were taken out and set into a different environment:

- dry cured in the laboratory conditions
- high moisture environment in the sealed vessel
- curing underwater

Curing in this environment was set to four weeks before weighting and mechanical testing.

2.3 Main findings

2.3.1 Choosing the geopolymer

The first experiment consisted of preparing samples of all three geopolymer recipes and adding a specific amount of metakaolin to determine which geopolymer has the best compressive strength properties.

In these samples, 5, 10, 15 and 20 wt.% more relevant metakaolin was added into the mixture as a binder for better performance. This modification resulted from previous experiments and consultations. Figure 3 compares the geopolymers Baucis LBNa, LNa and LK.

The best performance in the compressive strength test with adding extra metakaolin had Baucis LK with its compressive strength between values 50 to 80 MPa depending on the extra amount of added metakaolin. It was therefore determined as the most suitable for the subsequent experiments. Baucis LNa sample with 10 wt.% addition of metakaolin saw a drop in compressive strength compared to 5

wt.% addition, but samples with higher metakaolin addition had an increasing trend of compressive strength. Compressive strength values of Baucis LBNa samples decreased from 56 to 36 MPa with extra added metakaolin. The different compressive strength values between tested geopolymer mixtures are mainly due to their chemical composition. [3]

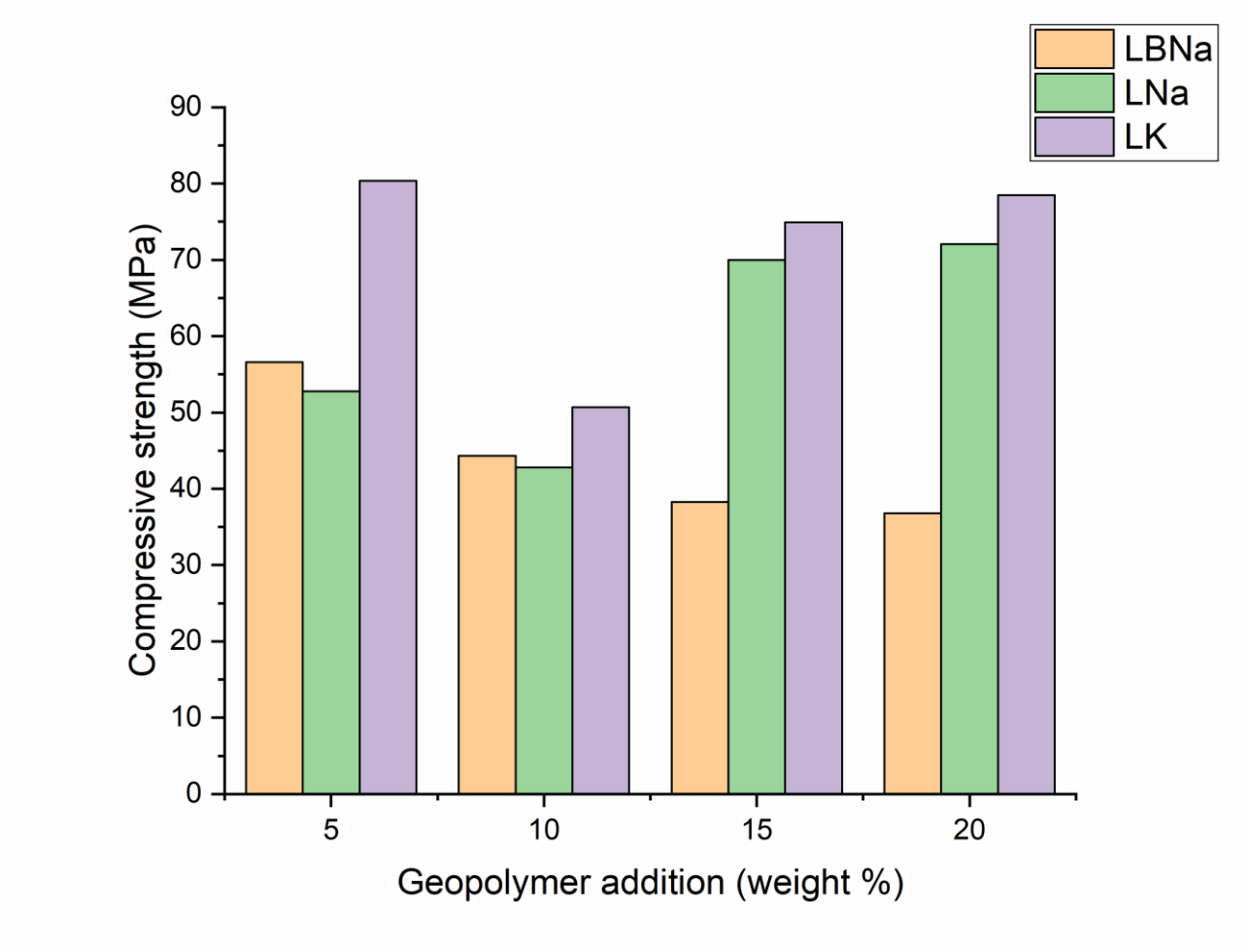

Figure 3: Comparison of compressive strength between different geopolymers.

To investigate the effect of curing time on the compressive strength, three sets of Baucis LK samples with the addition of 5, 10 and 15 wt.% of metakaolin were prepared (LK5, LK10 and LK15) and cured for the different time periods. The curing times were set at 7, 14 and 21 days. As shown in Figure 4, the curing time positively influenced the compressive strength values at all three geopolymer mixtures due to the continuous polymerisation process. Longer curing time resulted in higher compressive strength, similar to what was reported in other studies [4,5]. The LK5 mixture showed smaller compressive strength compared to LK10 and LK15. The highest compressive strength values were measured for LK15 and were 60, 72 and 82 MPa after 7, 14 and 21-day curing, respectively. It can be observed that the addition of the metakaolin on the top of the recipe increased the compressive strength values; however, more added metakaolin content also increases the mixture viscosity. Adding more than 15 wt. % of the metakaolin made mixing very difficult and increased the porosity of the samples, which then had a negative effect on the resulting geopolymer properties.

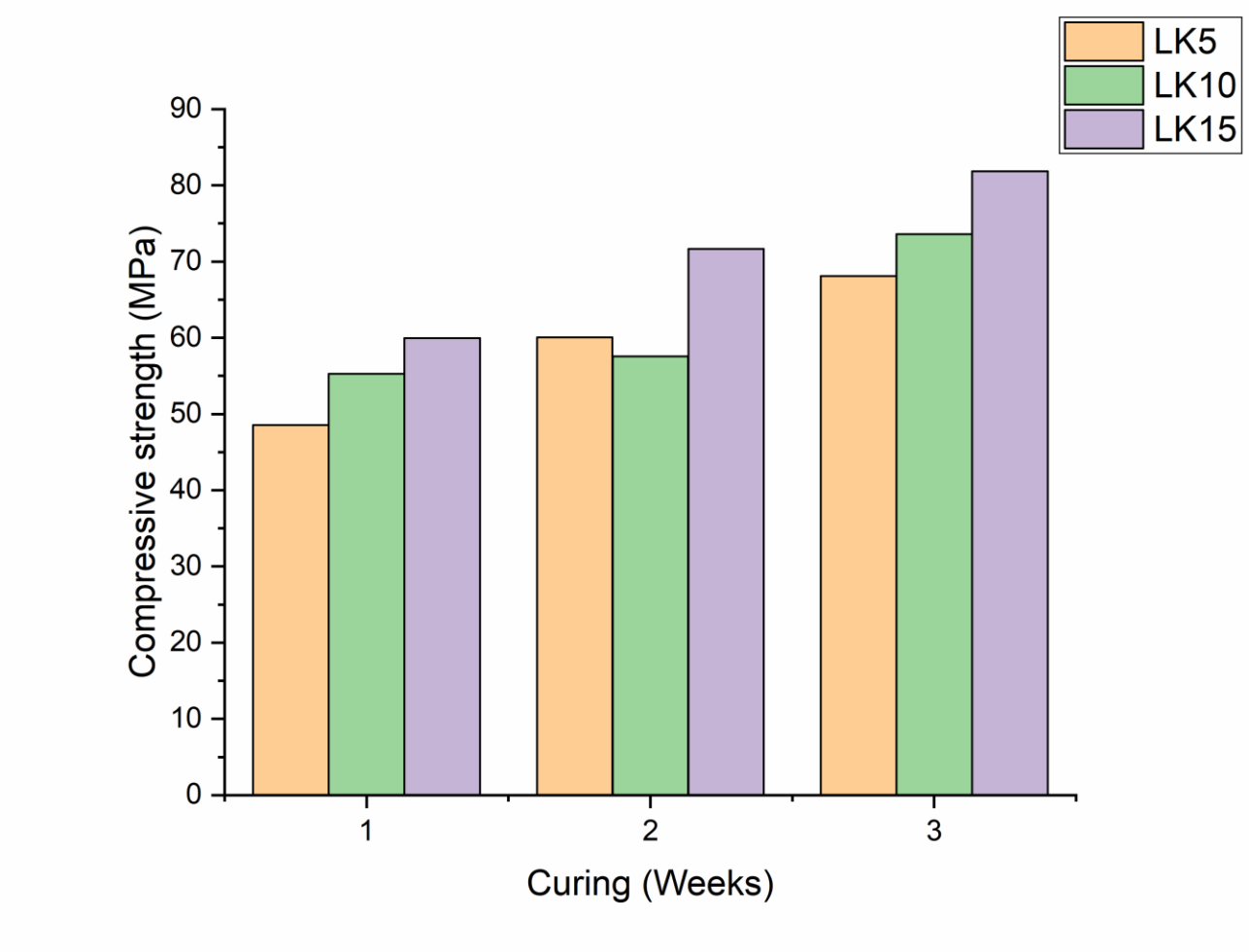

Figure 4:The effect of curing time on compressive strength of selected geopolymer.

As the LK10 and LK15 mixtures showed higher values of compressive strength in previous tests they were then used for the experiments where a set amount of an MSO spent salt was added to the mixture instead of metakaolin. The resulting samples after curing are shown in and the results of compressive strength analysis are shown in Figure *5*.

Both geopolymer mixtures had a similar compressive strength value at 10, 15 and 20 wt.% load of salt. Significantly higher compressive strength of 58 and 59 MPa was observed at samples LK10 with 25 and 30 wt.% salt additions, respectively, compared to the LK15 samples with the same amount of salt addition where the values were 23 and 16 MPa. It can be stated that adding more metakaolin together with higher loads of salt leads to higher viscosity and difficult mixability, which then negatively affects the strength properties. The unsatisfactory results of the LK15 mixture meant that further increase of metakaolin addition together with the addition of salt as a waste load was unsuitable. Because overall better results have been seen with LK10 it was then determined to use it for the temperature experiment.

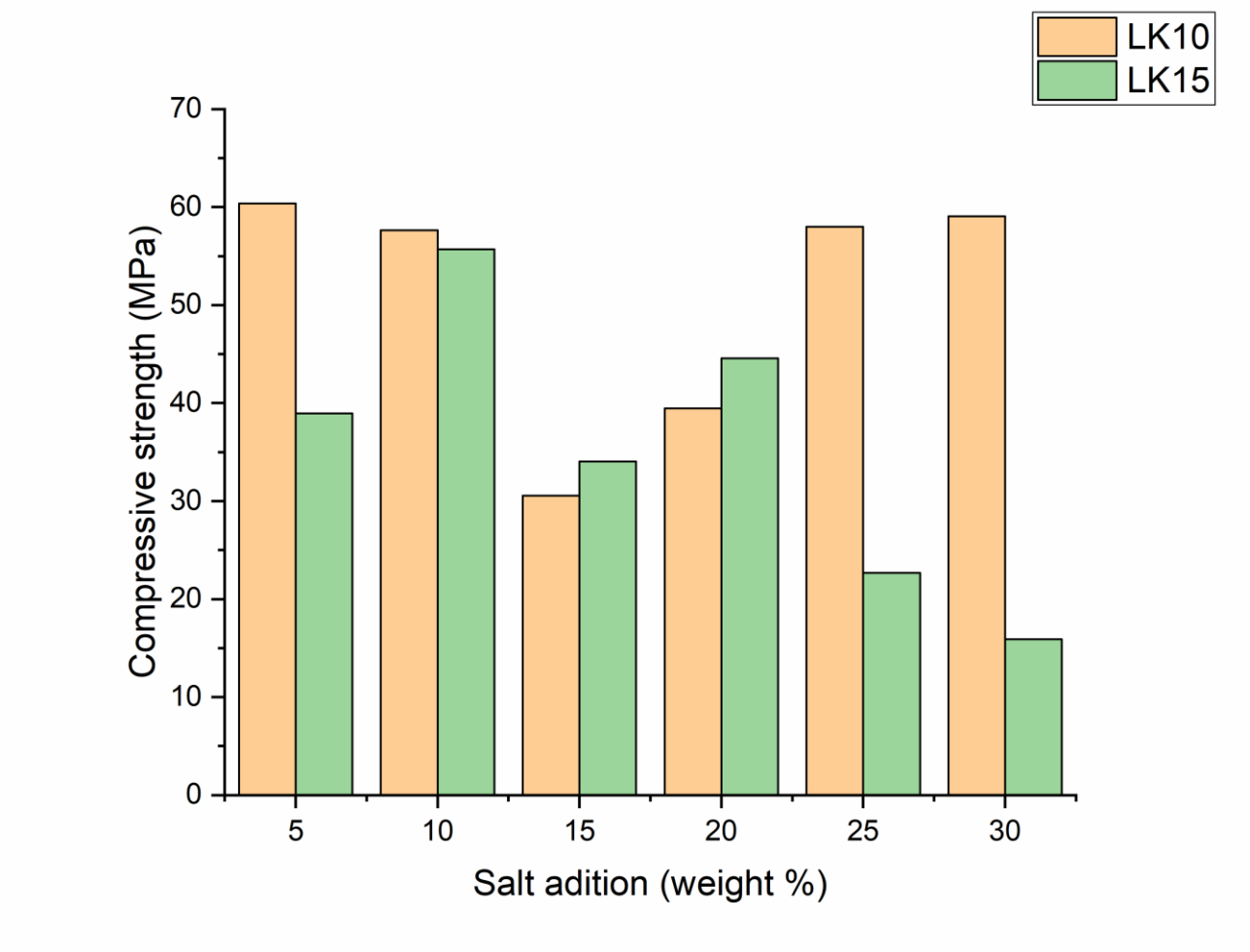

Figure 5: The difference of compressive strength between two recipes of LK geopolymer based on salt addition.

After this experiments the XRD analysis was performed to compare the resulting geopolymer with salt addition with Mefisto L05 metakaolin. The results are shown in the Figure *6*. The analysis has shown the presence of gaylussite and thermonatrite in the resulting geopolymer. Thermonatrite is an evaporite consisting of sodium carbonate and gaylussite is a hydrated form of the sodium-calcium carbonate, which is usually unstable and formed at an early stage in the activated geopolymer paste. It then slowly decomposes in H_2O, leaving $CaCO_3$ as stable calcite or aragonite. These two minerals are usually present in geopolymers where an alkalic activator which contains sodium is presented; however, geopolymer mix Baucis LK uses potassium silicate as an activator. The most probable reason for their formation is the presence of sodium in the MSO salt, which reacts with the geopolymer mix during the process.

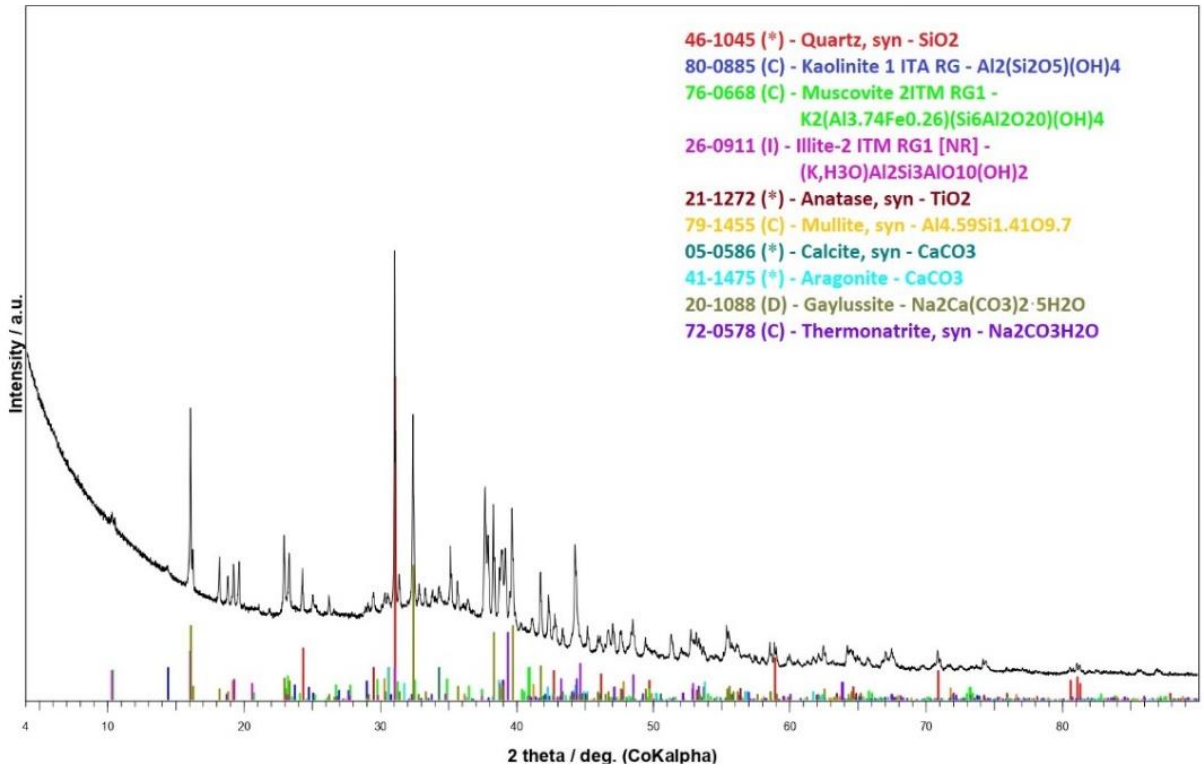

Figure 6: XRD analysis of the LK geopolymer mixture with MSO salt addition.

The temperature influence was also tested of used LK geopolymer mixture. One set of samples with 5, 10, 15, 20, 25 and 30 wt.% spent MSO salt addition was cured as the samples in the previous experiments. The other samples were removed from the mould after 24 hours and placed into the laboratory drier for 24 hours at 65 °C. The results presented in Figure 7 have shown that the standardly cured samples had overall higher compressive strength than the samples cured at a higher temperature.

Overall lower compressive strength values were seen in the samples which were cured at the higher temperature, which was in contrast to the results seen in another study [6]. It is possible that a sudden change in temperature influenced the microstructure of the samples, as some small cracks were observed on the surface. A gradual rise in temperature would therefore be more beneficial. The unexpected drop in the compressive strength values at samples with 15 and 20 wt. % salt addition was most likely caused by inhomogeneous moisture content in MSO salt. Sodium carbonate is very hygroscopic and even though the salt was homogenised, it is possible that the moisture content varied slightly in each batch used for sample casting. This variation in moisture content then affects the W/S ratio in the mixture and, subsequently, the reaction in the polymerization process.

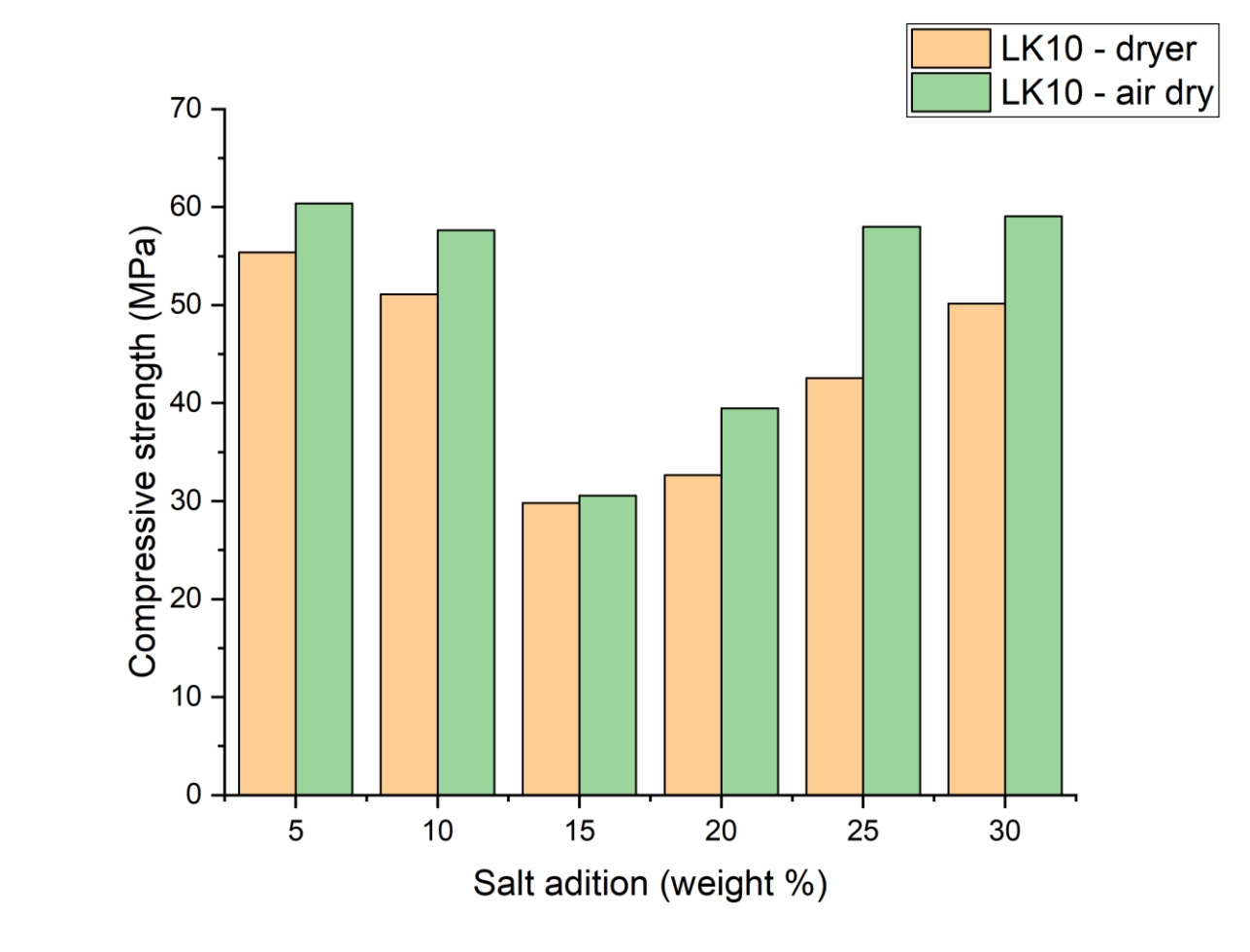

Figure 7: The effect of curing temperature on compressive strength of LK10 geopolymer mixture.

2.3.2 Properties of LK10 geopolymer

For the repeatability of the produced samples, more samples were prepared for compressive testing with SEM analysis to see any deformations or non-homogenous elements within the matrix. For each geopolymer, the six samples were prepared from 5 w.% of the waste salt up to the 25 w.% salts. The 30 w.% and more waste added was viscose, hard to mix and hard work with, so only 25 w.% were used. Samples were cured in the sealed bag environment, in the mould for four weeks and taken out before testing.

Figure *8* shows the compressive testing of the LK10 with 5 w.% of waste salt. It shows a range of mechanical strength from 67 MPa up to 105 MPa with a median of 89.95 MPa. The difference can be explained by the non-homogenous layout of waste salt in the mixture. Nevertheless, the samples show excellent mechanical strength corresponding to low waste loading. Figure *9* shows the preparations of the samples for the SEM analysis, also with the microscopic image of the selected part.

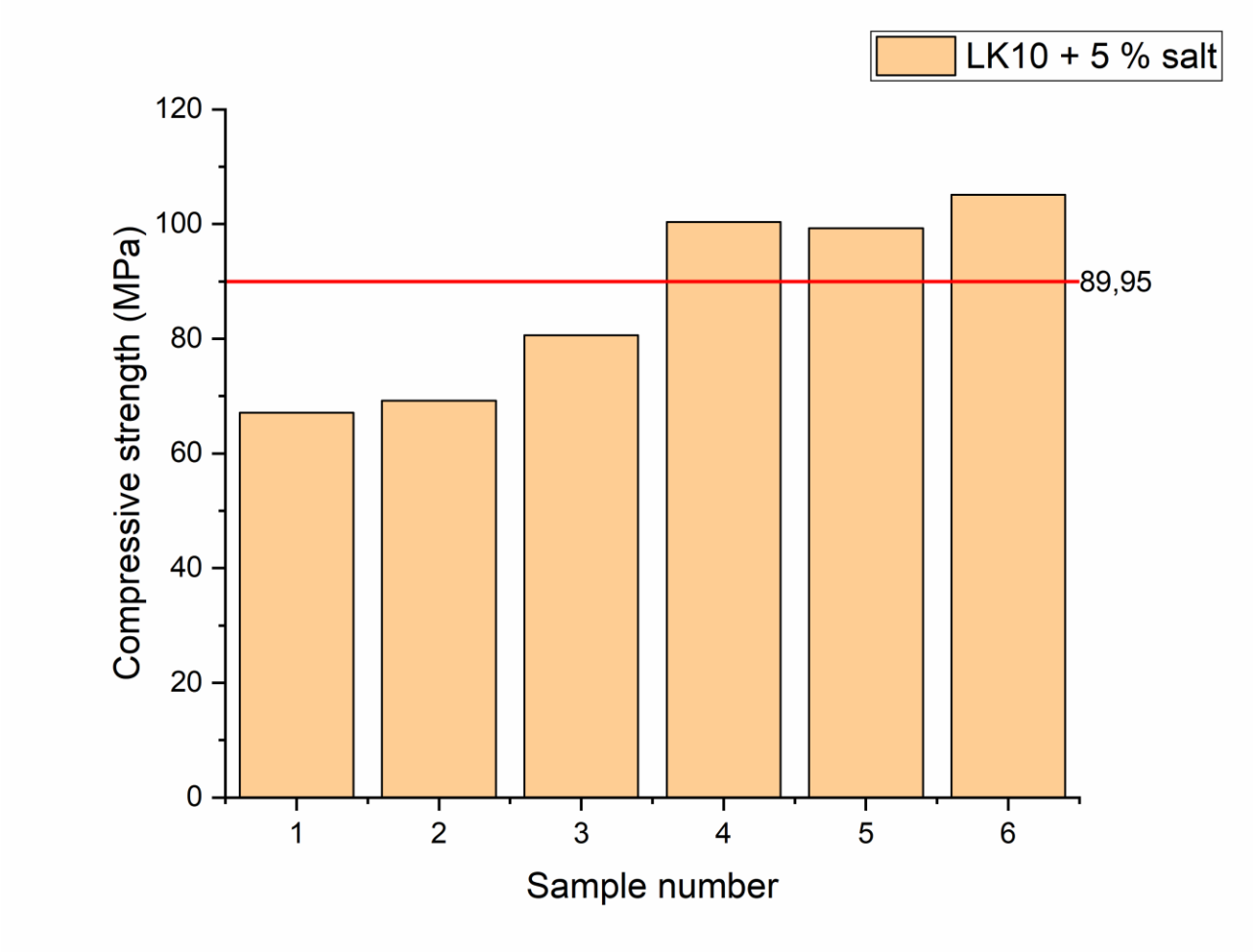

Figure 8: The compressive strength of LK10 geopolymer with 5 w.% waste added.

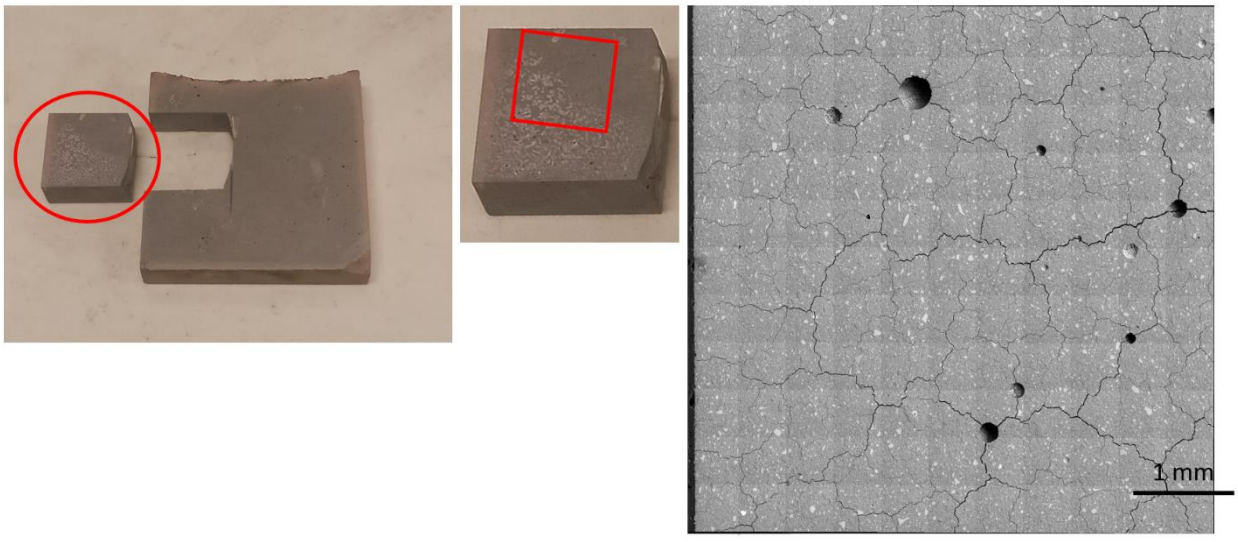

Figure 9: The samples cutting for SEM analysis.

The Figure *10* shows the BSE analysis with sample map of detected minerals. The geopolymer matrix had 90.7 %, Akermatinite + Merwinite had 5.8 %, Quartz 0.5 %, Calcite 0.3 % and Illite 0.6 %. The analysis shows good distribution of the waste in the bulk of the sample, but a blooming Figure *13* shows the mechanical strength of the LK10 geopolymer with 15 w.% of waste salt incorporated. These samples were more uniform in the mixture, as the minimum mechanical strength

was measured at 60 MPa, and the maximum was 64 MPa with a median set at 62 MPa. These samples showed lower mechanical strength than the 10 % samples, but the decrease was not steep, between 5% and 10%. The samples for SEM analysis were prepared the same way as the previous samples.

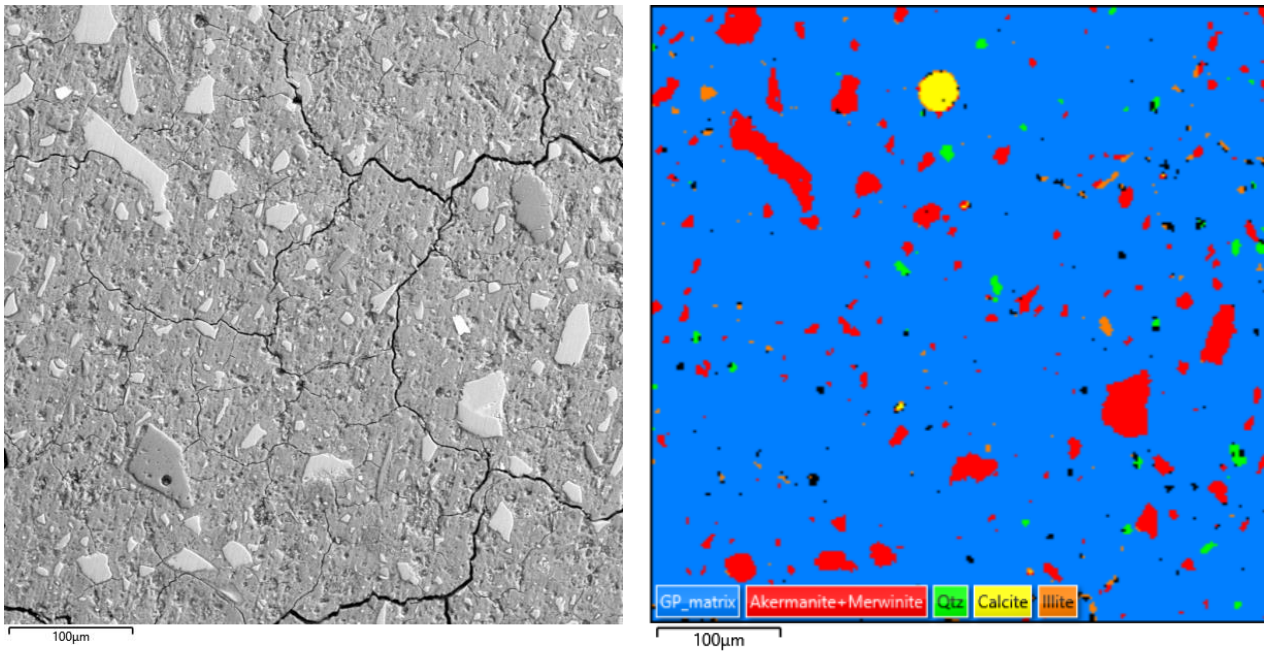

Figure 10: The BSE analysis of the LK10 geopolymer with 5 w.% of waste salt with phase map.

Figure *11* shows the compressive strength of the LK10 geopolymer with 10 w.% of waste salt incorporated. The minimum mechanical strength was measured at 57 MPa; the maximum was 85 MPa, with the median set at 68 MPa. These samples showed lower mechanical strength than the 5 % samples. The samples for SEM analysis were prepared the same way as were in the 5 w.%.

Figure 12 shows the BSE analysis with a phase map. The geopolymer matrix had 93.3 %, Akermatinite + Merwinite had 2.9 %, Quartz 0.9 %, and not determined Na-Ca-CO phase 1.5%. The last phase is shown with a larger amount of waste incorporated in the matrix, and the data collected from XRD mainly consisted of pirssonite and related sodium carbonates. As the sample cutting was undertaken with ethanol cooling, it may cause some sodium carbonate hydrates to lose water to form pirssonite, as the XRD spectra show gaylussite with more H_2O molecules than pirssonite. Also, these sodium carbonate hydrates undertake the blooming effect causing them to accumulate more water molecules, increasing the tensions of the matrix. This causes a decrease in the mechanical strength of the samples.

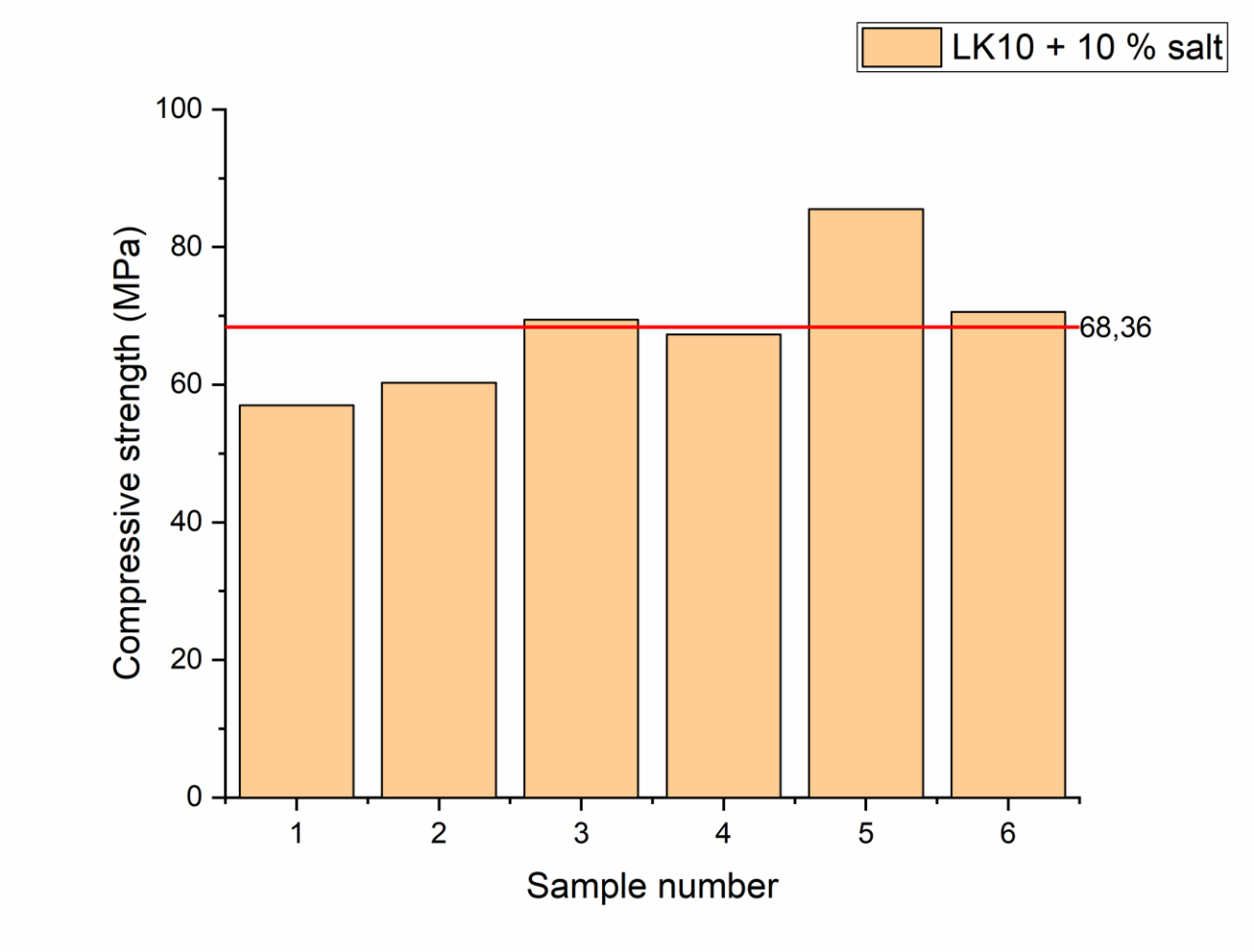

Figure 11: The compressive strength of LK10 geopolymer with 10 w.% waste added.

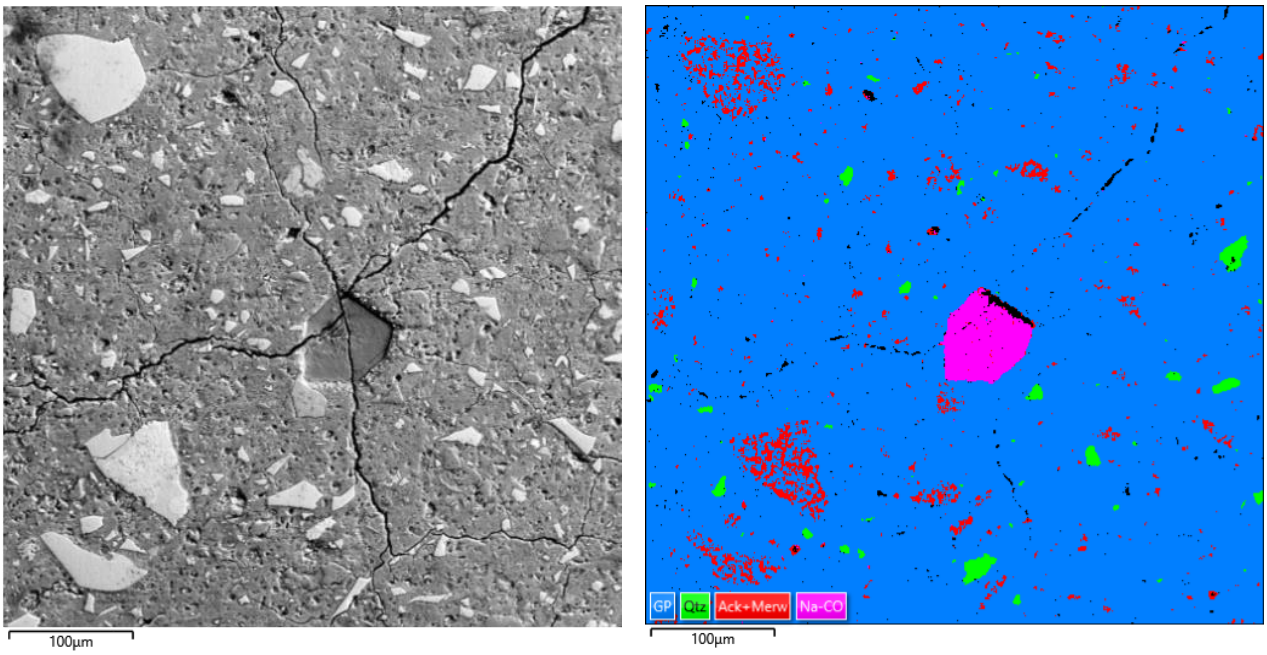

Figure 12: The BSE analysis of the LK10 geopolymer with 10 w.% of waste salt with phase map.

Figure *13* shows the compressive strength of the LK10 geopolymer with 15 w.% of waste salt incorporated. These samples were more uniform in the mixture, as the minimum mechanical strength was measured at 60 MPa, and the maximum was 64 MPa with a median set at 62 MPa. These

samples showed lower mechanical strength than the 10 % samples, but the decrease was not steep, between 5% and 10%. The samples for SEM analysis were prepared the same way as the previous samples.

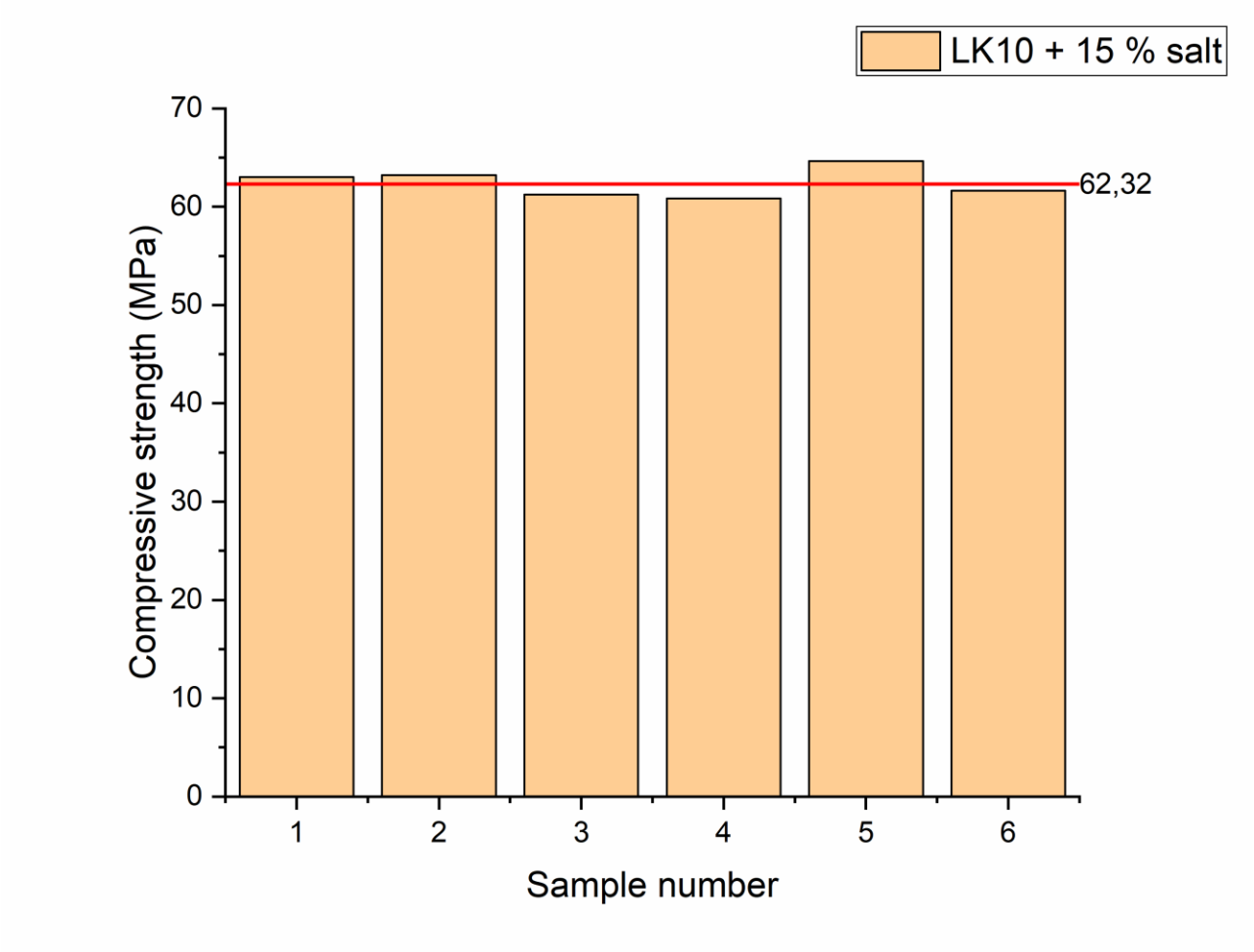

Figure 13: The compressive strength of LK10 geopolymer with 15 w.% waste added.

Figure *14* shows the blooming effect with higher waste added to the samples, and Figure 15 shows the BSE analysis with a phase map. The geopolymer matrix had 89.9 %, Akermatinite + Merwinite had 4.7 %, Quartz 0.9 %, Illite 1.2 % and Pores 2.2 % and not determined Na-Ca-CO phase 1.5%. The pore phase could be determined by cutting the samples and dissolution of sodium carbonates in ethanol, which may cause the high value of pores.

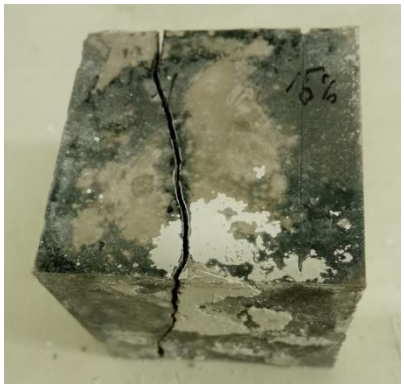

Figure 14: The blooming effect of the LK10 geopolymer with 15 w.% of waste loads.

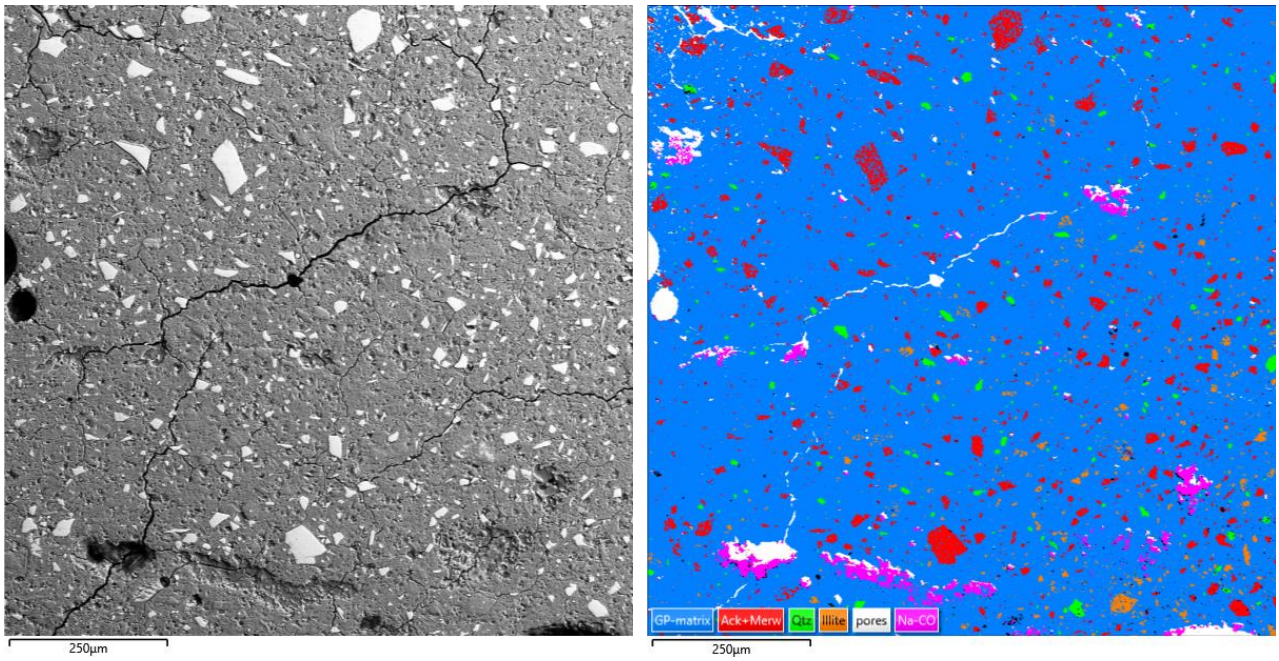

Figure 15: The BSE analysis of the LK10 geopolymer with 15 w.% of waste salt with phase map.

Figure *16* shows the compressive strength of the LK10 geopolymer with 20 w.% of waste salt incorporated. These samples show different mechanical strengths, with the minimum set at 36 MPa, the maximum set at 60 MPa, and the median set at 50 MPa. These samples showed lower mechanical strength than previous samples; this corresponds with previous measurements.

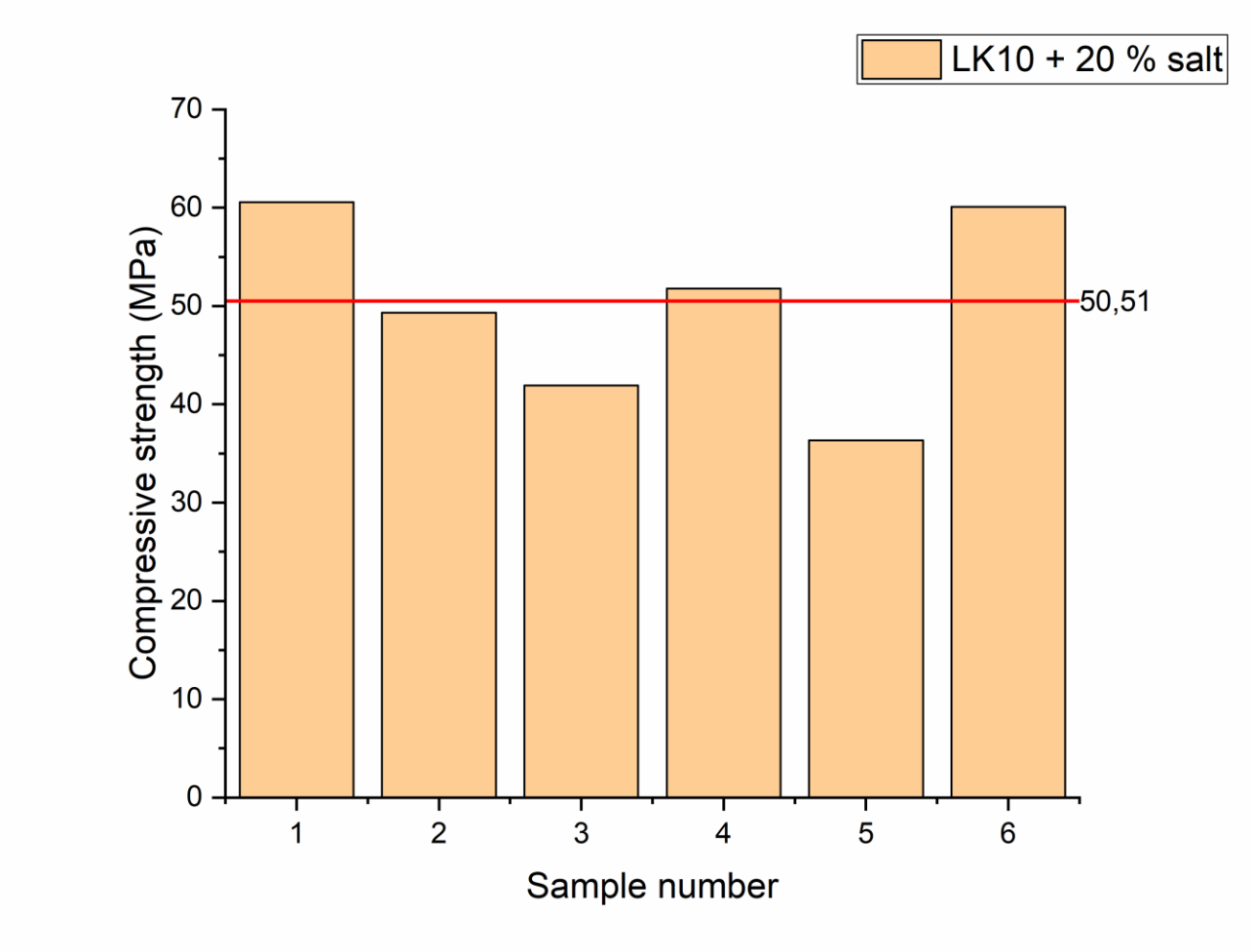

Figure 16: The compressive strength of LK10 geopolymer with 20 w.% waste added.

Figure *17* shows the blooming effect on the sample on the whole surface. Figure *18* shows the BSE analysis with a phase map. The geopolymer matrix had only 78.4 %, Akermatinite + Merwinite had 8.9 %, Quartz 1.8 %, Kaolinite 2.2 % and Calcite 2.2 % and not determined Na-Ca-CO phase rose to 6.3 %. This phase composition explains the lower compressive strength of the samples as a higher carbonate phase with a high blooming effect shows higher water absorption and sodium carbonates hydration causes swelling. This effect causes cracks in the geopolymer matrix.

Figure 17: The blooming effect of the LK10 geopolymer with 20 w.% of waste loads. All surface is covered with the blooms of sodium carbonate hydrates.

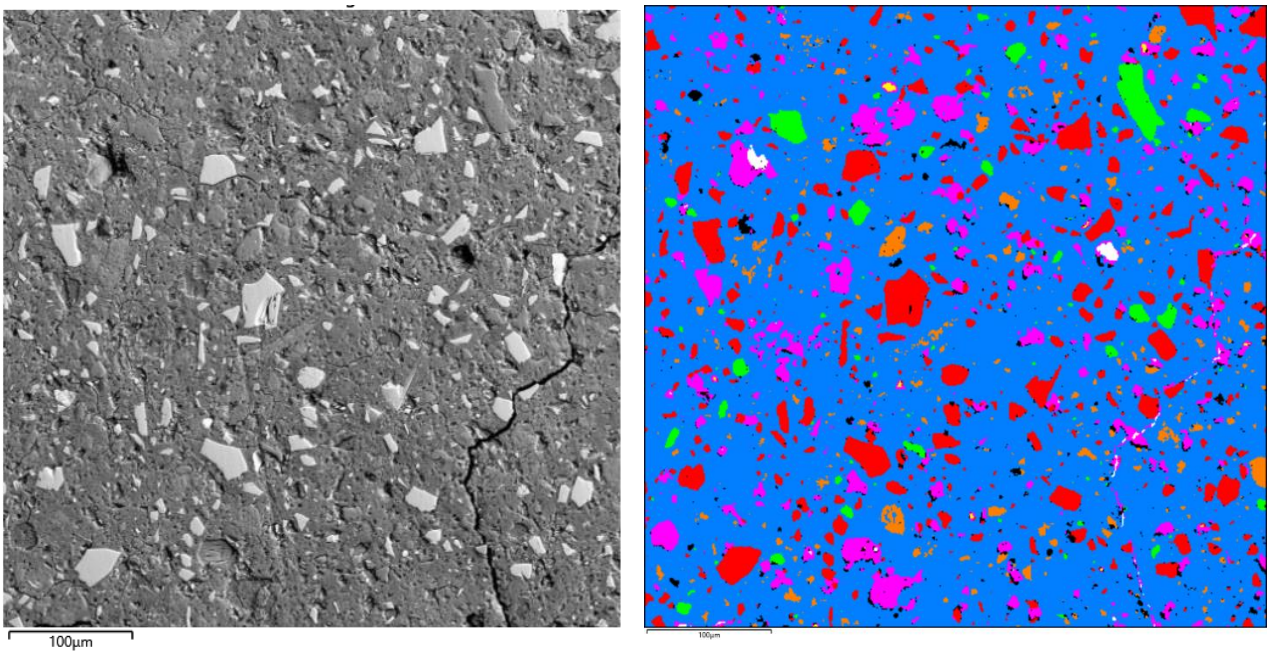

Figure 18: The BSE analysis of the LK10 geopolymer with 20 w.% of waste salt with phase map. The purple parts are the Na-Ca-CO phase which covers larger parts of the sample.

Figure *19* shows the compressive strength of the LK10 geopolymer with 25 w.% of waste salt incorporated. This compressive strength decreases with the minimum set at 28 MPa, the maximum set at 36 MPa, and a median set at 31 MPa. These results showed a rapid decrease in compressive strength compared to 20 % waste loads. Figure *20* shows the blooming effect on the sample, but practically the same as the 20 %. Figure *21* shows the BSE analysis with a phase map. The geopolymer matrix had almost the same as the 20 % sample: 77.5 %, Akermatinite + Merwinite had 7.2 %, Quartz 1.8 %, and not determined Na-Ca-CO phase rose to 9.9 %. The large cracks in the sample could be caused by the dissolution of the sodium carbonates in the cooling liquid of the saw. This would mean an even larger Na-ca-CO phase composition could be present. But the higher amounts of sodium carbonates and their hydrates show a compressive strength decreasing trend. The hydration of the carbonates is even higher and causes larger cracks and holes.

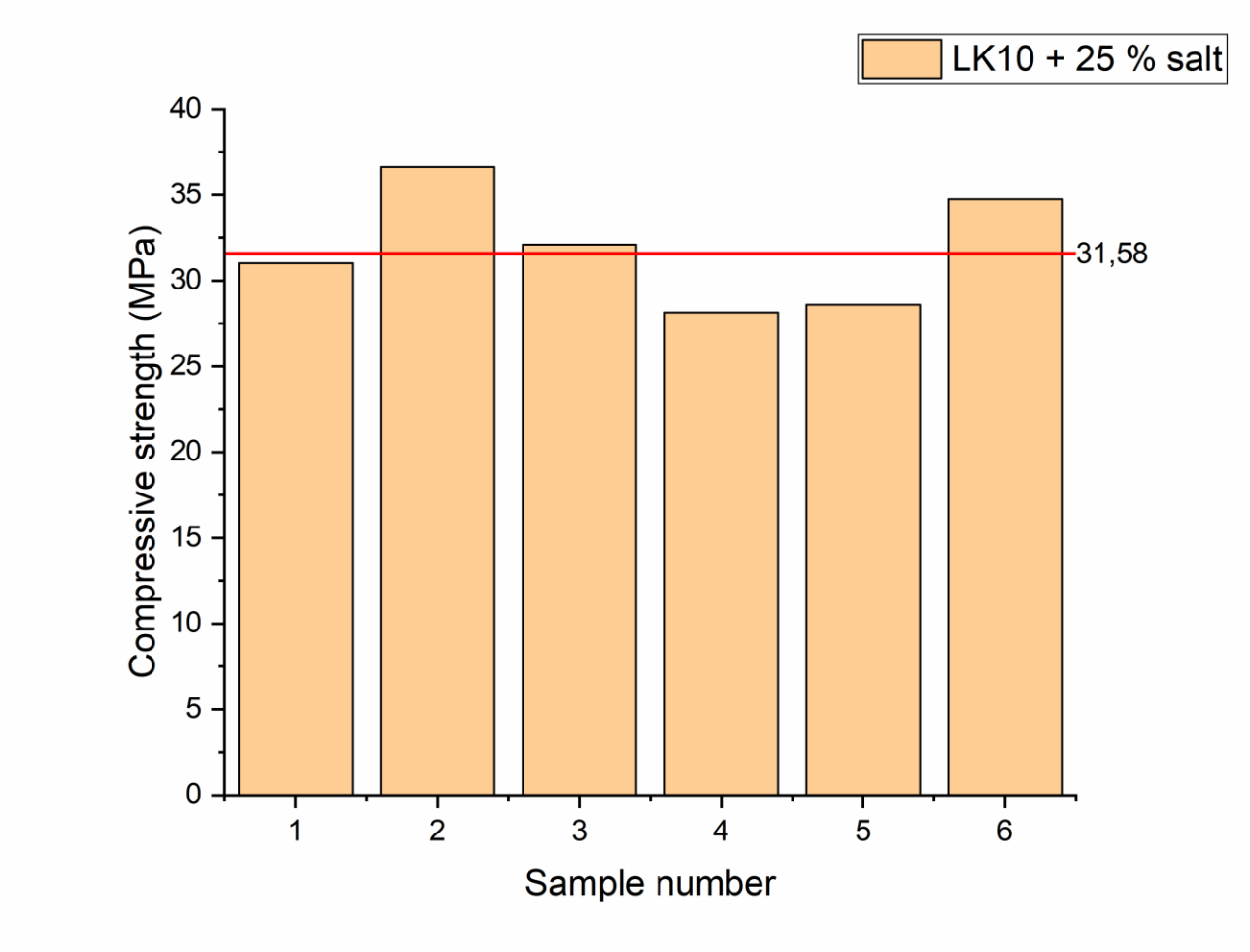

Figure 19: The compressive strength of LK10 geopolymer with 25 w.% waste added.

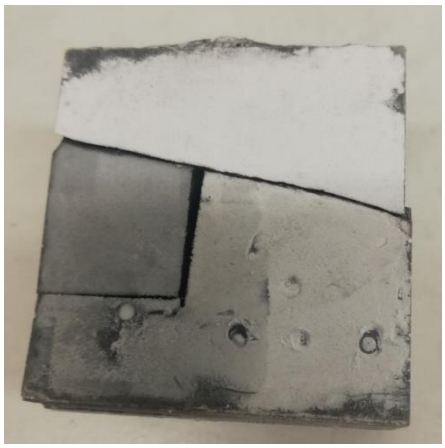

Figure 20: The blooming effect of the LK10 geopolymer with 25 w.% of waste loads.

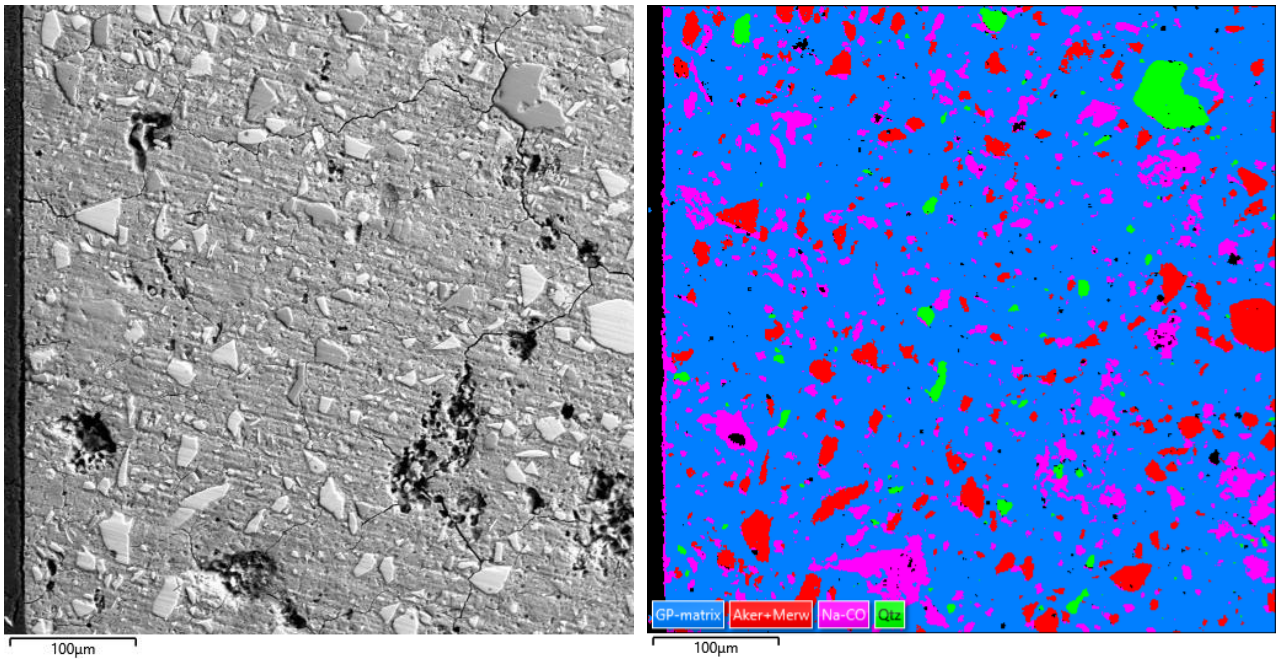

Figure 21: The BSE analysis of the LK10 geopolymer with 25 w.% of waste salt with phase map. The purple parts are the Na-Ca-CO phase located mainly in the cracks.

The properties of the LK10 geopolymer with the incorporation of the waste salt showed decreasing compressive strength with a higher amount of waste incorporated. The SEM analysis showed that with a higher amount of waste salt, the Na-Ca-CO phase rises, which tends to keep its hydrates and hydrate in laboratory conditions causing cracks which negatively affect the matrix. With 15 w.% and more salt, the samples were covered with bloom caused by sodium hydrates. The high number of pores and cracks were more frequent, but trona found by XRD analysis was not found during the SEM analysis, probably caused by dissolution in cooling liquid during the sample preparation. Ethanol was used as a cooling liquid for cutting the samples. Overall, samples show good distribution of waste salt in their matrix, which shows good mixture preparations.

Another series of experiments were made to understand reactions in different curing conditions of LK10 geopolymer. As the compressive strength and SEM analysis were determined in the sealed bag curing, the dry and wet environment and its properties on the matrix were also tested. The mixture preparation was done as in previous experiments, but they were removed from the mould after 3 days and put into observed conditions. Dry curing was done in laboratory conditions, and weight and volume differences were measured each week for up to four weeks. The following samples were put into a sealable vessel filled with water. The samples were put into a beaker so they were above water level. This environment simulated high-level moisture to observe any reactions. Figure *22* shows the scheme of a high-level moisture environment.

The dry-cured samples had good results with compressive strength, modulus of elasticity, weight and volume change evaluated. Figure *23* are shown the results of the compressive strength of dry-cured samples after four weeks in laboratory conditions. It is shown a difference against a sealed bag option, as with 25 w.% of salt, the samples had a very high compressive strength. All samples ranged from 55.6 MPa up to 89.2 MPa, both for LK10 5% salt. Other samples did not show a high range difference. The LK10 + 25 % salt shows excellent results with a range from 69.4 MPa up to 84.6 MPa.

In Figure *24*, the modulus of elasticity of LK10 geopolymer cured in dry conditions is shown. The modulus of elasticity shows the homogenous conditions of the sample. Higher means better. The interesting trend is that LK10, with 5 % of the salt, had the lowest values. This corresponds with low waste content, which could lead to a non-homogenous matrix with solid but brittle conditions. The

higher salt content, as with LK10 with 25 % salt meaning higher values, shows the waste lowers the inner tensions of the sample. This also corresponds with the higher compressive strength shown in Figure *23*.

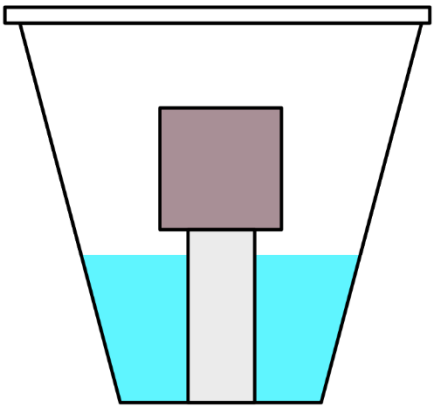

Figure 22: A sample in sealed vessel for high-level moisture environment experiments.

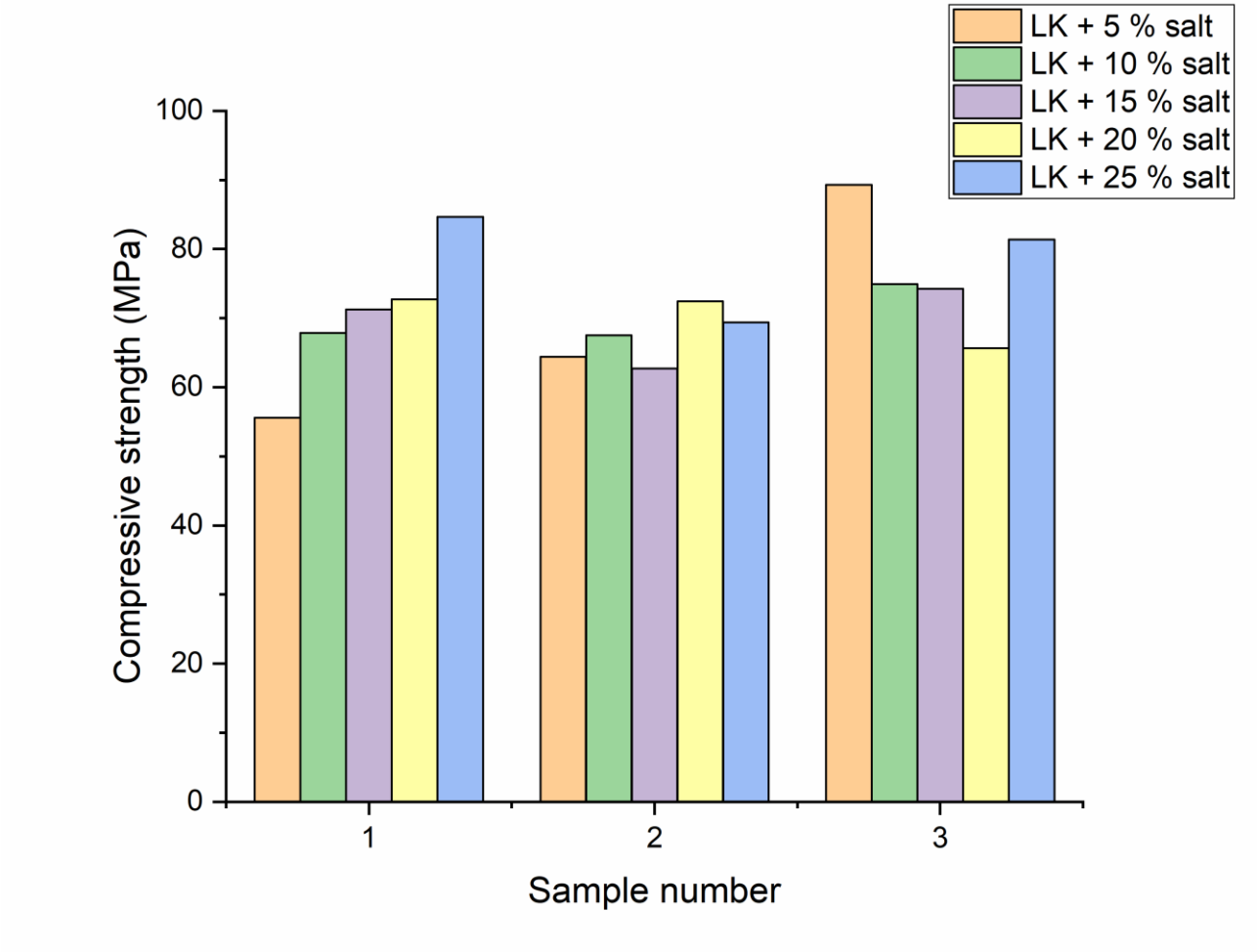

Figure 23: Compressive strength of LK10 geopolymer with salt addition cured in dry environment.

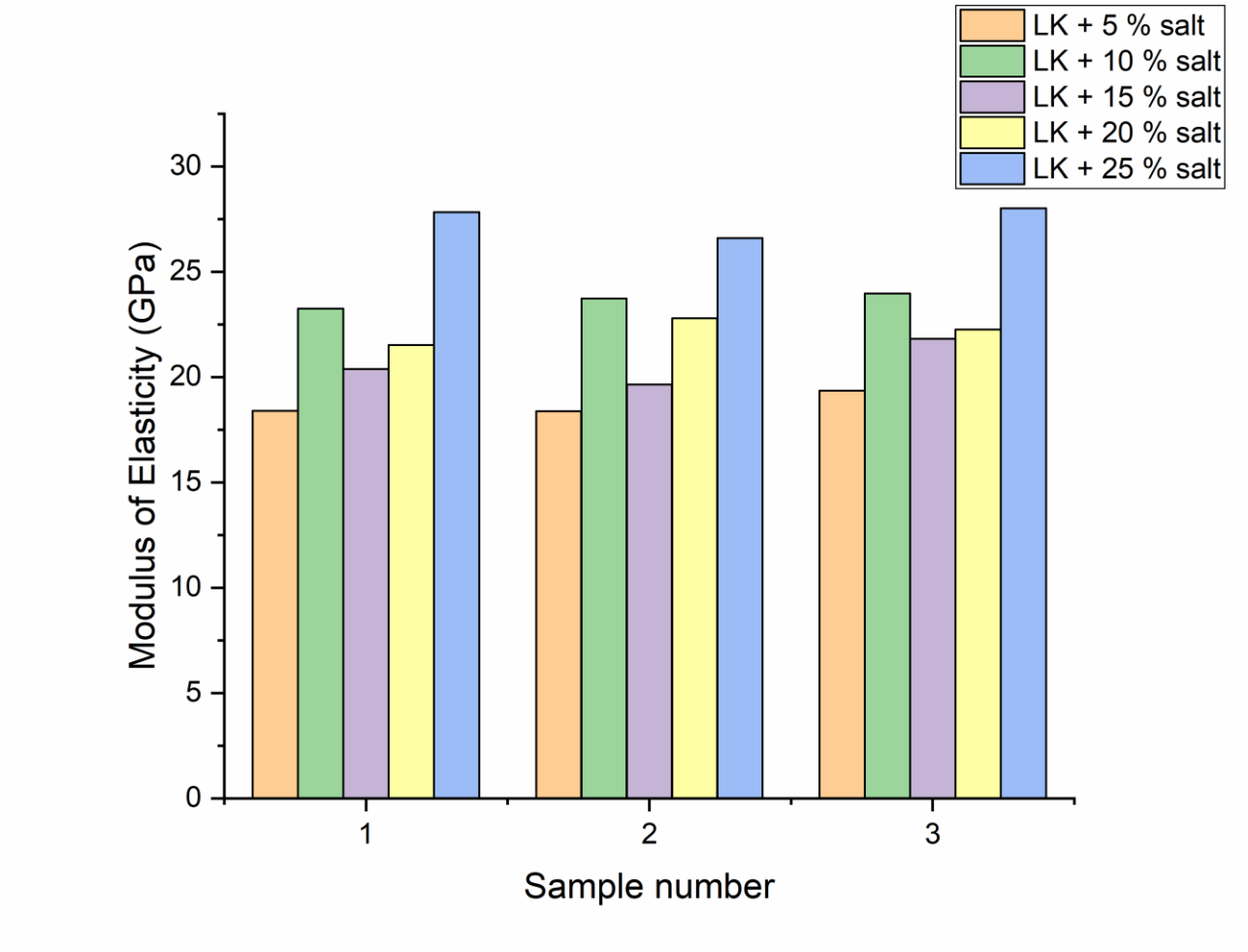

Figure 24: The modulus of elasticity of LK10 geopolymer with salt addition cured in dry environment for four weeks.

The weight difference of each dry-cured sample was measured to determine weight loss or gain during dry curing. Figure *25* shows the weight difference of each sample. The weight difference was measured each week, and each value was compared to the first values obtained after demoulding. The most weight loss was calculated for the LK10 with 5 % waste salt, and weight loss was lower with more waste salt added. This corresponds with the content of $Na_2CO_3.XH_2O$ is contained in the mixture as the water from hydrates slowly evaporates, changing the mineralogical compositions of high waste-loaded samples.

The weight difference experiments were conducted, but obtained results were not conclusive.

The samples cured in wet conditions were not easily obtained as dry-cured ones; samples with a waste load higher than 15 w.% were bloomed and cracked. Figure *26* shows the cracked sample with 20 w.%. This phenomenon was probably conducted by a high moisture environment and with high content of $Na_2CO_3.XH_2O$, the swelling and water absorptions occur, which cracks all samples, and therefore no results could be obtained. In Figure *27* are shown results of the compressive strength of samples cured in a wet environment for four weeks. Obtained results show good mechanical strength, even for 15 % waste load, ranging from 51.2 MPa up to 56.7 MPa. Interestingly the best results were measured with LK10 with 10 % of salt. The ideal filler could explain this phenomenon in the mix, enhancing the mechanical strength.

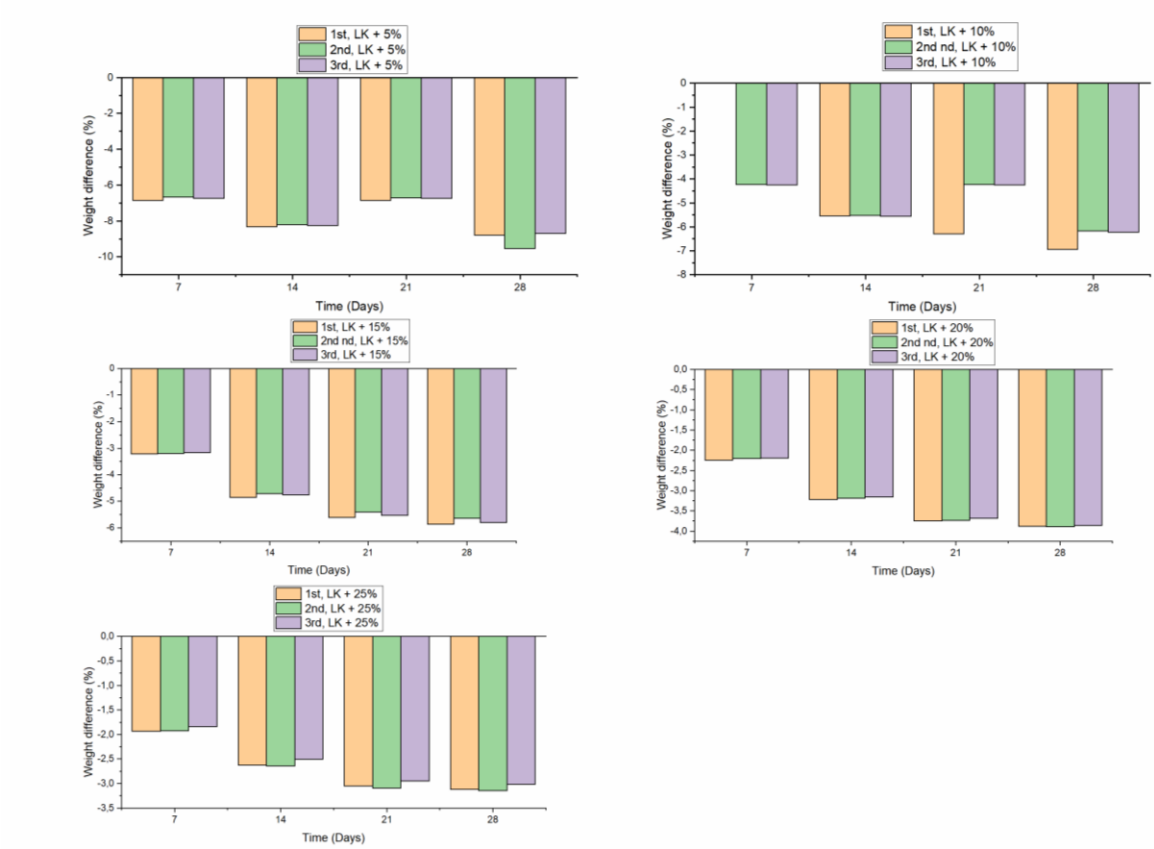

Figure 25: Weight difference of LK10 geopolymer with salt addition cured in dry environment.

Figure 26: A cracked sample with blooming effect.

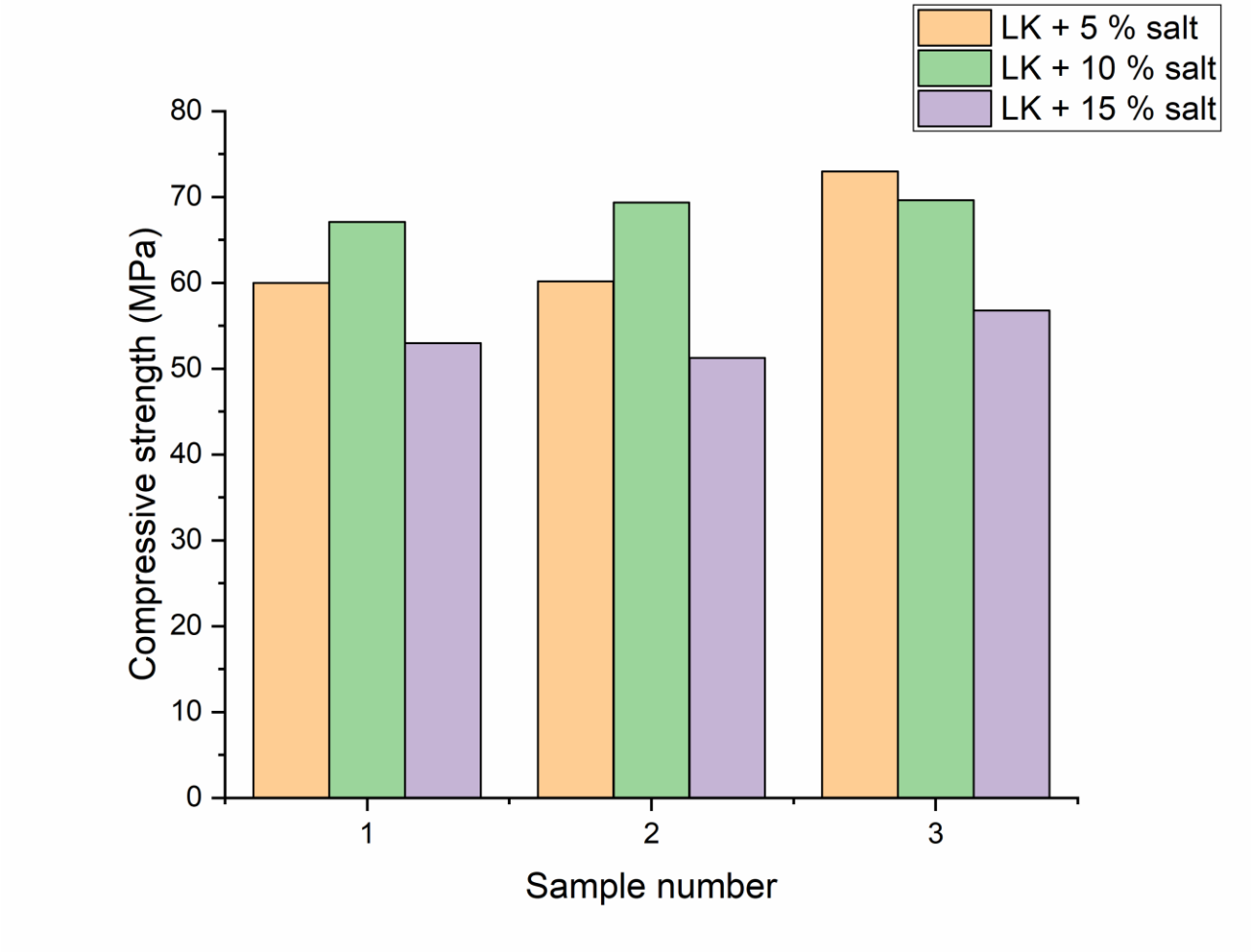

Figure 27: Compressive strength of LK10 geopolymer with salt addition cured in wet environment.

Figure *28* shows the modulus of elasticity of LK10 geopolymer cured in dry conditions. The modulus of elasticity shows the homogenous conditions of the sample. Also, the results are higher than in the dry-cured samples, mainly with low waste load. This could be explained as the samples were not losing any water, which did not result in the cracking of the samples, like in the dry-cured conditions.

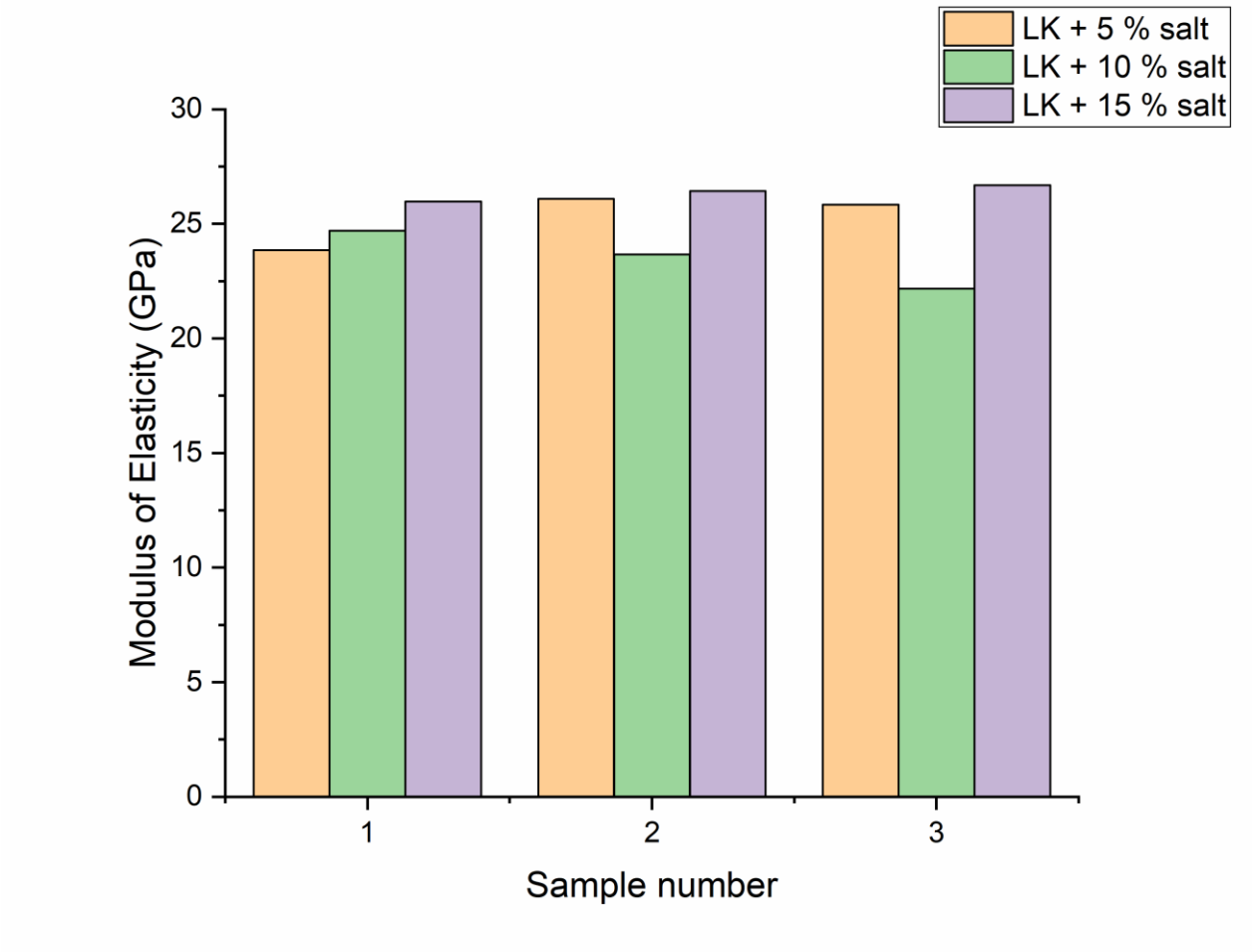

Figure 28: The modulus of elasticity of LK10 geopolymer with salt addition cured in wet environment.

The weight difference of the wet environment cured samples was measured the same as with dry-cured samples. The results are shown in Figure *29*. For the LK10 with a 5 % of waste load, the weight gain for all samples was up to 1 %. With a higher waste load, the measured weight gain was shrinking as in the samples LK10 with a 15 % waste load. After four weeks, the samples got practically the same weight as at the beginning of the experiment. This could be explained by water absorption at the beginning of the curing and dissolving of waste into the water. The waste that could be dissolved would have been on the walls of the sample.

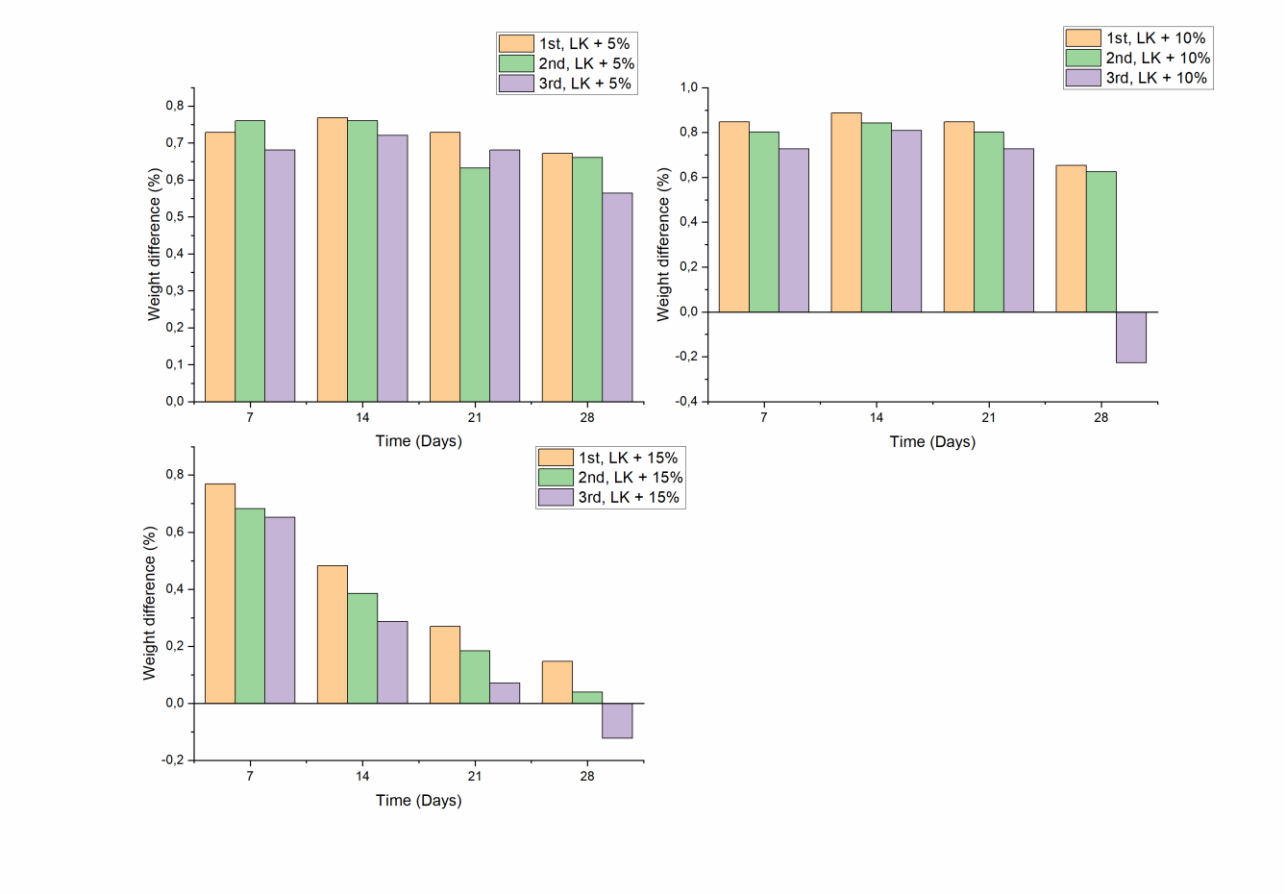

Figure 29: Weight difference of LK10 geopolymer with salt addition cured in wet environment.

2.3.3 Tuff addition

As partners in POLIMI had good results with volcanic tuff as part of their geopolymer mix, it was decided to use it as filler in LK10 geopolymer. POLIMI supplied volcanic tuff, and it was proposed as a more readily available and sustainable natural raw material [7,8] than metakaolin prepared by kaolinite clays, which needed high-temperature calcination before its use. The volcanic tuff's chemical composition is shown in Table *5*, provided by POLIMI [9].

Table 5: Chemical composition of Volcanic tuff in w.% [9]

	SiO_2	Na_2O	K_2O	Al_2O_3	CaO	MgO	Fe_2O_3	TiO_2	H_2O
Volcanic Tuff	52.09	0.51	6.08	17.13	5.77	1.94	3.69	0.52	7.98

The XRD analysis was performed for further analysis and eventually SEM analysis. The Figure *30* shows the spectra of pure volcanic tuff sample. The phase composition (in w.%) was Chabazite 46.3%, Sanidine 5.1 %, Philipsite 1.35 %, Kaolinite 1.62 %, Muscovite 3.8 %, and amorphus phase 42 %.

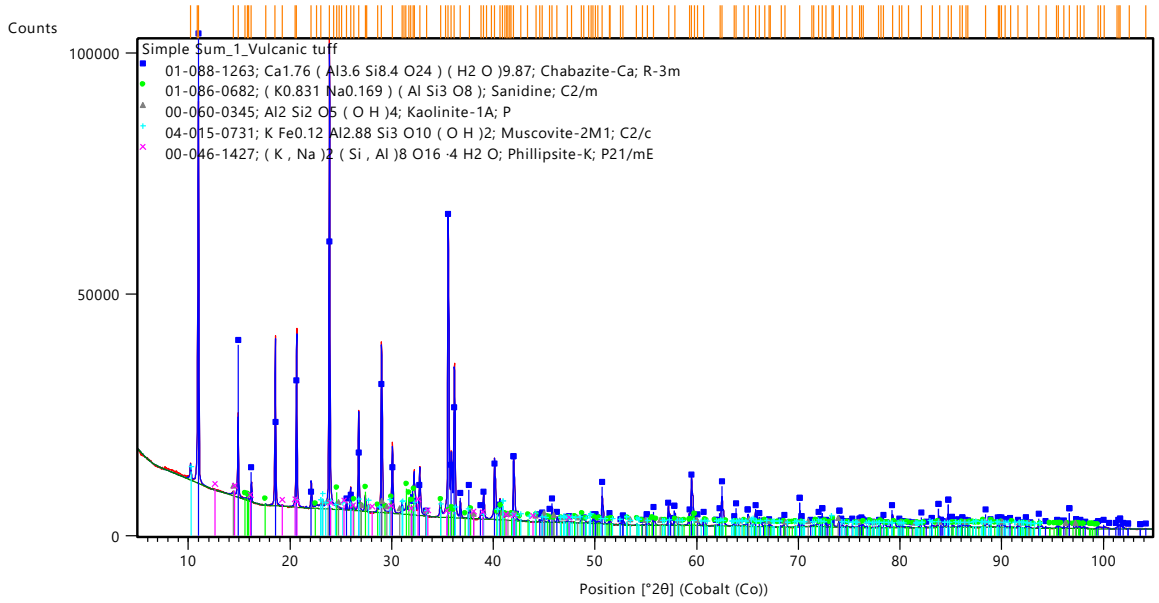

Figure 30:The XRD analysis spectra of volcanic tuff send by POLIMI.

The tuff was used in the LK10 recipe as filler with 10 w.% instead of added metakaolin. The samples were prepared the same way as in the LK10 mixture. The main difference was the high viscosity of the mixture, as tuff absorbed the most water, and the samples with 15 w.% of waste salt were very hard to mix. Therefore, the samples with 20 and 25 w.% of waste were not prepared. The demoulding process needed to be altered as samples were drying slowly. The first series of experiments broke up during the demoulding process (Figure *31*), as samples were not dry enough, so the demoulding of the samples was carried out 10 days after mixing. After demoulding, the samples were cured for 20 days to simulate the same conditions as LK10 geopolymer and were cured in three environments: dry cured, wet environment and water immersed. Figure *32* shows the results of the mechanical strength of the samples. The LK + volcanic tuff with 5 w.% had the best performance with dry-cured sample 79 MPa, but mechanical strength decreases with a high moisture environment and water immersed. The 10 w.% shows similar mechanical strength in all three environments, but the 15 w.% samples were cracked and only dry cured was ready for analysis. The samples were not fully solid after 30 days of curing, which led to low mechanical strength.

Figure 31: The broken samples during demoulding process (left) and not completely solid samples before Compressive testing (right)

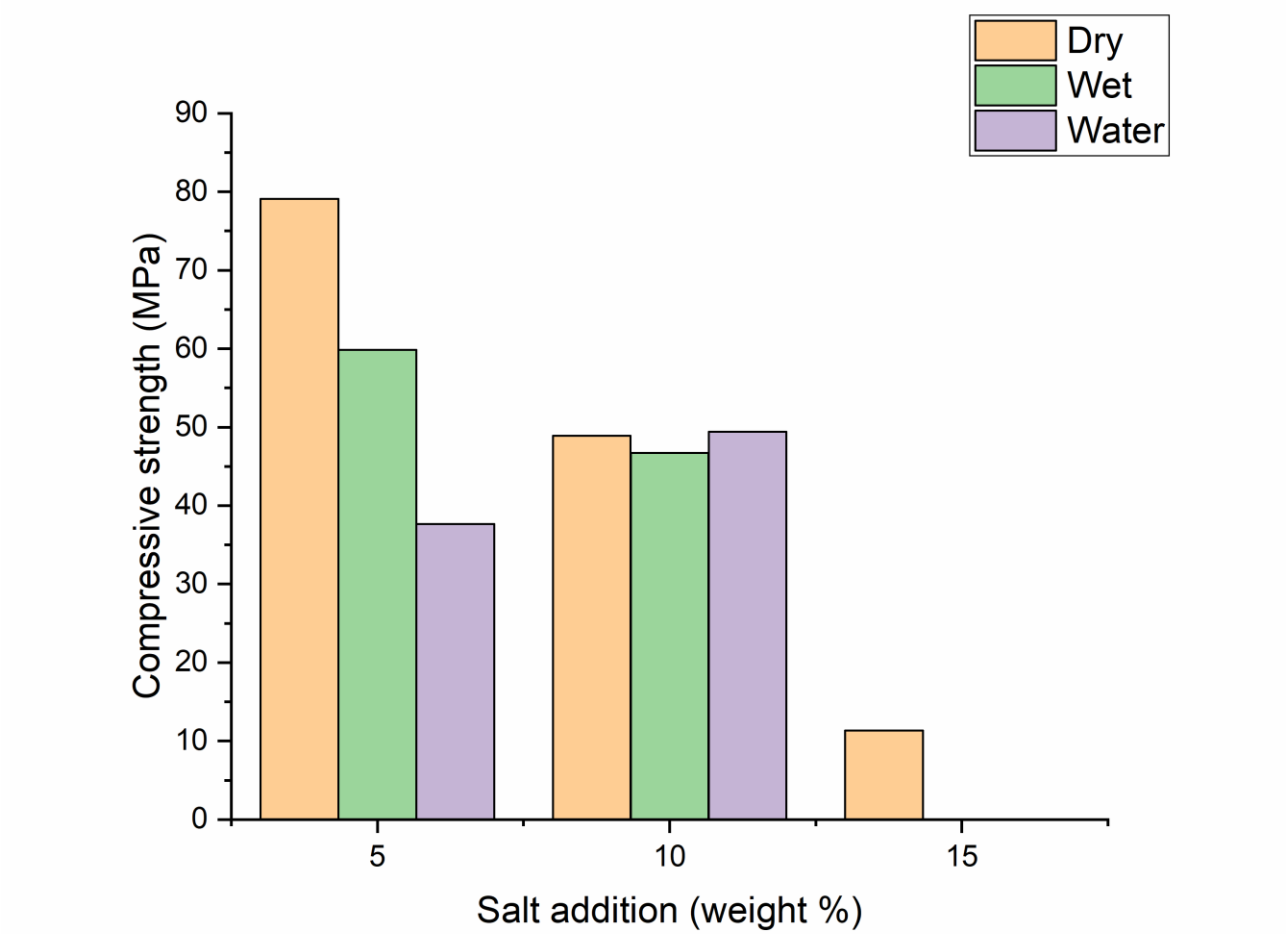

Figure 32: Compressive strength of LK geopolymer with 10 w.% of volcanic tuff and with salt addition.

2.3.4 Improved MSO salt

Due to the obtained results and results from other partners, it was shown that MSO waste is difficult to immobilize with no cracking, leaching or long-term stability of the samples. Therefore, improvements were made to change the MSO waste, mainly from $Na_2CO_3.XH_2O$ chemically into a $CaCO_3$-rich salt which would have better properties for leaching, mechanical and long-term stability.

As colleagues from SCK CEN and CSIC suggested, the ion-change reaction between Ca^{2+} a Na^+ ions is slow, and with the fast reaction, the encapsulation of Na_2CO_3 into a shell made from $CaCO_3$ could be a problem. Therefore, the slow dropping of chemical reagents needed to be performed. As the best reagent was determined, $Ca(OH)_2$ as other Ca^{2+} rich chemicals such as $Ca(NO_3)_2$, $CaCl_2$ or $CaSO_4$ could negatively affect the final mixture. Two experiments were prepared with the dissolution of MSO salt waste in the water, and $Ca(OH)_2$ solution was added by automatic pipette. The final product was decanted and filtered. After filtration, the product was dried up and analyzed by XRD analysis. The XRD analysis of the first and second experiments is shown in Figure *33* and Figure *34*. The resulting yield of this enhanced salt was 511 g from both experiments.

The analysis showed that the enhanced waste had 47.4 w.% of Calcite and 52.6 w.% of Gaylussite, chemically more stable than a mixture of $Na_2CO_3.XH_2O$. The analysis of the second experiment shows that waste had 40.8 w.% of Calcite and 59.2 w.%. During the second experiment, the dosing $Ca(OH)_2$ solution was performed faster, and therefore the Ca:Na is lower than in the first experiment. After analysis, the final product was mixed and processed in the LK10 geopolymer matrix. The samples with enhanced salt were prepared with the LK10 geopolymer recipe and with the same

conditions as volcanic tuff. With more addition of salt, the mixture had high viscosity and was hard to mix; therefore, only 15 w.% of the enhanced salt could be immobilized. The recipe needed to be upgraded with water addition for the immobilization of high values of enhanced waste. Samples were demoulded after 3 days and cured in 3 different conditions, same as the series with volcanic tuff. After curing, the samples were analyzed by mechanical stress test.

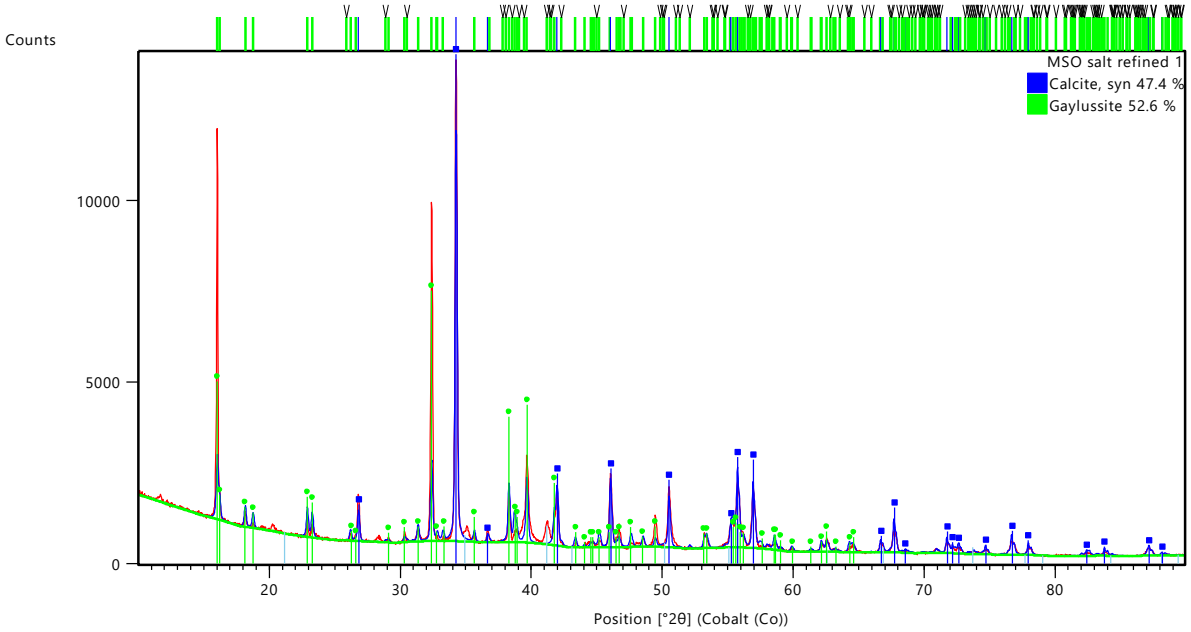

Figure 33: The XRD analysis of the first experiment to enhance MSO waste.

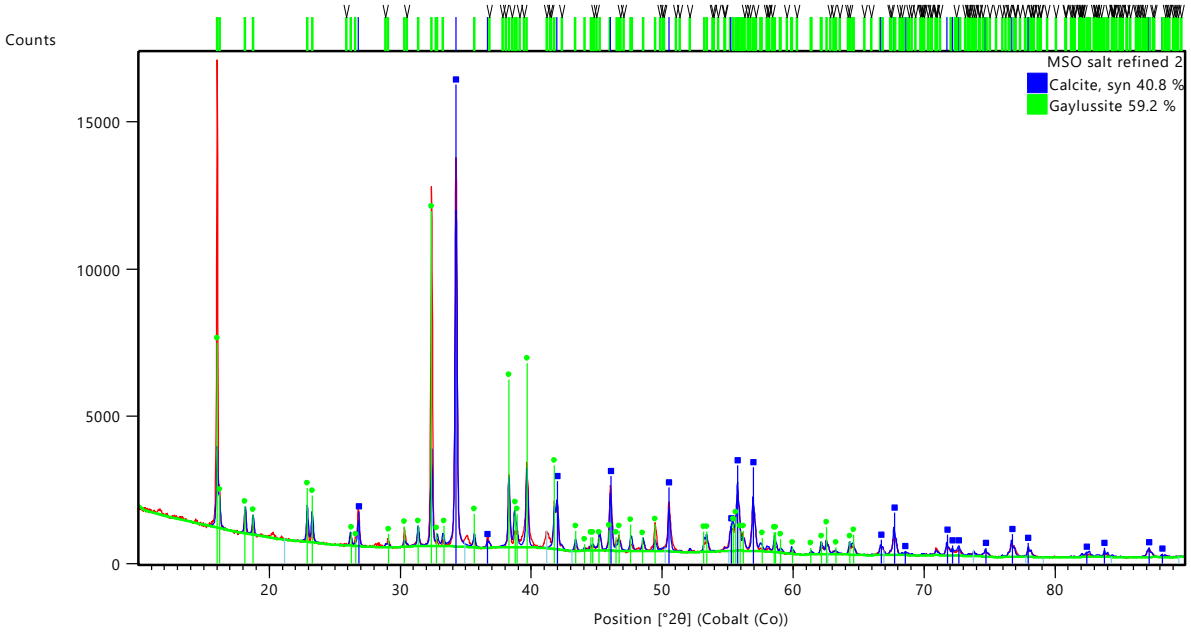

Figure 34: The XRD analysis of the second experiment to enhance MSO waste.

Figure 35 shows the results of the compressive strength analysis of the cured samples. The samples had high mechanical strength cured in all three conditions, as even water-immersed samples did not crack. The LK10 with 15 w.% of waste dry cured show lower mechanical strength, only 32 MPa. On the other hand, the wet sample had very high mechanical strength. This could be explained by the slower polymerization effect in humid conditions, which helped stabilize the sample with less cracking and a more flexible final product. Water immersion, on the other hand, helped the Na_2CO_3

inside the salt. Gaining hydrates leads to swelling, increasing the inner tension, which helps the cracking of the sample.

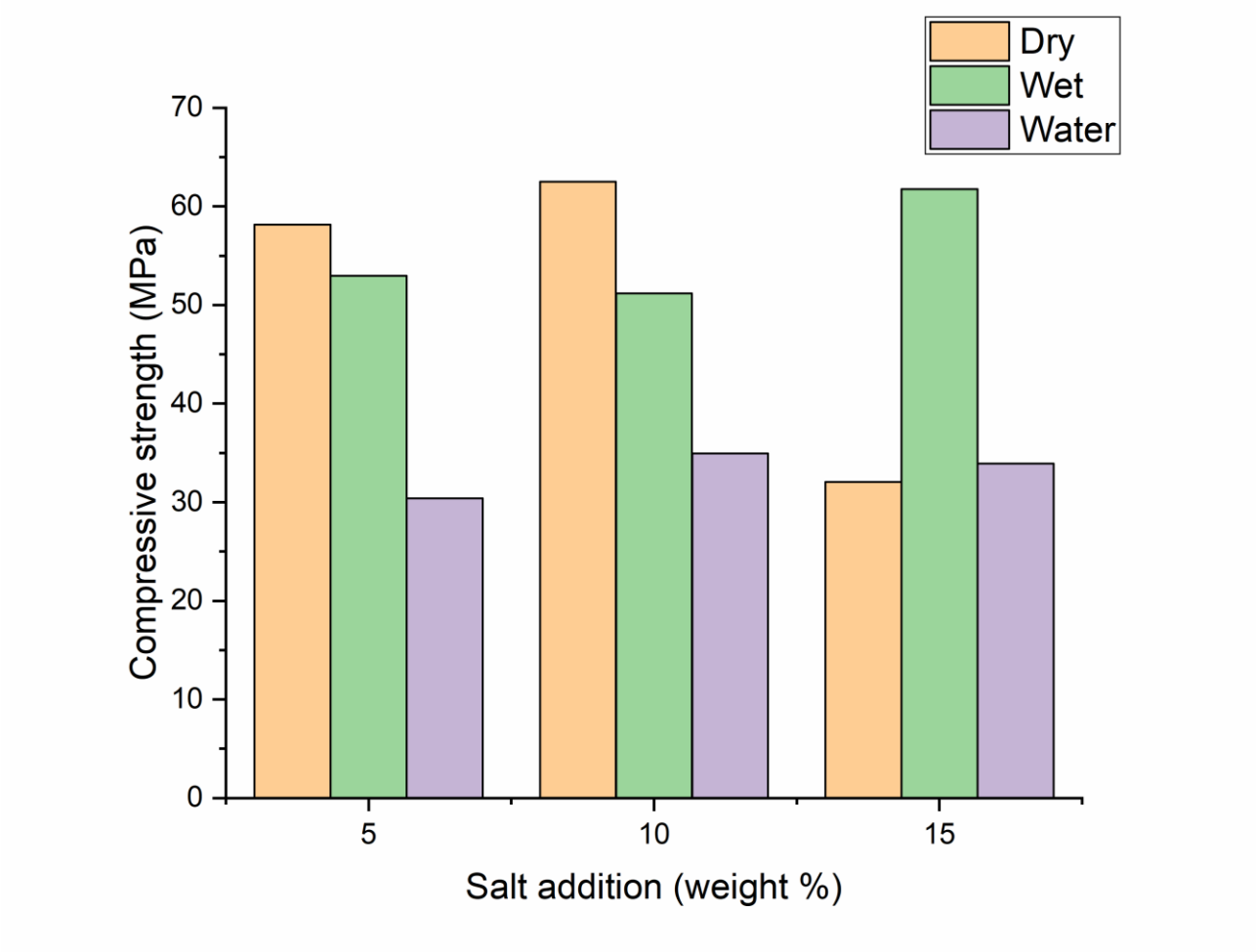

Figure 35: Compressive strength of LK10 geopolymer with enhanced salt addition.

2.4 Conclusions

The CVRez experiments were centred around utilising the commercial LK geopolymer based on metakaolin Mefisto L05 to immobilise the MSO waste generated from the incineration of the IER in molten salt. The salt was analysed and distributed to PREDIS partners within WP6, T6.4.

The first experiments determined the most suitable geopolymer formulation by considering metakaolin addition and mechanical strength. Previous data indicated the necessity of adding extra metakaolin to the standard recipe. The LK geopolymer exhibited the highest mechanical strength, ranging from 50 MPa to 80 MPa. Further analysis revealed that the addition of 15% metakaolin to LK yielded the highest mechanical strength, ranging from 60 to 82 MPa. This formulation was selected as the standard recipe. With the introduction of waste materials, challenges surfaced. Increased metakaolin addition negatively affected the mechanical strength of LK15 with higher salt content, resulting in a decrease from 55 MPa to 15 MPa. The LK10 recipe displayed more consistent compressive strength, achieving a minimum of 30 MPa with 15% salt addition and peaking at 60 MPa and 59 MPa with 5% and 30% salt addition, respectively. Finally, it was decided to use the LK10 recipe as standard for further experiments.

The next series of experiments was performed to assess the properties of the LK10 mixture under various curing conditions and its effects on the final mixture. XRD and SEM analysis were used to understand the mixture better. Higher salt addition led to decrease of the compressive strength of

the samples even in dry-cured conditions. SEM analysis revealed the formation of distinct Na-Ca-CO phases, leading to the identification of pirssonite from XRD results. The weight loss was also determined and showed that with increasing salt waste, the weight loss in dry-cured samples was lower than in samples with a lower waste load, attributable to higher Na2CO3.XH2O levels. The hydrates lost its bound water slowly and prevented fast drying of the samples. Wet-cured samples exhibited weight gain due to water absorption, a phenomenon more evident in high-salt-load samples. Samples with 20 and 25 w.% cracked and could not be measured after one week of curing.

Through cooperation with POLIMI, it was decided to incorporate volcanic tuff into the samples, which could benefit the properties of samples. The tuff addition, set at 10 w.% as filler instead of the metakaolin, exhibited slower hardening and needed to be demoulded only after 10 days. Therefore, the waste loading was performed only up to 15 w.%. The compressive strength results were comparable to the LK10 recipe, although the sample with 15 w.% collapsed during curing.

As MSO waste immobilisation has been proven difficult, the possibility of chemically stabilising the waste has been discussed. Dissolved waste underwent reaction with $Ca(OH)_2$ solution to undergo ion exchange forming $CaCO_3$, which would be easily immobilised. Two experiments yielded a total of 511 g of enhanced salt with a Ca:Na composition of 44,1:55,9. This product was used instead of MSO salt waste and mixed with LK10 geopolymer. The mixture set up very fast compared to standard waste, and therefore limited the waste loading to 15 w.%. The results of the compressive strength analysis were promising with values exceeding 50 MPa for dry and wet cured samples. Water-immersed samples displayed lower compressive strength of approximately 30 MPa. Interestingly, the 15% waste-loaded samples demonstrated different behavior; the dry-cured sample exhibited lower compressive strength (32 MPa) compared to the wet-cured sample (61 MPa). This could be explained by slower weight loss from the sample and longer polymerisation time with increased flexibility of the sample, and lower cracks from fast drying. The recipe requires a formulation upgrade for higher waste loadings, such as higher water content for improved mixing and slower setting times.

2.5 Publications

Reports:

- Hadrava, J., Galek, V., Sears, A., (2021) “Milestone 40 Delivery campaign of the geopolymer samples, June 29, 2022.
- Galek. V., Sears, A., Pražák, P., Vacek, M., Černoušek, T., Hadrava, J., (2023) “Geopolymer characterization from immobilization of MSO waste”, PREDIS Proceedings of May Workshop 2023, Mechelen, Belgium.
- Galek. V., Sears, A., Pražák, P., Vacek, M., Černoušek, T., Hadrava, J., (2023) “Immobilization of spent salt from MSO process”, PREDIS Proceedings of April Workshop 2022, Espoo, Finland.

Presentations in conferences

- CVRez, 4th PREDIS Workshop Meeting, May 22-26, 2022, Mechelen, Belgium.
- CVRez, 3er PREDIS Workshop Meeting, April 25-28, 2022, Espoo Finland.
- Černá, A., Galek, V., Pražák, P., & Hadrava, J. (2022). “Direct Conditioning Of Molten Salt Arising From The Thermal Treatment Of Solid Organic Waste”. 31st International Conference Nuclear Energy for New Europe.
- CVRez, 3er intermediate WP6 PREDIS Workshop Meeting, October 4, 2022, on-line.
-

- Galek, V.; Sears, A.; Pražák, P.; Hadrava, J.; Vacek, M.; Santi, A.; Mossini, E. IMPROVED GEOPOLYMERS FOR ENCAPSULATION OF MOLTEN SALTS FROM THERMAL TREATMENT PROCESSES. In Fuel cycle and radioactive waste, 32nd International Conference Nuclear Energy for New Europe, 11th – 14th September 2023, Portorož, Slovenia; , Ed.; 2023, Poster, Accepted for presentation.

3 CSIC, CIEMAT, UAM contribution

3.1 Introduction

This document describes the contribution of the CSIC regarding Task 6.4 for the conditioning of ashes of Radioactive Solid Organic Wastes (RSOW) by geopolymer and cement-based materials encapsulation. The main specific objectives of CSIC in task 6.4 are the development of Geopolymer binders and Portland Cement-based cementitious systems specially designed to immobilize three types of surrogate RSOW from different sources.

3.2 Work carried out

Figure 36 shows the types of RSOW (input from task 6.3) and the cementitious matrices that have been studied for their immobilization. Both the untreated ion exchange resin (UIER) and the thermally treated ion exchange resin (IER) waste were supplied by CIEMAT and consisted of a mixture of Spent Ion Exchange Resins of type Amberlite IRN-77 and IRN-78 in a 50/50 ratio, doped with B, Cs, Sr and metal traces of Cr, Co, Fe, Zn. The conditioned IER, obtained from calcination at 450°C of the UIER, was granular, with a mean particle size of 300 µm, hygroscopic, with a water content of 3% and had an acid pH ~ 2.4. The UIER was also granular but with a mean particle size of ~500 µm, a moisture content of 51%, and a slightly basic pH ~ 8.8. On the other hand, the Molten salt (waste) was provided by CVrez obtained from the Molten Salt Oxidation process; it was a combination of alkaline salts composed mainly of sodium carbonates and sodium carbonate hydrates (natrite, trona and thermonatrite; ~85%) sodium and potassium chlorides (~5%) and sodium and potassium sulfates (~5%). Cs^{+}, Co^{2+} and Sr^{2+} were added as trackers (1% wt. of each element) and others (2%). The MS showed a particle size between 0.2 and 1 mm and it was very hygroscopic, with an alkaline pH of ~11.4.

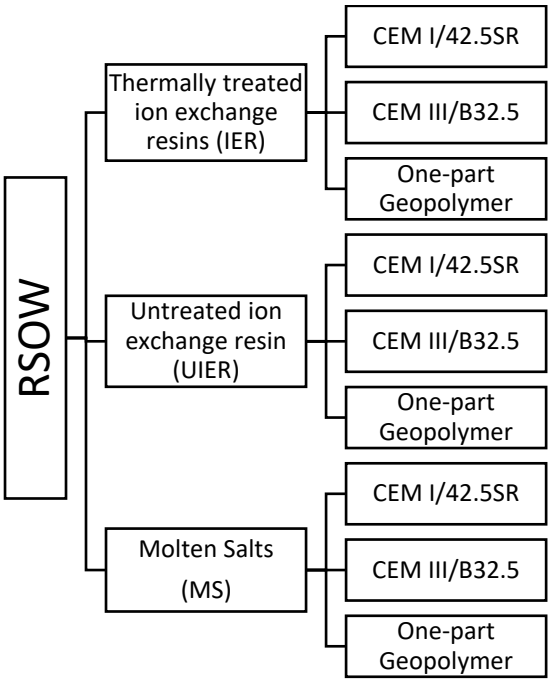

Figure 36. Types of RSOW and cementitious matrices studied by CSIC

For the conditioning of both RSOW surrogates, two types of cementitious systems were studied: i) one based on geopolymers and ii) one based on Portland cement, both specially designed for the immobilization of treated wastes. The geopolymer (GP) was designed based on "one-part" geopolymer matrices, formulated with mixtures of metakaolin (MK) and blast furnace slag (BFS) as precursors, and Na_2SiO_3/NaOH powders as solid activators. As Portland cement (PC) systems, a CEM I/42.5SR and a CEM III/B32.5 were evaluated; CEM I has been used as a reference, while the CEM III (with high content in BFS) was used as a special PC binder, usually employed in cementation processes in the nuclear power plants. All these raw materials were characterized from the chemical and mineralogical point of view (see Table *6* and Figure *37*). The PCs (CEM I and CEM III) have a chemical composition based on CaO and SiO_2, while the chemical composition of MK is based on SiO_2 and Al_2O_3 and that for the BFS shows SiO_2 and CaO as major oxides, with an important content in MgO and Al_2O_3.

Table 6. XRF Chemical composition of CEM I and CEM III, and MK and BFS precursors (% wt.)

	SiO_2	**Al_2O_3**	**Na_2O**	**MgO**	**CaO**	**K_2O**	**TiO_2**	**Fe_2O_3**	**SO_3**	**Others**	**LOI***
CEM I	17.4	4.7	0.2	1.8	60.3	0.3	-	5.0	3.2	2.9	4.2
CEM III	27.2	8.3	0.2	6.5	51.5	0.7	0.7	1.5	2.1	0.3	1.0
BFS	34.8	11.6	-	11.9	37.9	0.3	0.5	0.2	-	2.6	0.3
MK	55.9	38.9	-	0.1	0.1	0.5	1.6	1.2	-	0.3	1.4

*LOI: Loss of ignition 1000±5ºC

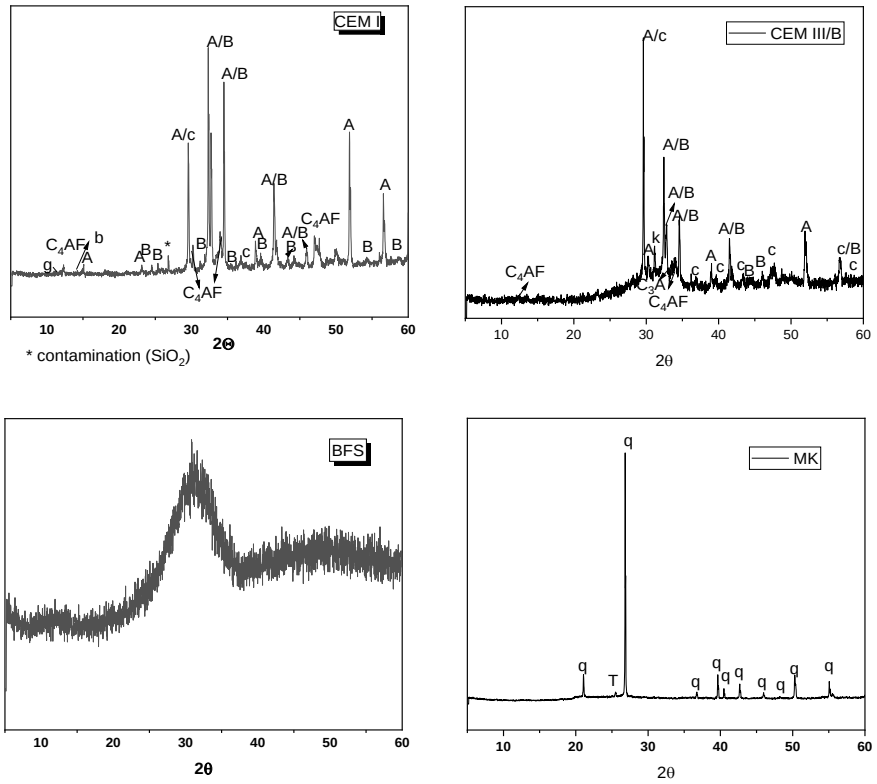

Figure 37. XRD patterns of the raw materials (a) CEM I (b) CEM III (c) BFS (d) MK. (Legend: A: Alite (C_3S) (COD 1540705); B: Belite (C_2S) (COD 9012789); C_4AF: Ferritic (COD 9003347); c: Calcite ($CaCO_3$ 2100189) (COD) g: Gypsum ($CaSO_4$) (COD 500039), k: Akermanite ($Ca_2Mg(Si_2O_7)$ (COD 2106179) q: Quartz (SiO_2) (COD 5000035), T: Anatase TiO_2 (COD 9009086)

CEM I shows the typical mineralogical phases corresponding to clinker (alite (C_3S), belite (C_2S), C_3A and ferrite phase C_4AF), together with gypsum, added as a setting regulator (See Figure *37*(a)). CEM III XRD pattern additionally shows akermanite and calcite coming from the BFS; the amorphous character of the latter was elucidated by a hump located between 20-35º 2θ. BFS used as a precursor in the design of the one-part geopolymer only shows the same hump (20-40º 2θ) associated with the amorphous phase, no crystalline phases were detected (Figure *37*(c)). The XRD pattern corresponding to MK (See Figure *37* (d)) shows that all kaolin has been dehydroxylated, and some minor crystalline phases, such as quartz and anatase were identified.

Each RSOW (IER, UIER and MS) was incorporated in the GP and PC cementitious systems in proportions from 0 to 30 % of the weight of binders (cement or MK/BFS + activators). Regarding the IER, an optimization of the concentration of alkaline activator and composition of the precursors was carried out on the one-part geopolymer to develop matrices of compressive strength comparable to PC systems and reduced porosity; the matrices studied for this purpose are shown in Table *7*. In the case of IER-incorporating PC systems, the water/cement ratio was adjusted to obtain 28-day compressive strengths above 70 MPa in the reference matrices (without the waste). After preliminary tests [10], a water/solid mass ratio (w/s) of 0.3 was fixed for all the matrices.

Table 7. Studied geopolymer and PC matrices for encapsulating the thermally treated IER RSOW.

System	**G1**	**G2**	**G3**	**G4**	**G5**	**G6**	**G7**	**G8**	**G9**	**G10**	**CEM I**	**CEM III**	**CEM I+20IER**	**CEM III+20IER**
%Na_2O	6	9	12	12	6	6	9	12	12	6				
MK/BFS	1	1	1	3	1/3	1	1	1	3	1/3				
%IER	0	0	0	0	0	20	20	20	20	20			20	20

CEM I											100		80	
CEM III												100		80

After optimizing the one-part geopolymer and adjusting the parameters of PC systems to encapsulate the IER, another experimental work was carried out to test the capability of the selected systems to confine the UIER; the studied matrices are shown in Table *8*. In this case, a w/s of 0.35 was fixed to obtain pastes with suitable workability in the fresh state.

Table 8. Studied geopolymer and PC matrices for encapsulating the UIER RSOW.

System	GPO	CEM I	CEM III	UIER
GPO	100			0
GPO+10%UIER	90			10
GPO+20%UIER	80			20
GPO+30%UIER	70			30
CEM I		100		0
CEM I +10%UIER		90		10
CEM I +20%UIER		80		20
CEM I +30%UIER		70		30
CEM III			100	0
CEM III +10%UIER			90	10
CEM III +20%UIER			80	20
CEM III +30%UIER			70	30

The formulations tested for the MS surrogate are shown in Table *9*. Due to the fluidification effect of the salt (water is present in sodium carbonates, main components of the waste), water/solid ratios were adjusted to have, in all cases, pastes of similar workabilities. In the case of the GP systems, two types were prepared, GP-1 and GP-2, which were formulated with practically the same BFS/MK mass ratio but different water/solid (w/s) ratios and different content of activators (NS+NH).

In all of the above mentioned matrices, prisms of 1x1x6 cm^3 were prepared and cured in a climatic chamber (at 21 ^{o}C and 99% RH) until the testing ages. The compressive strengths were determined after 3, 7 and 28 days of curing. At 28 days, changes in microstructure were evaluated by mercury intrusion porosimetry (MIP) and backscattering electron microscopy (BSEM), while the nature of the products formed (mineralogy) was determined by XRD, BSEM-EDX, FTIR and solid-state ^{29}Si and ^{27}Al MAS NMR spectroscopy. For the microstructural characterization, the reaction processes of the samples were stopped following some recommendations by Palacios et al. [11]. Calorimetry tests were also performed on selected samples to determine the effect of the RSOWs on the hydration of cement using a TAM Air isothermal calorimeter at a constant temperature of 25 ◦C. Further details regarding all these techniques can be found in the CSIC recent publication [12].

Table 9. Dosage of the cementitious systems prepared for conditioning the MS (weight %).

SYSTEM		CEM I	CEM III	MK	BFS	NS	NH	MS	L/S ratio*
Without MS	**CEM I**	100.00		-	-			-	0.40
	CEM III		100.00	-	-			-	0.30
	GP-1	-	-	43.00	40.00	10.00	7.00	-	0.42

	GP-2	-	-	39.00	36.00	18.40	6.50		0.32
With 10%MS	**CEM I + 10 % MS**	90.00	--	--	--		--	10.00	0.40
	CEMIII + 10 % MS	90.00	--	--	--		--	10.00	0.30
	GP-1+10 % MS	--	--	38.70	36.00	9.00	6.30	10.00	0.26
	GP-2+10% MS	--	--	35.10	32.40	16.60	5.80	10.00	0.28
With 30%MS	**CEM I + 30 % MS**	70.00	--	--	--		--	30.00	0.40
	CEMIII + 30 % MS	70.00	--	--	--		--	30.00	0.30
	GP-1+30 % MS	--	--	30.10	28.00	7.00	4.90	30.00	0.16
	GP-2+30 % MS	--	--	27.30	25.20	12.90	4.50	30.00	0.12

*L/S ratio: Liquid/solid ratio

3.3 Main findings

3.3.1 Conditioning of the thermally treated ion exchange resin (IER) RSOW

Figure *38* shows the compressive strengths of the geopolymer pastes without and with the incorporation of 20 % IER. The reference matrices (without IER), at 3 days of curing, achieved mechanical strengths higher than 70 MPa, with G1-G5 undergoing a slight increase over time. As expected, the incorporation of 20 % IER reduced the compressive strengths, but this effect was not the same for all the systems; matrices G6 and G10 showed the most substantial reduction while the opposite behaviour was observed for G7 and G9. In this way, the geopolymer composition of 9 % Na_2O and MK/BFS=1, and 12 % Na_2O and MK/BFS=3 underwent the best mechanical performance when the IER was incorporated; both formulation samples far exceed the waste acceptance criteria (WAC) of compressive strengths (10 MPa) [13], and substantially overcome those previously reported elsewhere in the preliminary tests [10].

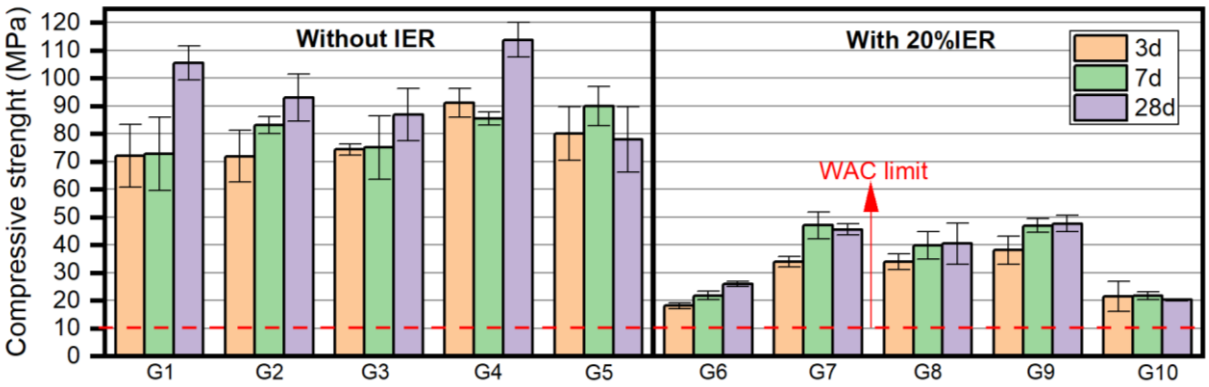

Figure 38. Compressive strengths of geopolymer paste samples without and with 20 % IER.

In agreement with the above, the reference samples with 9 % Na_2O-MK/BFS=1, and 12 % Na_2O-MK/BFS=3 showed very low total porosity (Figure *39*a). The incorporation of 20 % IER increased the total porosity and changed the pore size distribution, which was more remarkable in G9. The

deleterious effects of the IER agree well with the remarkable interface porosity between the IER and the geopolymer matrix (Figure *39*b and c). It should be noted that the IER does not affect the chemical composition of the reaction products, composed of a mixture (N,C)-A-S-H and C-A-S-H gels (Figure *39*d).

As shown in Figure *40*, the XRD pattern of the geopolymer pastes formulated with a) 9 % Na_2O-MK/BFS=1, and b) 12 % Na_2O-MK/BFS=3 showed, in all cases, the formation of an amorphous hump between 25 and 37°2θ, which is associated with the precipitation of geopolymer gels ((N,C)-A-S-H + C-A-S-H) as identified in the BSEM/EDX analysis. Small diffraction lines of calcite and other phases associated with gismondine were also identified as secondary reaction products. It is noteworthy that the incorporation of 20 % IER does not introduce the formation of new crystalline phases.

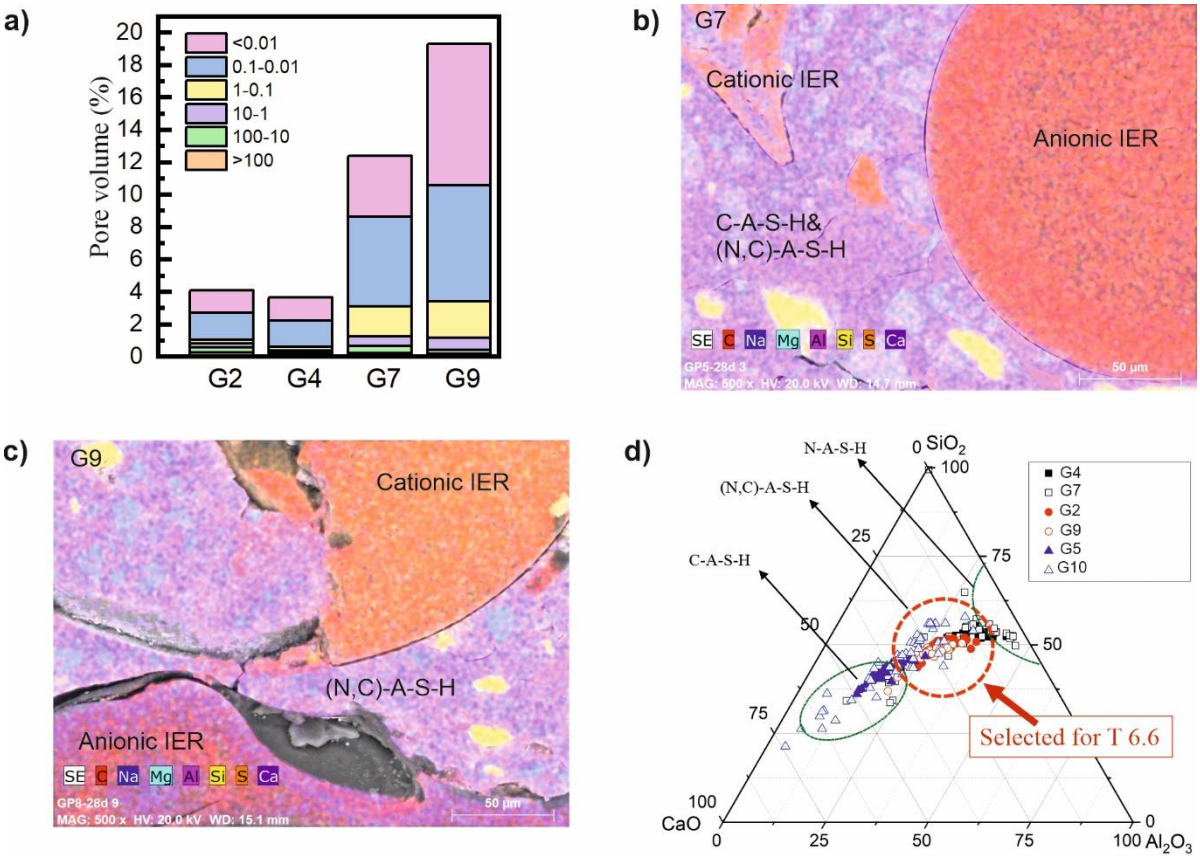

Figure 39. a) Pore volume (%) of samples with the best mechanical performance; mapping BSEM analysis of samples with 20%IER: b) G7 and c) G9, and d) composition of reaction products.

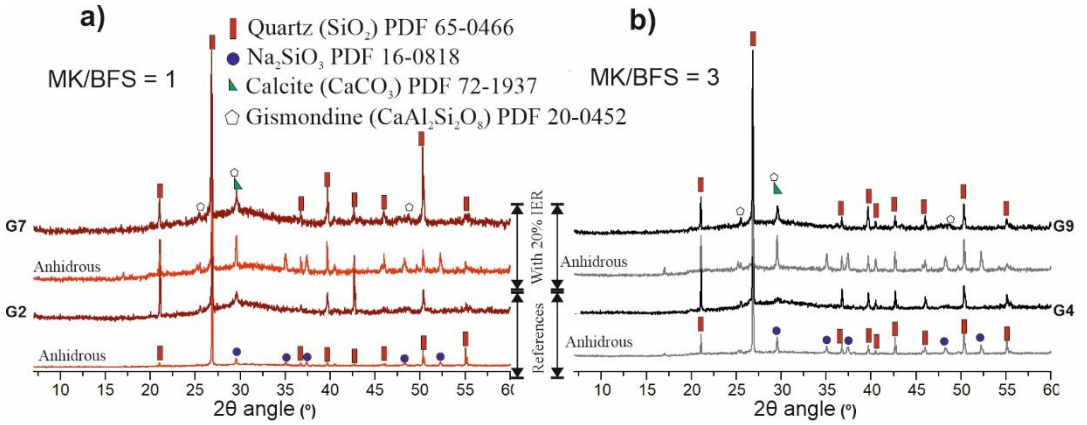

Figure 40. XRD patterns of geopolymers, without and with 20% IER, formulated with a) 9%Na_2O-MK/BFS=1, and b) 12%Na_2O-MK/BFS=3.

The ^{27}Al MAS NMR spectra (Figure *41*a) show that the incorporation of IER did not substantially affect the Al uptake in the (N,C)-A-S-H/C-A-S-H reaction products of systems with a composition MK/BFS of 3 (G4 and G9) and 1 (G2 and G7), since the positions between reference samples and those containing 20 % IER are practically the same. However, in the system with high content of BFS (G5 and G10), the incorporation of IER substantially reduced the FWHH from 15.2 to 14.0 ppm, associated with the lower content of Ca^{2+} in the (N,C)-A-S-H/C-A-S-H gels [14]. Additionally, the lineshape position of the system with high BFS content shifted towards lower chemical shifts (from 59.8 to 57.6 ppm) upon the incorporation of IER, which indicates a decrease of the Al atoms in the neighborhood of the central Al atoms [15]. This behaviour is also supported by the ^{29}Si MAS NMR analysis (Figure *41*b), which shows substantial differences in the systems with high BFS content (G5 and G10) when the IER was incorporated; quantitative analysis by spectral deconvolutions (data not presented here) have shown that the amount of reaction products was reduced by ~38%, consistent with the reduction of the mechanical strength observed in Figure 38.

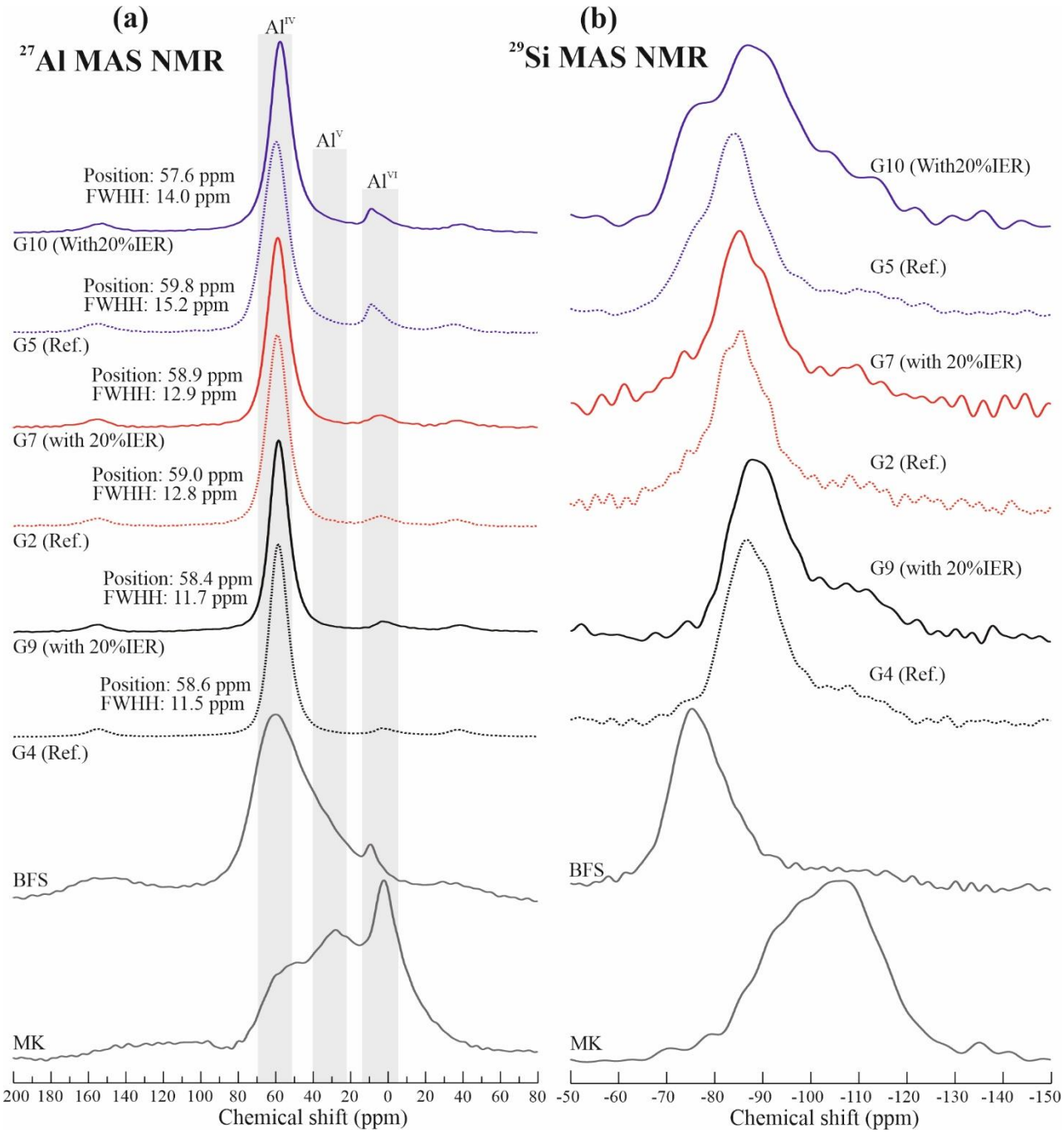

Figure 41. (a) ^{27}Al and (b) ^{29}Si MAS NMR spectra of precursors and GP pastes without (G4, G2 and G5) and with 20%IER (G9, G7 and G10).

Considering the results shown above, the geopolymer formulated with 9 % Na_2O-MK/BFS=1 was considered as the best candidate for conditioning the IER waste. This formulation labelled as GPO was selected for further long-term studies, together with PC-based systems with an optimized water/cement of 0.3; the compressive strength results up to 28 days in matrices with 30 % IER and up to 1 year in those with 20%IER, cured under standard conditions (21 ºC and 99 % RH) are shown in Figure 42. The three reference matrices show comparable 365-day compressive strengths, with GPO having higher values at early ages. This behaviour was preserved when 20 % IER was incorporated, but the compressive strengths decreased by about 50 %, in which CEM I underwent the lowest values; despite this, all the matrices achieved the WAC of compressive strength [13]. After incorporating 30 % IER, both PC-based systems did not achieve the WAC, in which CEM III failed to set; however, the GPO achieved the WAC within 3 days of curing making it the best candidate in terms of mechanical properties for conditioning IER RSOWs.

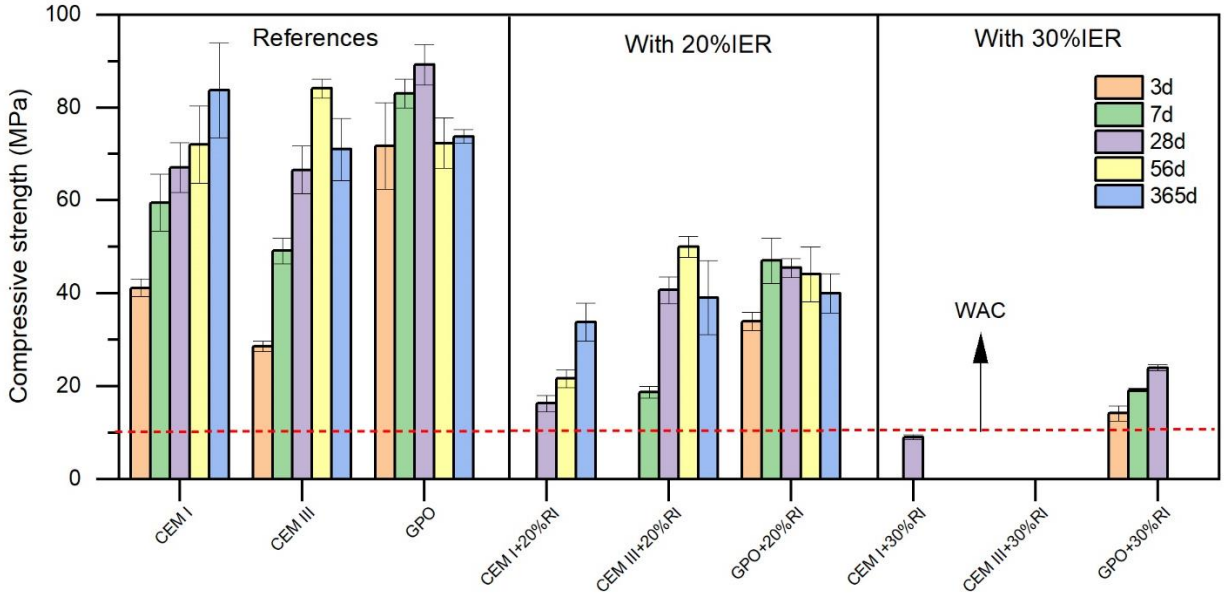

Figure 42. Compressive strengths of selected PC and geopolymer systems with up to 30%IER.

Isothermal calorimetry tests in PC systems elucidated that the cement hydration was delayed with 10 % IER and practically inhibited when 30 % of IER was incorporated (Figure 43a). CEM III+10 % IER underwent lower heat flow than CEM I+10%IER in the first 85h. In addition, the total heat reduced from 250-300 J/g to <50 J/g in both PC samples with 30% of IER (Figure 43b). The acidic character of the IER clearly delays and inhibits the PC hydration. The deleterious effect of the IER on the alkaline activation (GPs) was less evident; although the heat flow was reduced in the first 20 hours due to the IER incorporation, the total heat was recovered after 40 hours of reaction (Figure 44).

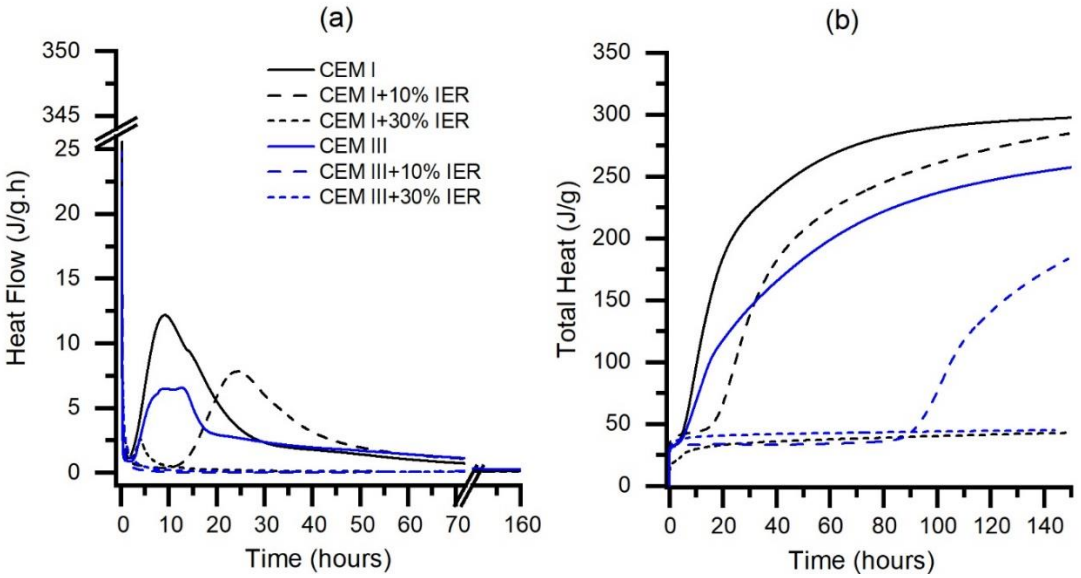

Figure 43. (a) Heat flow and (b) Total heat of CEM I (black lines) and CEM III (blue lines) without (solid lines) and with 10% (dash lines) and 30% (short dash lines) of IER.

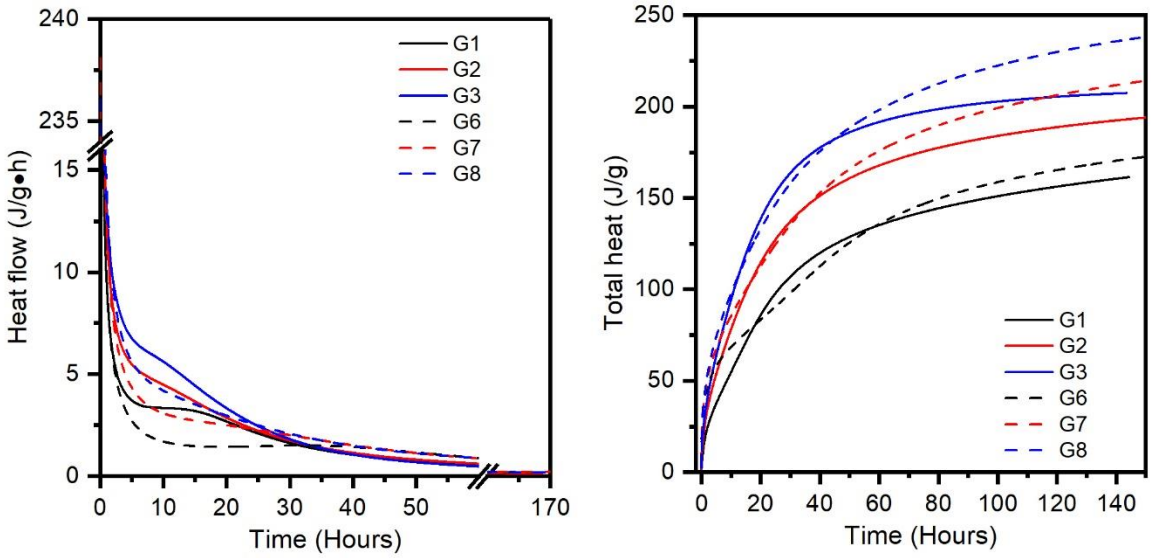

Figure 44. Heat flow and total heat of GP systems without (solid lines) and with 20%IER (dash lines)

3.3.2 Conditioning of the untreated ion exchange resin (UIER) RSOW

Figure 45 shows the effect of the untreated ion exchange resins (UIER) on the compressive strength development of PC and GP systems. As a general trend, compressive strengths decrease with the increasing the UIER content; however, the magnitude of this effect is not the same for the different systems. Similarly as for IER ashes, the setting was delayed for PC systems (Figure 46), wherein CEM I+30 % IER did not achieve the WAC of compressive strength during the evaluated period, while CEM+30 % IER only achieved it after 28 days of curing. In contrast, although the compressive strengths in GPO were also reduced with increasing the UIER content, the effect was less significant. In this case, GPO+30 % UIER strengths achieved the WAC within the 3 days of curing, and the compressive strengths increased over time, achieving up to 30 MPa after 28 days. As shown in Figure 46, the setting time in the GPO was also less affected than in PC systems upon the UIER incorporation. In agreement with this, Figure 47 shows that the pH values, in the first hours of hydration, were reduced with increasing the UIER content, with more remarkable effects in PC systems with 30 % UIER, while the GPO systems recorded pH >13 in all studied contents of UIERs. It seems that pH has an important role in the kinetics of the reactions.

Consistent with the above, the total porosity in PC and GP paste samples increased with increasing the UIER content (See Figure 48). The reference samples (without the UIER) showed similar total porosity of 12.9 % for CEM I, 14.6 % for CEM III and 12.3 % for GPO, but these values increased up to 33.2, 25.3 and 24.6 %, respectively, when 30 % of the UIER was incorporated. Furthermore, the PC-based systems show a substantial increase in the pore size diameter after incorporating the UIER, this effect being more evident in CEM I. Similarly as occurred with the thermally treated IER ashes, the increased porosity in both PC and GP systems upon the UIER can be related with a remarkable interface porosity between the UIER particles and the cementitious matrices (Figure 49) and with a reduction in the amount of reaction products (as the reactions can be delayed/inhibited). XRD patterns of the GP systems do not show visible changes upon the UIER incorporation, as the reaction products are mostly amorphous; however, in PC systems, the intensity of the unreacted alite and belite phases is increased with the increasing the UIER content (Figure 50).

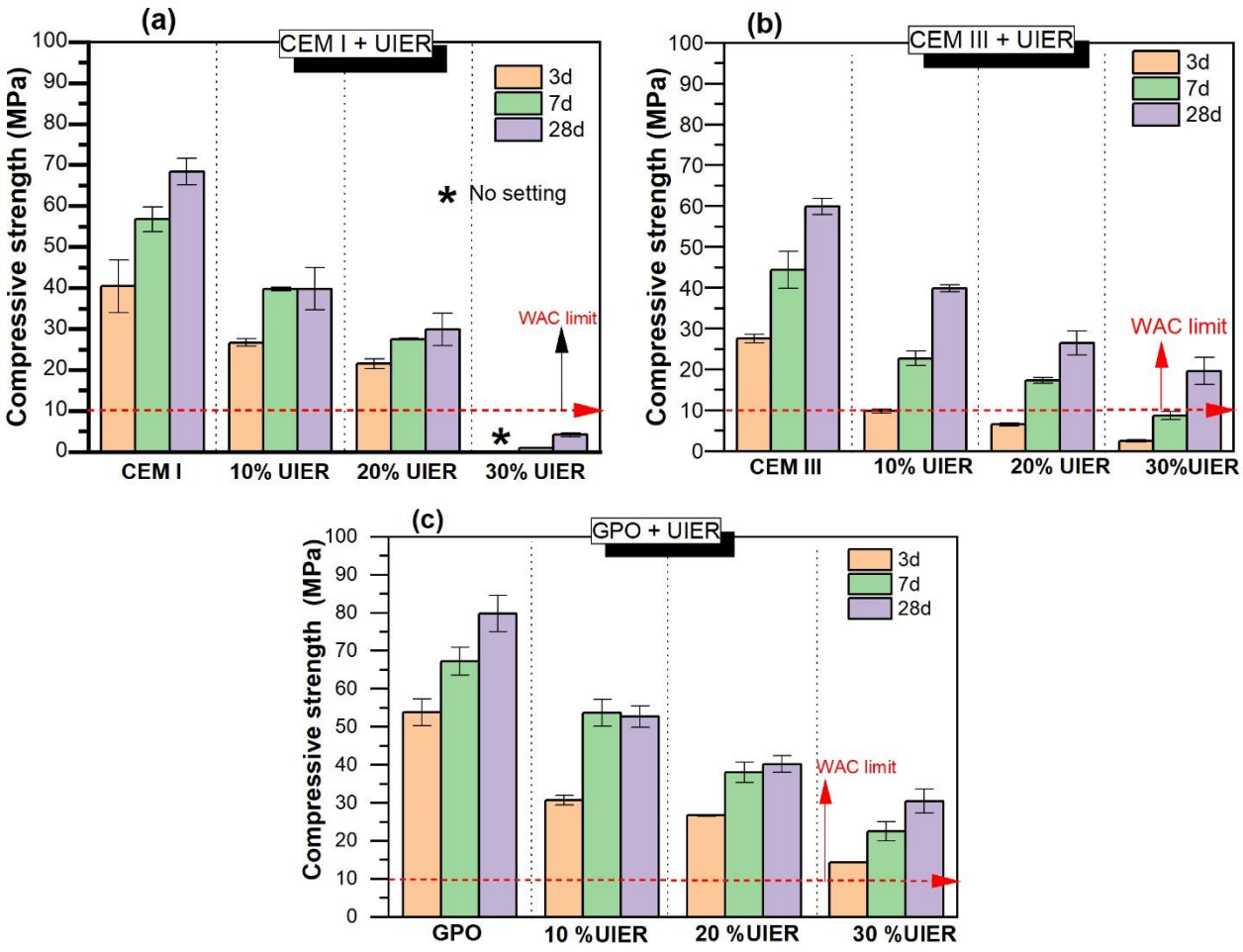

Figure 45. Effect of the UIER on the compressive strength development of selected PC and GP systems, (a) CEM I, (b) CEM III and (c) GPO.

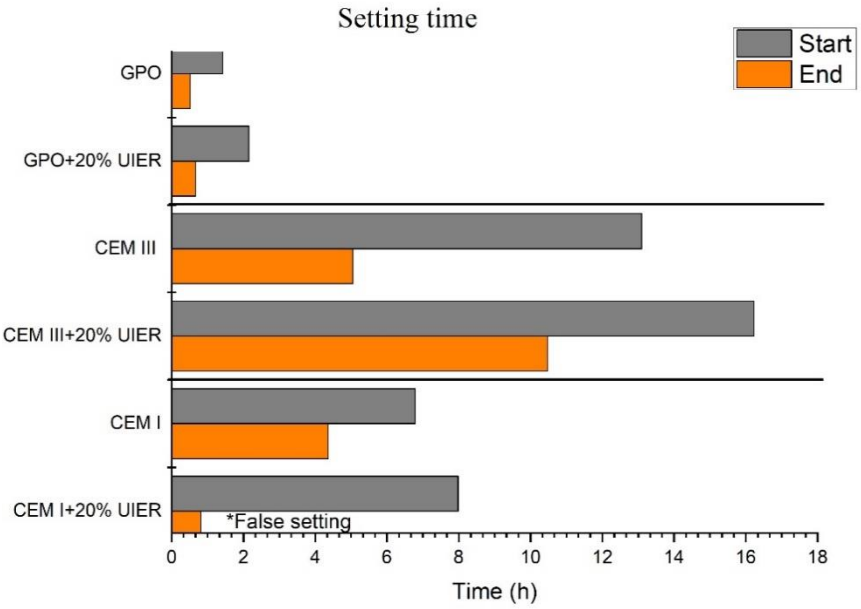

Figure 46. Setting time of pastes of PC and GP systems without and with 20% of UIER

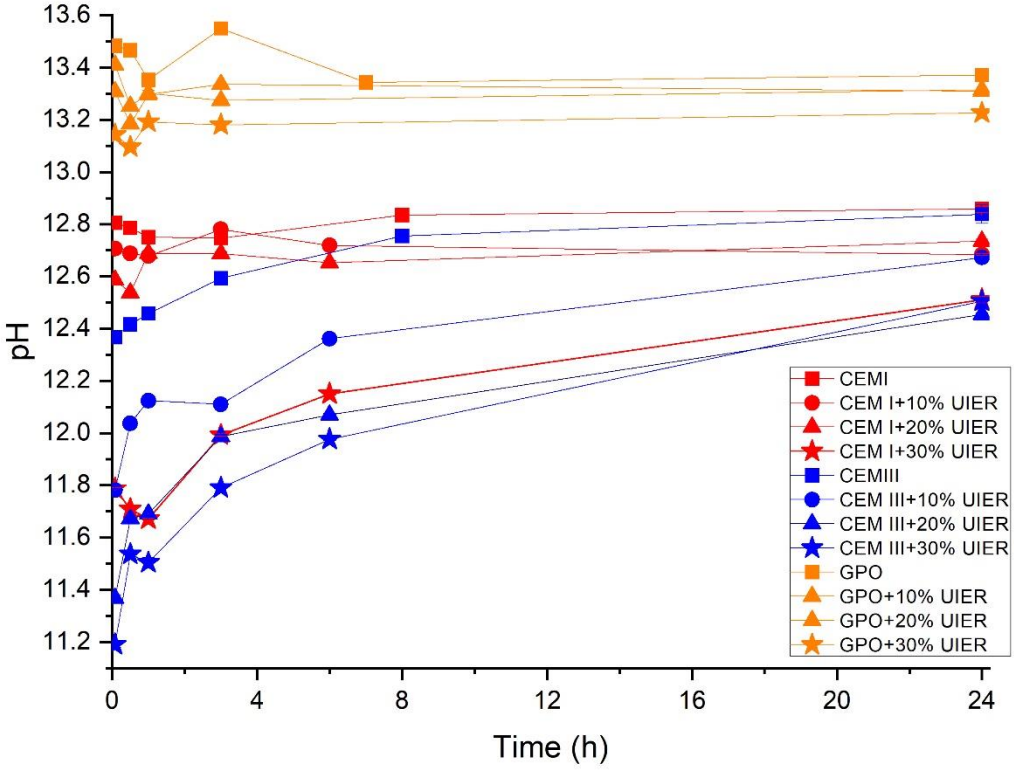

Figure 47. Effect of the UIER on the pH of the PC and GP pastes in the first hours of reaction.

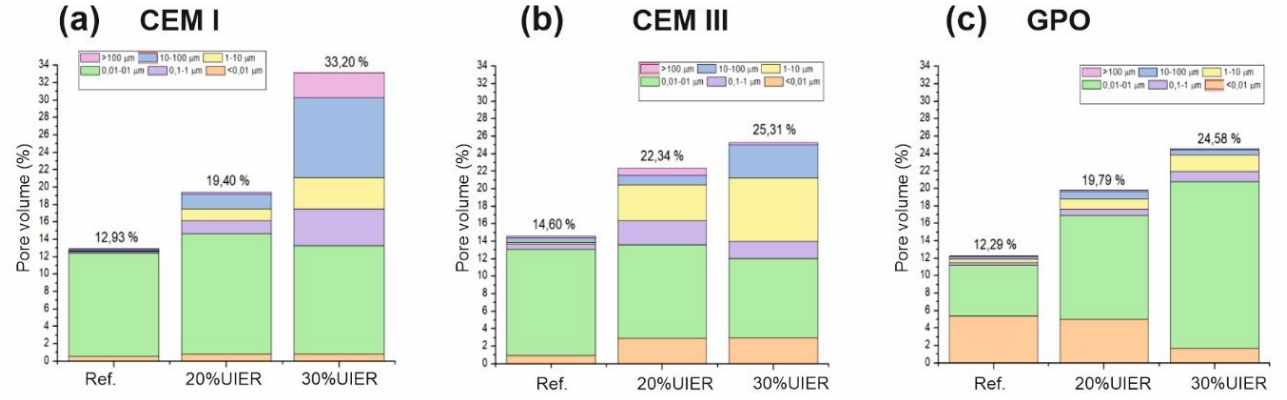

Figure 48. Effect of the UIER on the porosity of (a) CEM I, (b) CEM III and (c) GPO paste samples.

It is important to notice that PC-based samples with 30 % of UIER, exhibited deformation since the first 28 days of curing (Figure 51). After 90 days in the chamber (21 ºC and 99 %RH), the deformation became much more evident in both PC-based samples with 30 %of UIER, in which the CEM I+30 %UIER samples were highly deteriorated (Figure 52a). At this age, as shown in Figure 52b, the CEM I+20 % UIER samples broke while the CEM III+20 % UIER samples exhibited small deformations. In contrast, the GPO samples have not exhibited deformations due to the UIER content during the evaluated period.

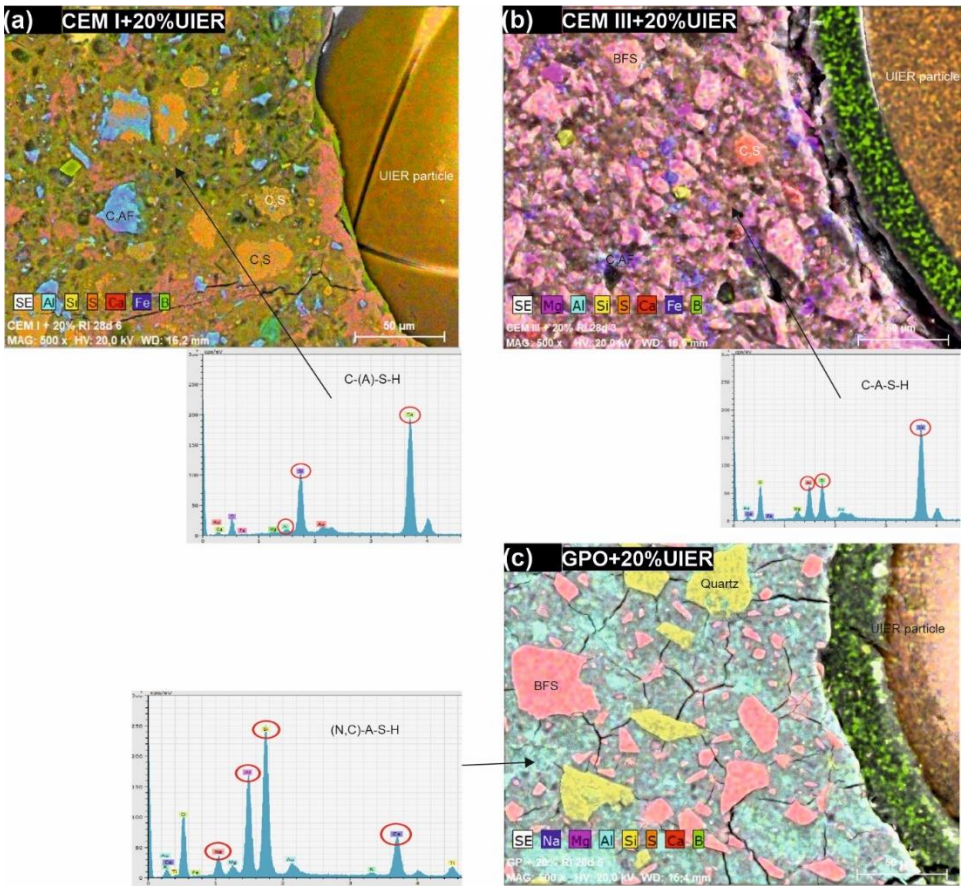

Figure 49. BSEM images of (a) CEM I, (b) CEM III and (c) GPO paste samples incorporating 20% of the UIERs.

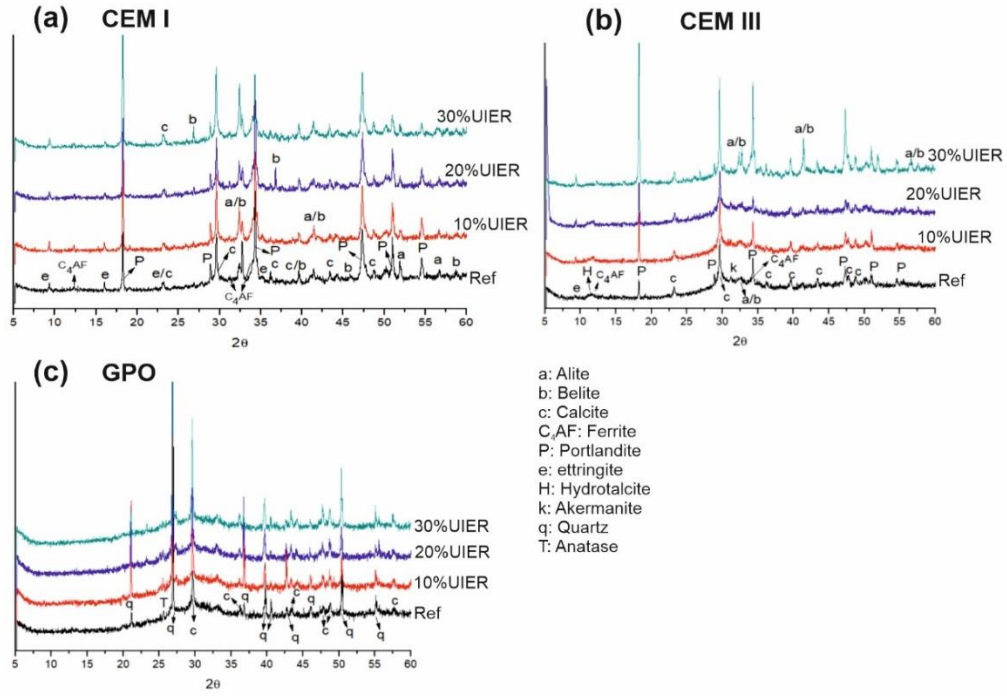

Figure 50. XRD patterns of (a) CEM I, (b) CEM III and (c) GPO paste samples incorporating 0, 10, 20 and 30% of the UIERs.

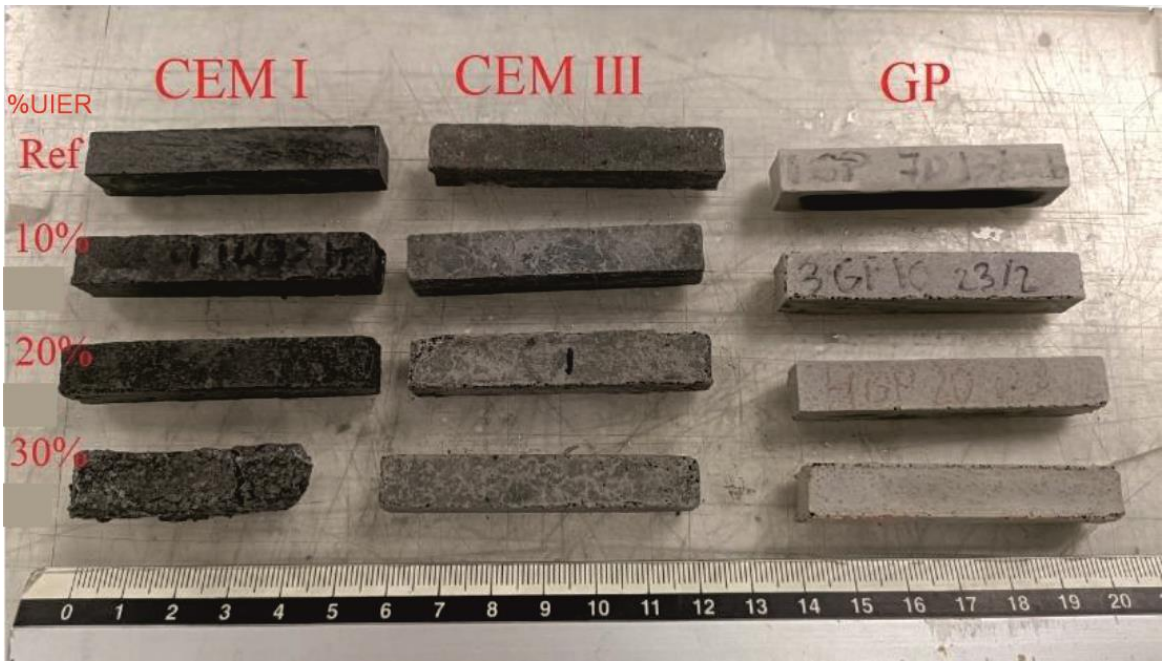

Figure 51. Visual aspect of representative paste samples at 28 days of curing at 21ºC and 99%RH.

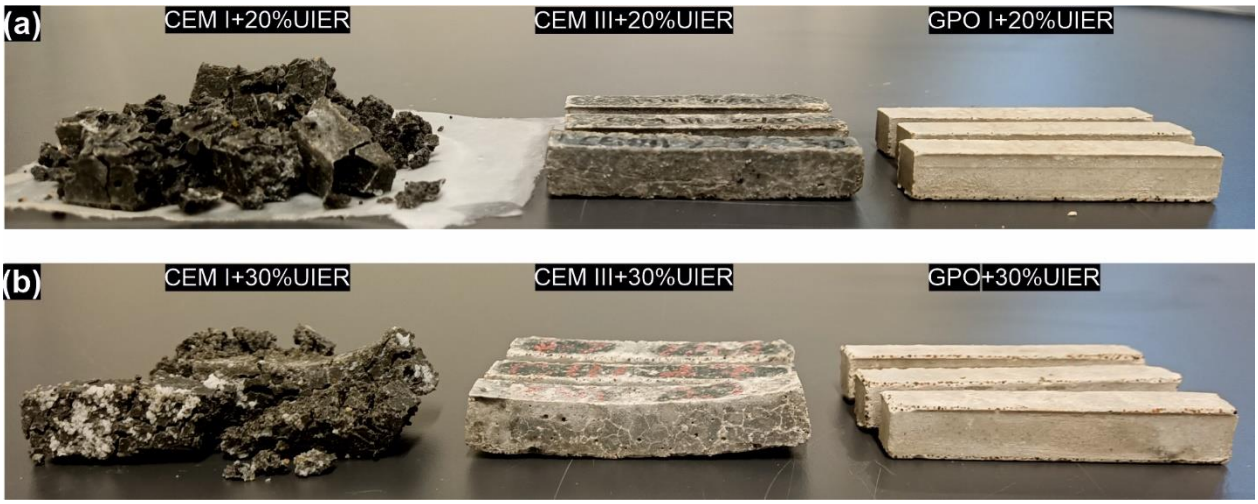

Figure 52. Visual aspect of paste samples with (a) 20%UIER and (b) 30UIER after 3 months at 21ºC and 99%RH

3.3.3 Conditioning of the Molten Salt (MS) waste

3.3.3.1 Geopolymer matrices

As shown in Figure 53, the reference GP-2 underwent higher strength gain than its counterpart GP-1, indicating a positive effect of increasing the alkaline activator dose and reducing the l/s ratio. After incorporating 10 % MS, GP-1 showed a clear decrease in the compressive strengths with values just at the WAC limit, while the opposite occurred in GP-2, which underwent a significant strength increase reaching values of 50 MPa after 28 days of curing. In the latter case, the MS could play a role as an extra activator, forming a more compact structure (Figure 54), which justifies the higher mechanical strength development. So, the incorporation of 10 % MS in GP-2 system was beneficial from the microstructural point of view, with a notable reduction in the total porosity (from 25% to 18%) and with a refinement in the microstructure (see Figure 54(b)); this is also in concordance with its very good mechanical strengths.

In agreement with the above, the microstructure of GP-2+10 % MS was denser than GP-1+10 % IER, which is another indicative of the extra activator effect of the MS, in which the incorporation of 10% of MS in GP-2 favoured the dissolution of the precursors, densified the microstructure and improved the mechanical properties. The presence of microcracks in GP-2+10 % MS could be mainly associated with well-known dry shrinkage after alkaline activation of BFS [16]. An EDX analysis of the cementitious matrix of samples without and with the MS showed that it is composed of two types of gels (C-A-S-H + (N,C)-A-S-H). GP-2 showed a chemical composition slightly richer in Si than GP-1 due to the higher Na_2SiO_3 content. In both GPs, the incorporation of 10 % of MS, practically does not modify the chemical composition of the gels. The formation of C-A-S-H + (N,C)-A-S-H gels was also elucidated by the amorphous XRD hump between 25 and 37º 2θ (Figure 57). Calcite, vaterite and aragonite were identified as well, as secondary reaction products in both systems. At 7 days, the incorporation of 10% MS in both systems, practically do not modify the XRD pattern for the references ones (GP-1 and GP-2), while at 28 days some small diffraction lines assignable to gayslussite ($Na_2Ca(CO_3)_2.5H_2O$) were identified.

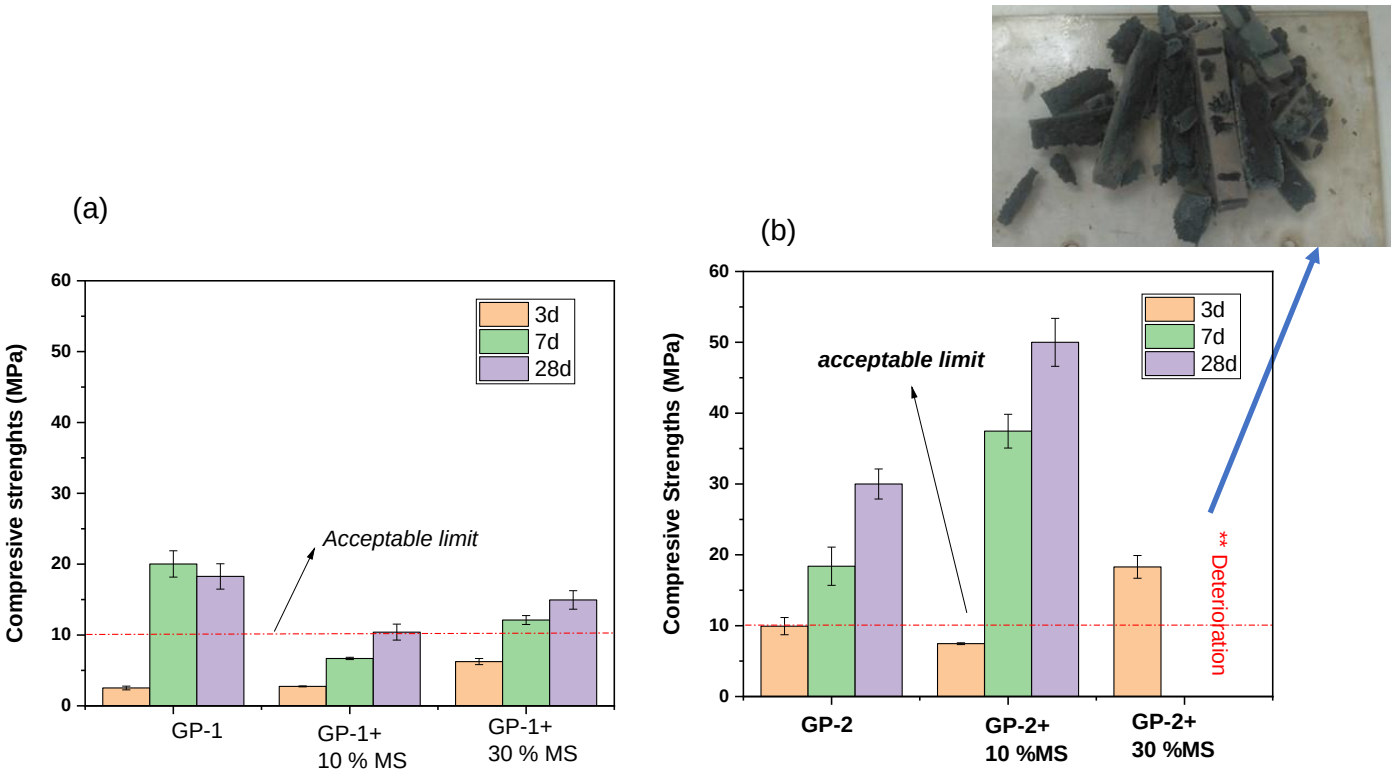

*Figure 53. Mechanical strengths at 3, 7 and 28 days of curing in (a) GP-1 and (b) GP-2 without and with 10 and 30% of the MS (** Specimens were highly deteriorated after 7 days of curing).*

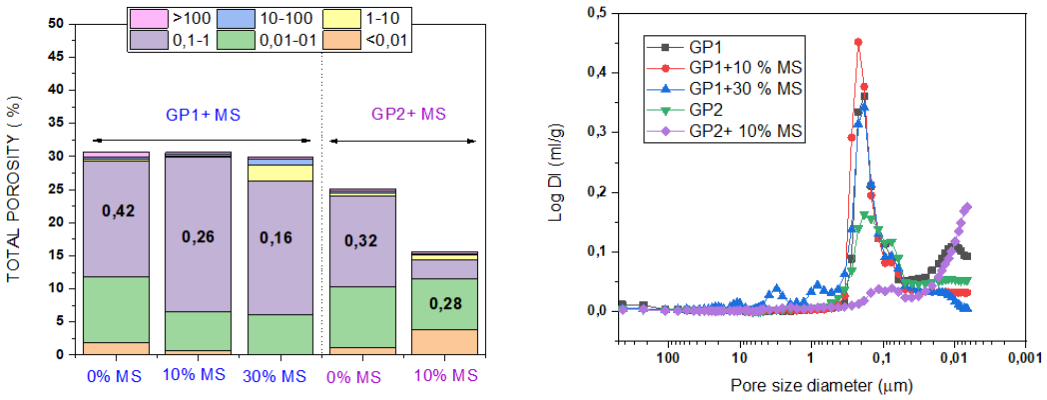

Figure 54. Total porosity and pore size distribution of GP-1 and GP-2 without and with the MS after 28 days of curing.

The behaviour changed completely in the pastes after incorporating 30 % of MS RSOW. Regarding to the mechanical strengths, at early ages (3 days of curing at 98 % RH), they were even higher than those observed in the reference GP-2 (~ 18 MPa)). However, after 7 days of curing the GP-2+30 % MS specimens spontaneously broken in fragments (see photo Figure 53(b)).

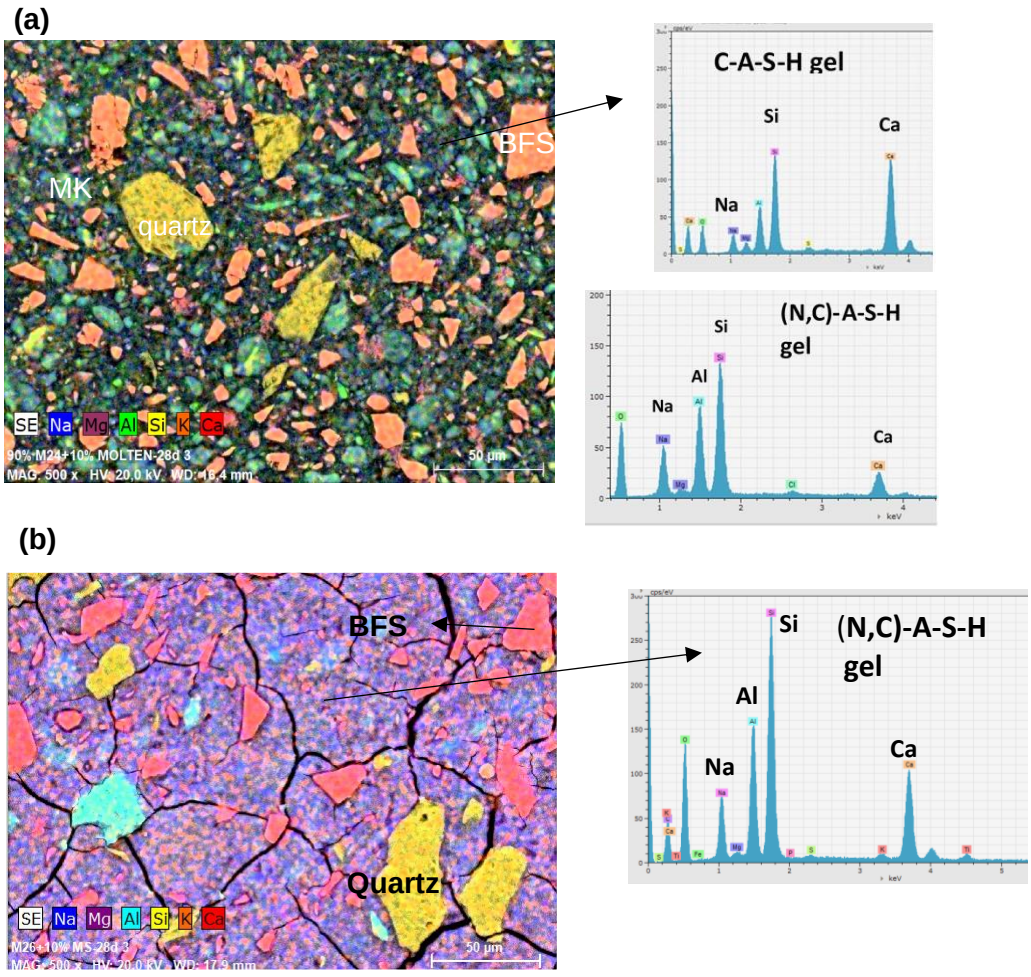

Figure 55. BSEM mappings of (a) GP-1+10 % MS and (b) GP-2+ 10 % MS (28 days of curing).

The deleterious effects of the incorporation of 30 % of MS on the microstructure are shown in Figure 58. BSEM mapping of GP-1+30 % MS (Figure 55(a)) shows that most of the EDX analysis corresponded with a (N,C)-A-S-H gel, where part of the Na has been replaced by a small amount of Ca. However, the BSEM image also shows the presence of big plates with a chemical composition based on Na and Ca, which can be associated with the precipitation of sodium-calcium carbonates (mainly gaylussite identified in the XRD, Figure 57) during the curing process. It seems that Ca^{2+} released during the dissolution of the BFS, reacts preferably with CO_3^{2-} anions and Na^+ cations, coming from the MS, precipitating this kind of carbonates. A detail of a representative micrograph of GP-2+30 % MS (Figure 58b) showed a massive formation of carbonates, in which the EDX analysis shows a chemical composition based mostly on C, Na and Ca. As shown in Figure 56, in GP-1+30 % MS practically all the points analysed correspond with a (N,C)-A-S-H gel, with a low content of calcium. It seems that Ca available in this system preferably reacts with carbonates as confirmed by the XRD analysis, which showed a massive precipitation of sodium-calcium carbonates hydrates. Specifically gaylussite $Na_2Ca(CO_3)_2.5H_2O$, pirsonite ($Na_2Ca(CO_3)_2.2H_2O$), thermonatrite ($Na_2CO_3.H_2O$) and trone ($Na_2CO_3.NaHCO_3.2H_2O$) were identified in GP-2 samples at 7 d. Gaylussite and trone have a molar volume of 148.8 and 108 cm^3/mol, respectively, which are much more higher than the molar volume of calcite (36.93 cm^3/mol) [17]. So, the formation of such a combination of sodium carbonate-based salts has an expansive behaviour, and is responsible for the high deterioration of the specimens. The deleterious effects of these expansive salts on the concrete products have been previously reported [18].

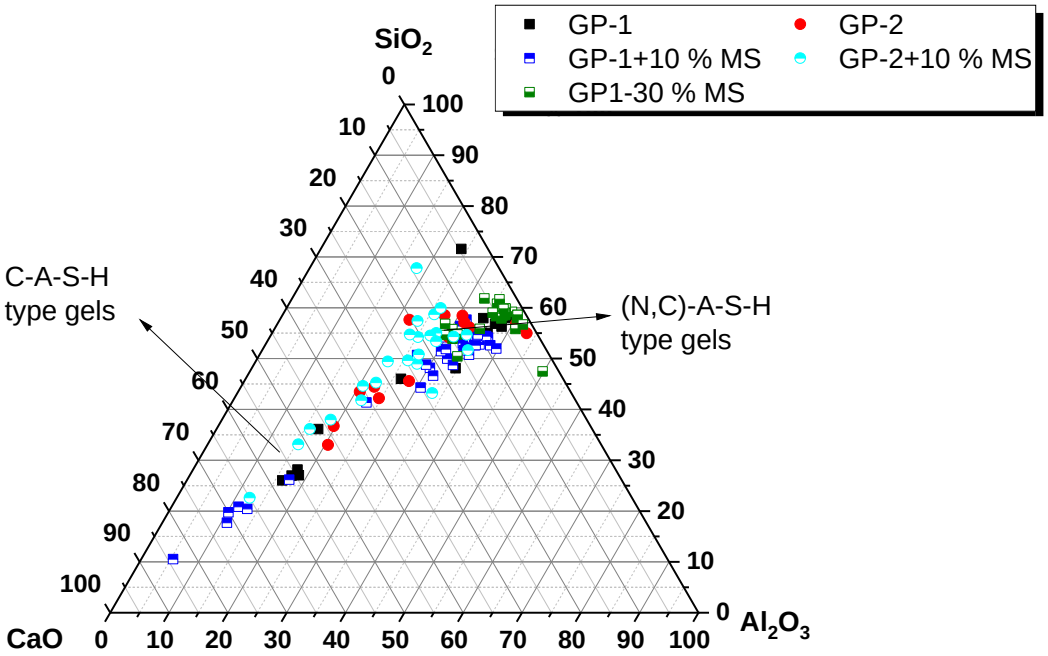

Figure 56. EDX analysis of the binding phase in the GP-systems without and with the MS RSOW.

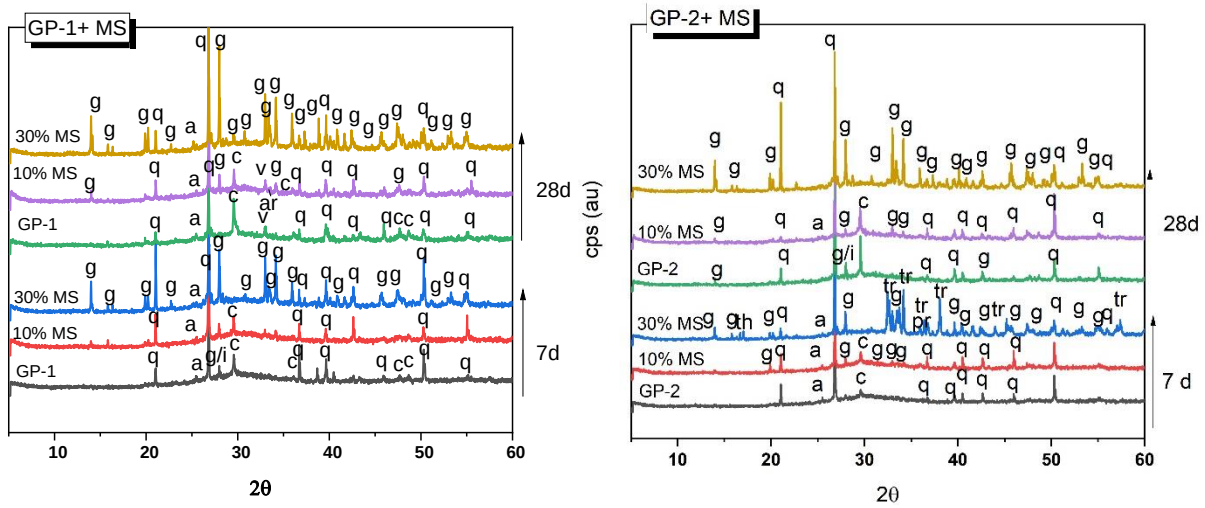

Figure 57. XRD patterns of the GP-1 and GP-2 systems after 7 and 28 days of curing (a) GP-1+MS (b) GP-2+MS. (Legend: q: quarzt (COD 1011172), a: anatase (COD 5000223) , i: illite (COD 9009665) , g: gaylussite (COD 9009890), pr (pirsonnite) (COD 90009889) tr: trone (COD 9007656), th: Thermonatrite (COD 9011153), c: Calcite (COD 7020139), v: Vaterite (COD 9016547), ar: Aragonite (COD 9014935).

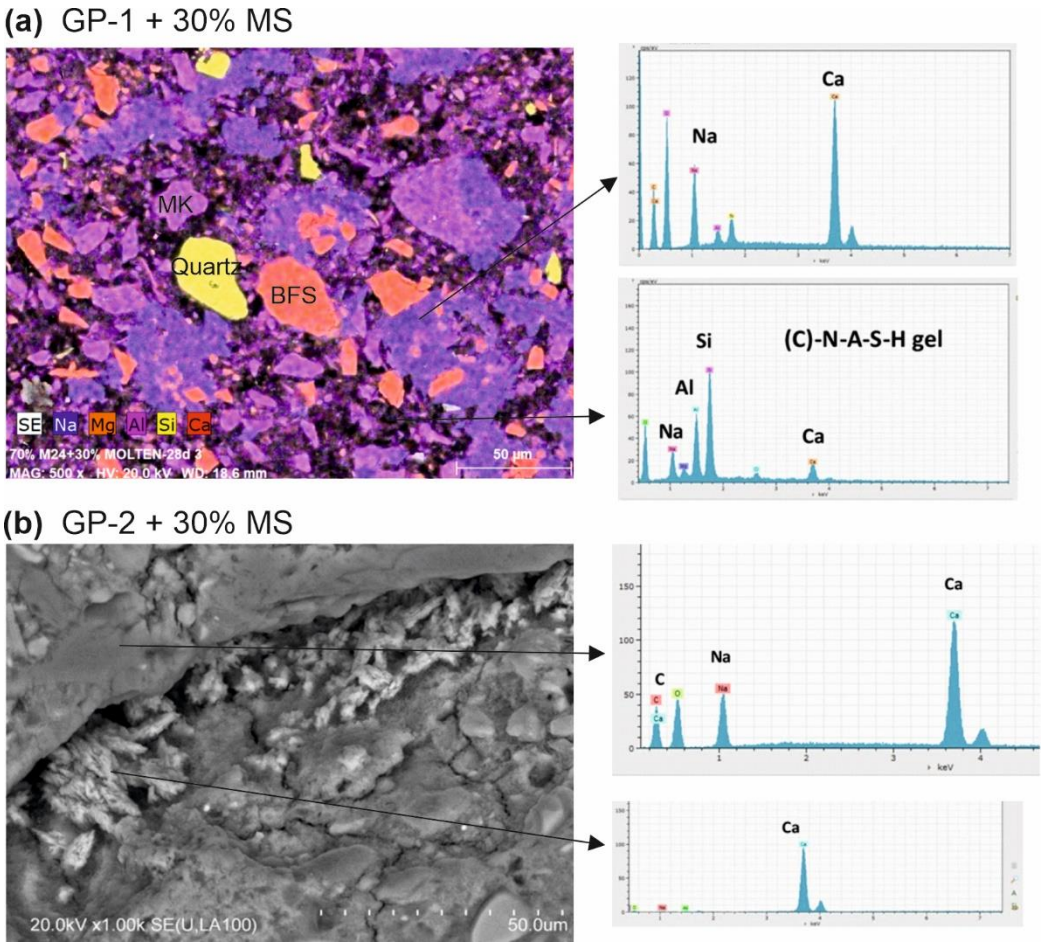

Figure 58. (a) BSEM Mapping of sample GP-1 + 30 %MS at 28d and (b) Detail of a micrograph of sample GP-2+ 30 % MS (x1000).

3.3.3.2 Portland cement-based matrices

Regarding the conditioning of the MS RSOW by PC systems, both CEM I and CEM III underwent a decrease on their compressive strengths, when 10 % of the MS is incorporated (Figure 59(a) and (b)); more remarkable in CEM I. Despite this, in both cases the mechanical strengths achieve the WAC limit for conditioning RSOW [13].

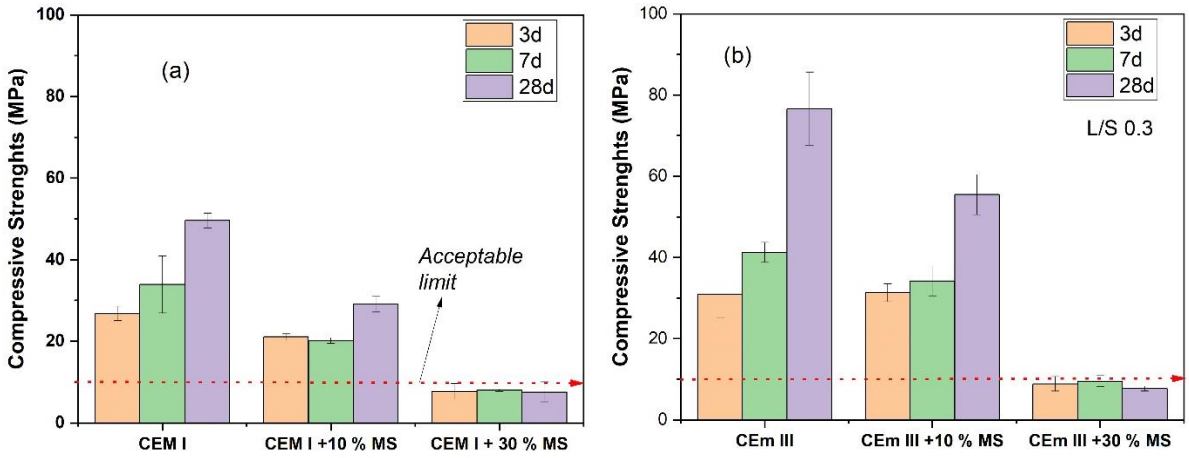

Figure 59. Mechanical strengths of (a) CEM I and (b) CEM III without and with 10 and 30 % MS.

PC-based systems also underwent some important issues when 30% of the MS was incorporated. Both CEM I and CEM III pastes with 30 % of MS, showed a dramatic decrease in the compressive strengths, dropping even under the 10 MPa considered as an acceptable limit for this type of application [13]. In this case, no further evolution in the compressive strengths with time was observed (at 28d samples are still under the 10 MPa). Measures of pH during the first hour of hydration of both PC showed a substantial increase in the pH upon the incorporation of MS (Figure 60), which was accompanied by a flash setting in CEM IIII+30 % MS after 10 min of hydration.

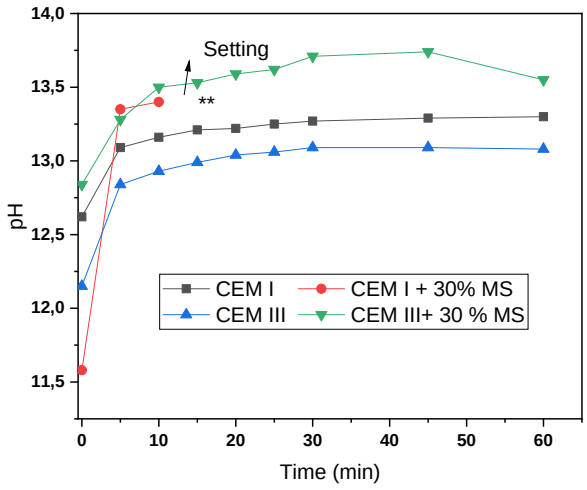

Figure 60. pH value in PC pastes without and with 20 % MS during the first hour of reaction.

To understand this behaviour, the kinetic of hydration was analyzed by isothermal calorimetry. Figure 61 shows a representative example of the effect of MS on the cement hydration of CEM I; further details can be found in our previous publication [12]. A new signal with a maximum located at 2.8 h appeared in both CEM I+10 % MS and CEM I+30 % MS systems (Figure 61(a)); this signal is mainly associated with the precipitation of calcium carbonates, whose early formation could occur from the reaction between CO_3^{2-} from the MS dissolution and Ca^{2+} dissolved from the surface of the cement

grains and that from the portlandite. CEM I+30 %MS showed two additional signals: one at 0.6 h related to the dissolution of the carbonates from the MS, and another of low intensity at 6.4 h associated with the precipitation of the PC hydration products. As a result of the very quick dissolution/precipitation of the carbonates, the cumulative heat curves showed a steeper exponential growth in the early hours; however, the total heat released after 10-12 h was substantially reduced with increasing the MS content (Figure 61(b)), indicating that the cement hydration has been shortened and/or inhibited.

The formation of calcium carbonate upon the incorporation of MS was confirmed by XRD analysis (Figure 62) and BSEM-EDX analysis (Figure 63). Figure 64 shows that, in both PC systems, the incorporation of the 30% MS increases considerably the total porosity (almost two times in the paste of CEM I, and three times in the paste of CEM III), and changes the pore size distribution, shifting the pore size diameter towards higher values; all this in good agreement with the decrease of the compressive strength (Figure 59).

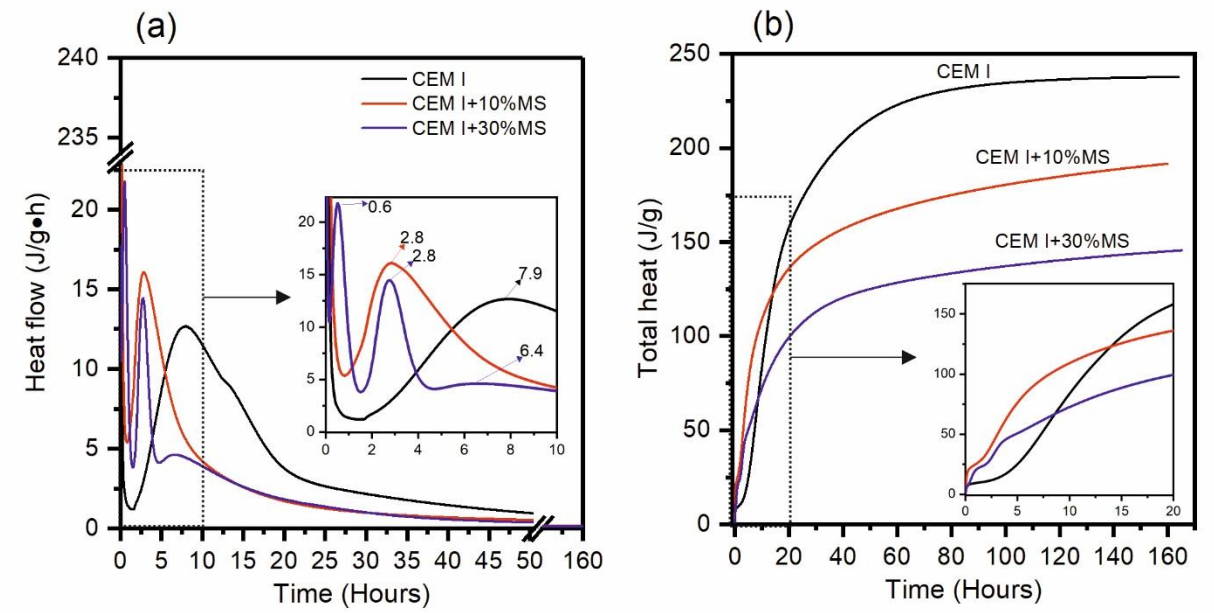

Figure 61. (a) Heat Flow and (b) Total Heat of CEM I with and without the MS waste.

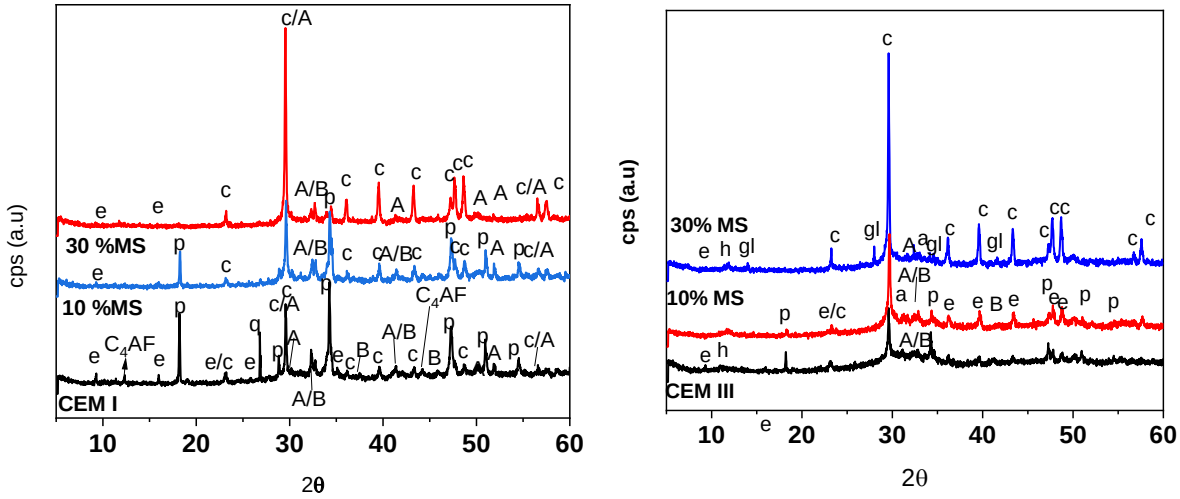

Figure 62. XRD patterns at 28 days of samples (a) CEM I and (b) CEM III, without and with 10 and 30 % MS. (Legend: c: Calcite ($CaCO_3$, COD 7020139); g: Gaylussite ($Na_2Ca(CO_3)_2 \cdot 5H_2O$, COD 9009890); p: portlandite ($Ca(OH)_2$, COD 1008780); e: ettringite ($3CaO \cdot Al_2O_3 \cdot 3CaSO_4 \cdot 32H_2O$, COD 9011103) A: Alite (C_3S, COD 1540704) B: Belite (C_2S, COD 9012793) C_4AF: Ferritic phase (COD 9015305); h: Hidrotalcite ($Mg_6Al_2CO_3(OH)16.4H_2O$; COD 9009272).

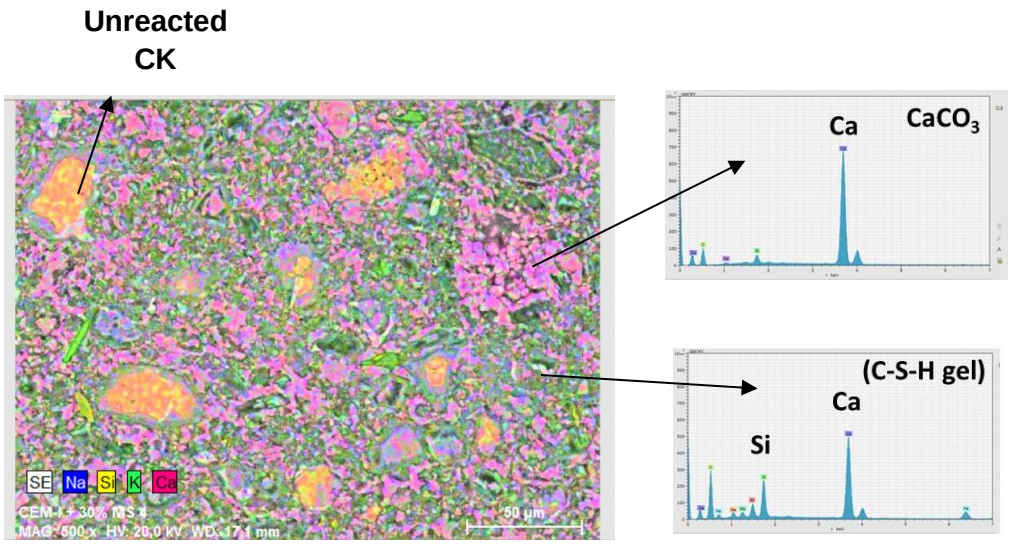

Figure 63. (a) Mapping of the sample CEM I + 30 %MS (b) EDX analysis of the binding phase (C-S-H gel) and $CaCO_3$ detected

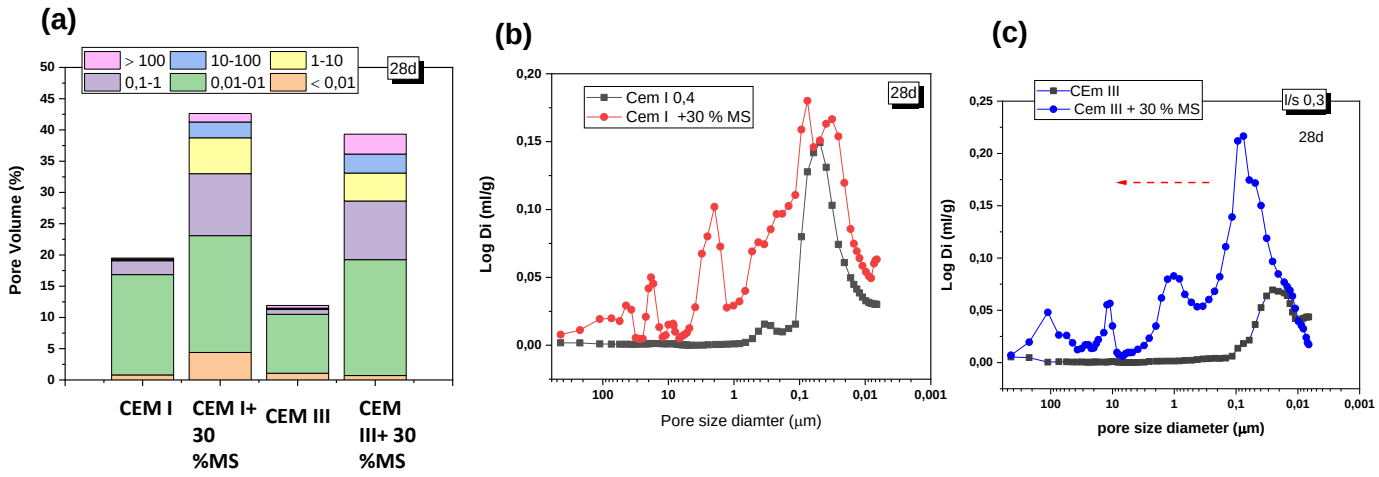

Figure 64. Changes in the microstructure analysed by MIP in the PC based systems (a) Total porosity (b) (c) Log DI vs pore size diameter (CEM I and CEM III) with and without 30% of the MS, after 28 days of curing

3.4 Conclusions

CSIC contribution highlights that each RSOW requires a specific confining cementitious matrix for an adequate and safe immobilization. Designing and developing any cementitious systems is going to be highly depended on the typology of the RSOW to immobilize it, being necessary a case-by-case assessment. The customization of the cementitious matrix, depending on the type of RSOW, will therefore be necessary to obtain a robust system. The future validation of the performance of the wasteform matrices at higher tailor-readiness level (scale-up) is fundamental.

Based on the CSIC results, the following technological conclusions and recommendations are given:

3.4.1 Conditioning of the thermally treated ion exchange resin RSOW

CSIC contribution highlights the significance of considering the composition of precursors and the concentration of alkaline activators when designing/developing geopolymer matrices for confining thermally treated ion exchange resins (IER). Taking this into account, geopolymer matrices can confine up to 30% (%wt) of IER. In Portland cement systems, the IER loading is limited to 20% to meet the waste acceptance criteria (WAC) of compressive strength of at least 10MPa after 28 days. Table 10 shows the geopolymer and Portland cement systems that achieve the WAC.

Table 10. One-part geopolymer and Portland cement matrices with acceptable WAC for conditioning the thermally treated ion exchange resin (IER) RSOW.

System	MK/BFS	%Na_2O	%IER	w/s ratio	28-day compressive strength
GPO+20%IER	1	9	20	0.30	45 MPa
GPO+30%IER	1	9	30	0.30	25 MPa
CEM I+20%IER			20	0.30	33 MPa
CEM III+20%IER			20	0.30	45 MPa

CSIC results also found that the performance of the Portland cement systems is very sensitive to the batch of the IER because slight changes in the calcination procedure of the IER can seriously affect the cement hydration due to changes in the acidic character of the waste, and thus the hardened properties of the final wasteform. The batch effect was not observed in the geopolymer matrices, which together with its higher capacity of confining IER, make them promising robust matrices for the immobilization of thermally-treated SIERs.

3.4.2 Conditioning of the untreated ion exchange resin RSOW

In the conditioning of the untreated ion exchange resins (UIER), Portland cement matrices perform differently and adjustments in the water/solid ratio are needed to achieve suitable workability of the fresh pastes. The performance of the selected one-part geopolymer was similar to that observed for conditioning the thermally treated ion exchange resins. Table 11 shows the geopolymer and Portland cement systems that achieve the WAC of compressive strength. CSIC results show that while the geopolymer matrices can be confined to up to 30% of UIER, the amount of this RSOW should be limited to up to 10% in Portland cement systems in order to avoid deformations and the collapse of the samples. So, the selected one-part geopolymer seems to be the best candidate for encapsulating this type of RSOW.

Table 11. One-part geopolymer and Portland cement matrices with acceptable WAC for conditioning the untreated ion exchange resin (UIER) RSOW.

System	MK/BFS	%Na_2O	%UIER	w/s ratio	28-day compressive strength
GPO+20%UIER	1	9	20	0.35	40 MPa
GPO+30%UIER	1	9	30	0.35	30 MPa
CEM I+10%UIER			10	0.35	40 MPa
CEM III+10%UIER			10	0.35	40 MPa

3.4.3 Conditioning of MS RSOW

Regarding the Molten salt (MS) waste, CSIC results show that this type of RSOW interacts completely different with the studied cementitious matrices. As the MS is mainly composed of sodium carbonate salts (alkaline nature), it could act as an extra activator, having positive or negative effects depending on the MS content and the composition of the cementitious matrix. Therefore, adjustments are needed in the cementitious matrices to achieve stable wasteforms. The geopolymer and Portland cement systems that achieve the WAC of compressive strength are shown in Table 12.

Table 12. One-part geopolymer and Portland cement matrices with acceptable WAC for conditioning the Molten Salt (MS) RSOW.

System	MK/BFS	%Na_2O	%MS	w/s ratio	28-day compressive strength
GP+10%MS	~1	~18.9	10	0.28	50 MPa
CEM I+10%MS			10	0.40	30 MPa
CEM III+10%MS			10	0.30	57 MPa

CSIC results show that the content of molten salt waste in both geopolymer and Portland cement-based matrices is limited to 10% of MS to obtain suitable mechanical and microstructural properties. The neutralization of the sodium carbonates from the MS with $Ca(OH)_2$ and other lines of action reported in the recent CSIC publication [12] could be explored to improve the conditioning of the MS RSOW.

3.5 Publications

JCR Papers:

- P. Perez-Cortes, I. Garcia-Lodeiro, F. Puertas, M.C. Alonso, “Effect of incorporating a molten salt waste from nuclear power plants on the properties of geopolymers and Portland cement wasteforms,” Cem Concr Compos. 142 (2023) 105210. https://doi.org/https://doi.org/10.1016/j.cemconcomp.2023.105210, (Q1, I.F.=10.5).

- P. Perez-Cortes, I. Garcia-Lodeiro, F. Puertas, M.C. Alonso, “Microstructural changes of the (N,C)-A-S-H gels after incorporating a thermally treated ion exchange resin radioactive waste,” In preparation.

Reports:

- Alonso, M.C., Puertas, F., Garcia-Lodeiro, I. & Perez-Cortes, P. “Milestone 41 Delivery campaign of the cement based materials samples, June, 28, 2022.

- Perez-Cortes, P., Puertas, F., Garcia-lodeiro, I., Alonso, M.C. (2023) “Immobilization of thermally treated ionic exchange resins in geopolymer matrices”, PREDIS Proceedings of May Workshop 2023, Mechelen, Belgium.

- Alonso, M.C., Puertas, F., Garcia-Lodeiro, I., Perez-Cortes, P. (2022) “Immobilization of the treated wastes by geopolymer or cement-based materials encapsulation”, PREDIS Proceedings of April Workshop 2022, Espoo, Finland.

- Torres, E., Marugán, E., Alonso, M.C., Garcia-Lodeiro, I., Puertas, F., Perez-Cortes, P., Fernández, R., Ruiz, A.I., Dieguez, M., “Physico-Chemical characterization of reconditioned waste form and stability testing”, PREDIS Proceedings of April Workshop 2022, Espoo, Finland.

Presentations in conferences

- CSIC, 4th PREDIS Workshop Meeting, May 22-26, 2022, Mechelen, Belgium.

- CSIC, 3er PREDIS Workshop Meeting, April 25-28, 2022, Espoo Finland.

- Puertas, F. “Immobilization of the solid wastes by cement-based and geopolymer materials”, PREDIS Overview: Innovations in Predis-disposal Radioactive Waste Management, June 10, 2022, On-line Course.

- CSIC, 3er intermediate WP6 PREDIS Workshop Meeting, October 4, 2022, on-line.

- I. Garcia-Lodeiro, F. Puertas, E. Torres, M.C Alonso, et al., “Encapsulation of simulate radioactive waste in cementitious systems”, NUWCEM 4th International Symposium on Cement-Based Materials for Nuclear Wastes May 04 to 06, 2022 Avignon.

- Perez-Cortes, P., Garcia-Lodeiro, I., Torres, E., Alonso, M.C. & Puertas, F., “Capability of traditional and geopolymer cementitious systems for the immobilization of a thermally treated ion exchange resin”, The 16th International Congress on the Chemistry of Cement 2023 (ICCC2023), September 18-22, 2023, Bangkok Thailand, accepted for presentation.

4 POLIMI's contribution: Encapsulation of treated wastes in tuff-based geopolymeric matrix

The conditioning of treated wastes consists of encapsulating them into a matrix to obtain the waste form, i.e., the system composed of the treated waste and the matrix, which should be endowed with stability and durability over time. The latter characteristics are influenced by many variables, including the combination of the properties of the treated waste, the matrix, and the properties of these two coupled materials [19].

4.1 Tuff-based geopolymeric matrix

To pursue the goals of durability of waste forms and sustainability of waste management strategy, along with the objectives of circular economy, POLIMI has developed a geopolymer matrix based on natural materials and industrial by-products. Specifically, the matrix is composed of:

- a micronized volcanic tuff (VT), rich in zeolites (Zeolite Fertenia™);
- ground granulated blast furnace slag (BFS);
- fly ash (FA).

Alumina and sodium hydroxide, both technical grade, are added to balance the Si/Al stoichiometric ratio and to activate the precursor, respectively. Grouts are activated by NaOH dissolved in water to obtain the desired workability [20]. A small amount of sodium silicate solution (35 wt.%, technical grade) is employed as well to provide the fresh grout with reactive Si-based species. The schematic representation of the synthesis of the geopolymeric matrix is reported in Figure 65.

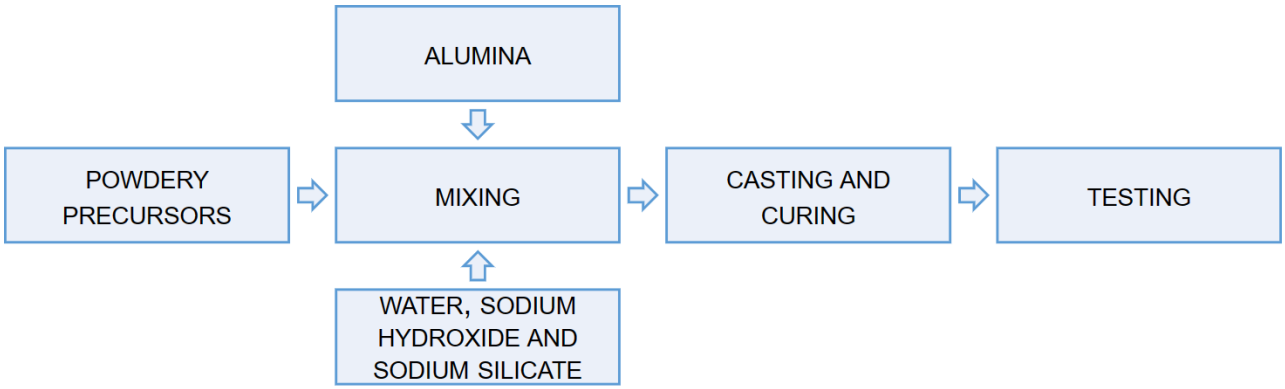

Figure 65: Scheme of the synthesis and testing of the tuff-based geopolymeric matrices.

The solid precursors and the activation solution are mixed in a planetary mixer for 5 minutes until the grout becomes homogeneous. Then it is poured in a mould and cured for a total period of 28 days. Different curing conditions have been investigated, as described below.

4.1.1 Investigation of the role of the zeolites in the matrix

To motivate the use of the volcanic tuff as a precursor for the synthesis of the geopolymeric matrix, besides its worldwide availability and its low environmental impact, a preliminary study was conducted to determine the cation-exchange capacity of this material. A literature overview showed that zeolites are effective trappers of chemicals species [21, 22], and chabazite, of which the VT is rich, is very effective in chelating Cs^+ ions, which are known to be very mobile [23, 24]. The investigation was performed using analytical-grade nitrate salts of Co, Ni, Sr, Cs, Nd, and Eu, because of their different chemical behaviour and the representativeness of the common activation and fission products.

The salts were dissolved in ultrapure water and contacted with the VT, and the supernatant was analysed via ICP-MS afterwards to assess the retention of the metal ions by the material. A second set of experiments was performed as a reference using metakaolin (Imerys), which is a typical precursor used for the synthesis of geopolymers. Selected cations turned out to fix from 20 % to 1100 % more in the VT with respect the metakaolin.

To understand whether zeolites in the VT can provide the geopolymeric matrix with effective binding capabilities for cations, their stability during the geopolymerisation reaction was investigated. XRD analysis on pristine VT and the geopolymers showed common peaks related to the zeolitic species (see Figure 66). Hence, zeolites are preserved during the synthesis of the matrix and can work as a chemical barrier to confine the mobile species in the waste, in addition to the physical barrier provided by the geopolymeric matrix itself.

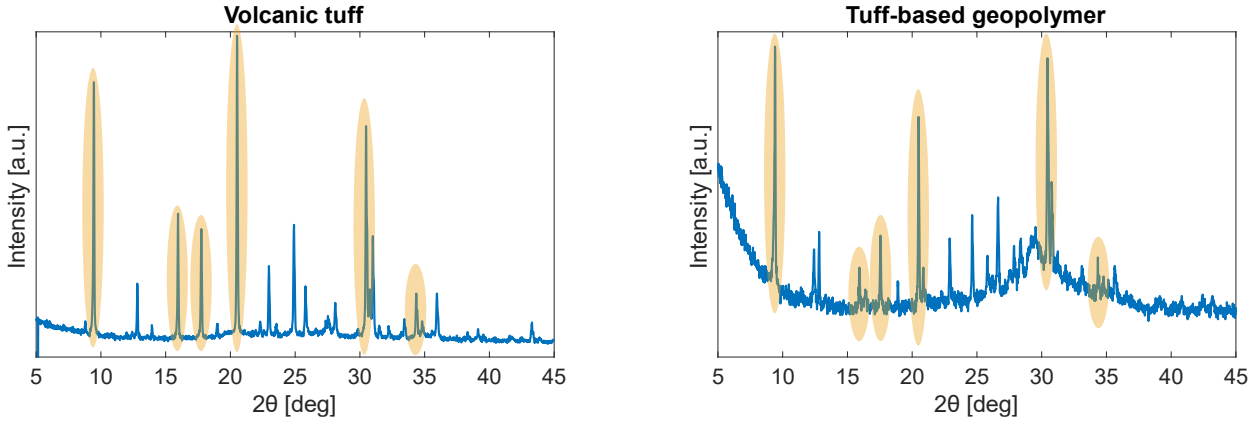

Figure 66: Comparison of VT and tuff-based geopolymer XRD.

4.1.2 Development of the tuff-based formulation

A set of samples with different composition of the raw materials was prepared to assess the most performant combination in terms of compressive strength and stability towards lixiviation in water [20]. The minimum requirements for the two tests were selected according to the Italian guide for conditioned low- and intermediate-level waste, namely 10 MPa at 28 days for the compressive strength and a leachability index of 6 (ANSI/ANS-16.1-2019 protocol) for matrix constituents and contaminants (especially Cs), concerning the stability towards lixiviation in water [25]. The screening of the different formulations allowed to set a reference recipe for the synthesis of the matrix, which is reported in Figure 67.

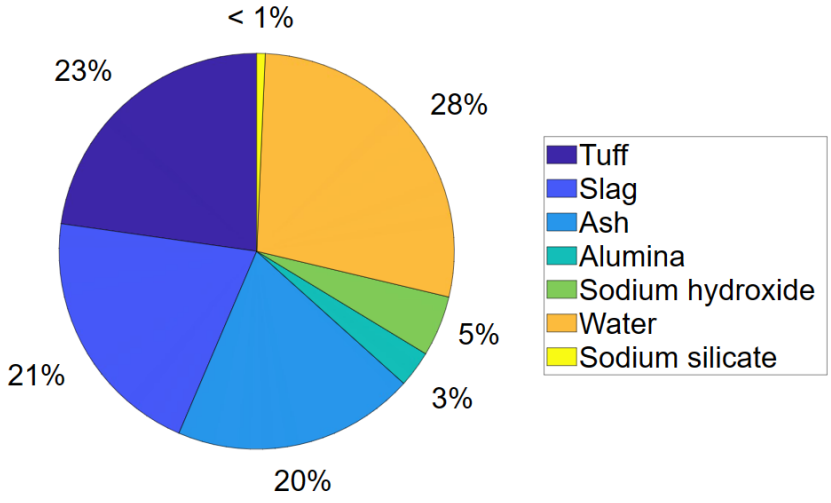

Figure 67: Composition of the tuff-based geopolymeric matrix.

A screening of the curing conditions followed. More specifically, three different environments were tested: (a) demoulding and in-air curing; (b) in-mould curing (endogenous conditions); (c) demoulding and curing in climatic chamber, at 22 °C ± 2 °C and > 90 %RH. The third environment proved to improve the mechanical resistance of the matrix and to increase its stability [20]. For this reason, it was chosen as the standard protocol for curing the matrix and the waste forms. The properties of the fresh and hardened pastes are reported in Table 13 [20]. Workability is measured with a flow table (BS EN 12350-5:2019 standard), while setting time was derived with a VICAT needle apparatus (BS EN 196-3:2016 standard). The compressive strength of the bare matrix is above 20 MPa. The formulation was tested with different BFS and FA and proved robust.

Table 13: Properties of the fresh and hardened tuff-based matrix.

Quantity	Value		Leachability indices	
Density	2.1 ± 0.1	g/cm^3	Na	7.3 ± 0.2
Workability	50 ± 5	%	Ca	12.6 ± 0.5
Initial setting	0.7 ± 0.1	h	Si	11.1 ± 0.3
Final setting	1.2 ± 0.1	h	Al	11.7 ± 0.3

4.2 Encapsulation of treated wastes

Within the Work Package 6 of the PREDIS project, POLIMI developed and tested the tuff-based matrix to encapsulate four different treated wastes:

- cation-exchange resins thermally degraded at POLIMI via oxidative pyrolysis;
- mixed-bed ion-exchange resins treated by Fenton-like wet oxidation at POLIMI;
- ashes of solid organic waste treated by the IRIS pilot plant managed by the CEA;
- residues of solid organic waste treated at CVŘež by means of molten salt oxidation (MSO).

The composition of the matrix is kept constant regardless of the waste, but the order of addition of the materials varies according to the waste to encapsulate, which can be added to the fresh grout before or after the activation of the latter. The tuff-based matrix exhibited remarkable versatility in encapsulating the different wastes up to significant loading factors. For the purposes of this document, the loading factor of a conditioned waste form is expressed as the ratio of the mass of the waste over the sum of the masses of the waste and the matrix.

4.2.1 Preliminary verification of compatibility with wastes

Prior to the full-scale encapsulation of wastes, a preliminary experimental campaign was conducted. The matrix stability was assessed in presence of some chemical species typically found in the treated wastes, namely sulphates and chlorides. Small cylindrical samples of tuff-based matrix were synthesised by loading the precursors with salts of Na and Sr, as reported in Table 14, and in-mould cured for 28 days. Grouts successfully hardened and proved stable towards one-month immersion in water, i.e., without crack formation, swelling, or dimensional changes as evidenced by visual inspection. Full-scale encapsulation of the wastes followed.

Table 14: Samples prepared for the preliminary verification of compatibility between treated wastes and the tuff-based matrix.

Sample ID	Loading
A	10 wt.% Na_2SO_4 + 10 wt.% $SrSO_4$
B	10 wt.% NaCl + 10 wt.% $SrCl_2$

4.2.2 Cation-exchange resins thermally degraded via oxidative pyrolysis

The oxidative pyrolysis process developed in the framework of Task 6.3 transforms cation-exchange resins into an inorganic, powdery material composed of oxides and sulphates of the cations fixed in the resin beads. Because of the high mass reduction achieved by the process and because of its level of development, there is scarce availability of treated residues to run conditioning tests, and the preparation of a surrogate residue was necessary. Hence, analytical-grade sulphates and oxides of a wide variety of metals, namely Fe, Co, Ni, Sr, Cs, were mixed to obtain a representative surrogate waste. Furthermore, lanthanides (e.g. Ce, Nd, Eu, Gd), Th, and U contained in ICP multi element standard solution were added in trace amounts.

Samples of tuff-based matrix loaded at 10 and 20 wt.% with the surrogate residue were synthesized by mixing the latter with the precursors prior to grout activation. Cubic samples of 5 cm were cast to assess the compressive strength of the resulting waste forms. Specimens were demoulded after seven days and completed the 28 days of curing in a climatic chamber with saturated humidity at the controlled temperature of 22 ± 2 °C. Pictures of the samples are reported in Figure 68.

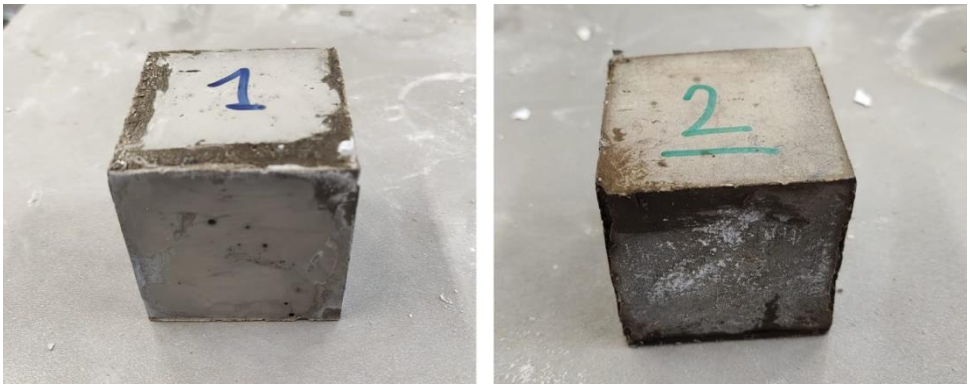

Figure 68: Examples of cubic specimens loaded with 10 wt.% (left) and 20 wt.% (right) of surrogate residues.

The encapsulation of the surrogate residue from oxidative pyrolysis did not compromise the properties of the matrix. Waste forms loaded at 10 and 20 wt.% exhibited minor losses in compressive strength with respect to the unloaded matrix, still meeting the Italian waste acceptance criteria (WAC) [25]. The investigation of greater loading ratios is being carried out in parallel with the assessment of the durability of the waste forms, to find the highest loading value satisfying the WAC.

4.2.3 Ion-exchange resins treated by Fenton-like wet oxidation

The treated waste downstream of the homogeneously catalysed Fenton-like wet oxidation developed in the framework of Task 6.3 comprises a sludgy residue rich in sulphuric acid, reported in Figure 69. Three different routes were tested to encapsulate such a sludge in the tuff-based matrix:

1. the sludge is directly mixed with the freshly activated geopolymeric paste;
2. the grout is synthesized with an excess of activator to cope with the acidity of the sludge, which is encapsulated afterwards by mixing it with the fresh paste;
3. the pH of the sludge is neutralized using sodium hydroxide prior to encapsulation in the matrix.

A fourth route was tested, which involves the synthesis of a metakaolin-based geopolymer activated with phosphoric acid and the subsequent encapsulation of the sludge in it. The matrix was composed as follows: 41 wt.% phosphoric acid (analytical-grade 40 wt.% solution, Fluka), 35 wt.% volcanic tuff, and 24 wt.% metakaolin (Imerys). Such a matrix was not characterized in detail, but its hardening was achieved and its resistance towards water immersion up to one month was experimentally assessed prior to its use with the sludge.

Figure 69: Sludge obtained downstream of the Fenton-like wet oxidation process.

Because of strong acid-base reactions occurring between the fresh paste and the sludge in the first two routes, the temperature of the fresh pastes increased excessively due to the uncontrolled development of heat. Hence, hardening of the matrices was compromised and the grouts did not set. The same unsatisfactory result was obtained with the encapsulation in the metakaolin-based geopolymer due to the reaction of phosphoric acid with sulphuric one, leading to very poor mechanical performances of the resulting waste form.

Encapsulation route number 3 allowed to obtain suitable waste forms. The neutralization of the sludge was performed one day before the conditioning operation, to dissipate acid-base reaction enthalpy. Cubic samples of 5 cm were cast to assess the compressive strength of the resulting waste forms. Specimens were demoulded after seven days and completed the 28 days of curing in a climatic chamber with saturated humidity at the controlled temperature of 22 ± 2 °C. Hardening of the waste forms was achieved up to 40 wt.% of sludge loading. The mechanical resistance was verified up to 20 wt.%: the compressive strength was reduced with respect to the bare matrix but met the Italian WAC (10 MPa). Besides, samples with loading factors greater than 20 wt.% did not prove stable towards water immersion as they showed evident cracks and swelling after few hours of immersion.

4.2.4 Ashes from the IRIS plant

The ashes obtained from the incineration of surrogate radioactive solid organic waste in the IRIS pilot plant comprise an inorganic material rich in aluminosilicates, thus compatible with the geopolymerisation. Such a waste was weighed and mixed with the powdery precursor prior to the activation of the paste. Small cylindrical samples at 10, 20, 30, 40, and 50 wt.% were prepared to preliminary assess the encapsulation of the waste. Afterwards, cubic samples of 5 cm loaded at 10 and 20 wt.% were cast to assess the compressive strength of the resulting waste forms. Specimens were demoulded after seven days and completed the 28 days of curing in a climatic chamber with saturated humidity at the controlled temperature of 22 ± 2 °C. Higher loading factors could not be tested in detail yet because of the limited availability of the treated waste.

The compressive strength does not appreciably vary with increasing loading factor up to 20 wt.% and remains above the WAC set by the Italian regulator [25]. Conversely, the density of the conditioned forms slightly decreases with increasing waste loading (of about 7% with 20 wt.% loading), while setting of the matrix is significantly delayed. Indeed, both initial and final setting times for fresh pastes loaded at 20 wt.% increase of about six times [20]. Specimens loaded at 10 and 20 wt.% with the IRIS ashes proved stable towards immersion in water up to one month. Indeed, the specimens did not show crack nor swelling formation and the leachability index of matrix constituents resulted above 6 [20]. Pictures of the immersed samples are reported in Figure 70.

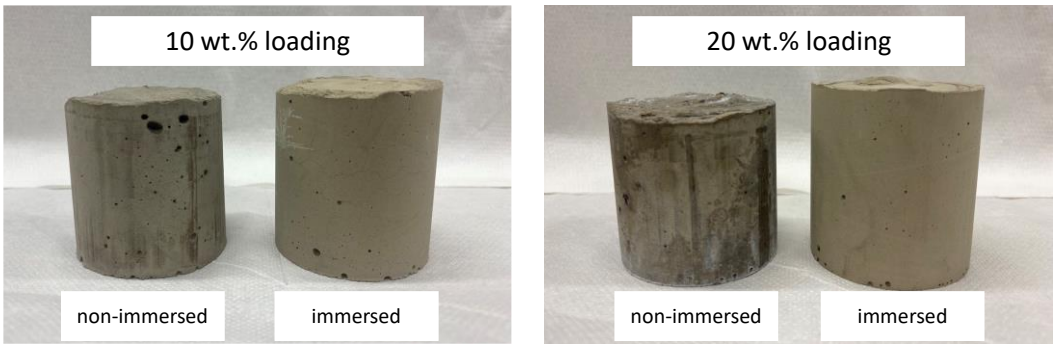

Figure 70: Cylindrical specimens, immersed and non-immersed, loaded with 10 and 20 wt.% IRIS ashes.

4.2.5 Residues from molten salt oxidation (MSO)

The MSO process run at CVŘež degrades the organic waste into a mixture of carbonates. Such residues proved challenging to encapsulate in the tuff-based geopolymeric matrix as they stand. They have been blended prior to encapsulation in the matrix to break the agglomerates and obtain a finer powder, and then added to the geopolymer precursors and mixed with them; activation of the grout followed.

A preliminary test was performed at 25 wt.% waste loading on a small cylindrical sample, achieving hardening of the form and its stability towards water immersion for one month. Subsequently cubic samples of 5 cm and cylindrical ones (diameter and height of 3 cm) loaded at 15, 25, and 35 wt.% were cast to provide more details about the compressive strength and the immersion stability. Specimens were demoulded after seven days and completed the 28 days of curing in a climatic chamber with saturated humidity at the controlled temperature of 22 ± 2 °C. The compressive strength drops with MSO waste loading factor above 15 wt.% and the Italian WAC is not met [25]. Because the MSO waste is mainly constituted of sodium carbonate, the reasons for such a behaviour could be the hydration of carbonate phases, which have an unstable volume and cause internal stresses in the waste forms. Further experimental confirmation is ongoing. Conversely, visual inspections confirmed that waste forms loaded up to 25 wt.% are stable towards one month of water immersion, while the 35 wt.% sample did not withstand 1 hour of immersion.

4.3 Ongoing activities

Some experimental activities are still ongoing to complete the task.

Concerning the tuff-based matrix development, the ongoing activities aim at replacing as much BFS and FA as possible in the recipe with materials for which there is less concern about availability-related aspects, while preserving the sustainability and the performance of the formulation.

Regarding the encapsulation of the treated wastes, further activities are ongoing to explain some observed behaviour or to improve some results (e.g., the waste loading factor). For example, investigation of the waste-matrix interactions is ongoing to comprehend the durability of the waste forms containing residues from homogeneous wet-oxidation treatments. Moreover, some trials are ongoing to encapsulate the residues from heterogeneous wet-oxidation treatments. In the next months, further attempts will be made to successfully encapsulate MSO residues in the tuff-based geopolymer.

5 SCK CEN Contributions

Some radioactively contaminated solid organic waste streams are problematic to dispose of by direct immobilization in known matrices (e.g. cementitious binders), as they can potentially degrade after disposal, possibly resulting in the release of radionuclides. Within work package 6 of the PREDIS project, techniques for the treatment and disposal of these waste streams are investigated [26]. One of the possible ways of treatment is the molten salt oxidation (MSO) process, in which the bulk of the organic waste can be oxidized at a high temperature in the presence of a sodium carbonate salt [27]. The residue after the MSO process is a salt containing radionuclides in a carbonate form. The goal of this study is to investigate whether it is possible to immobilize this salt residue in an alkali-activated or blended cementitious matrix which has good mechanical properties while showing good long-term durability. Initial experiments with direct mobilization of the salt into these matrices has shown that the hygroscopic minerals contained within the salt pose significant issues with regard to shrinkage and expansion under variable humidity and temperature. Therefore, the salt will first be pretreated to increase the compatibility with its matrix. After ensuring good mechanical properties, thermodynamic modelling of the system is performed to understand the stability of the salt-related phases.

5.1 Methods

5.1.1 Characterization of salt residue

Initial characterization of the salt revealed it to be highly waterlogged at a water content of 60 wt.% after drying at 100°C. In order to improve reproducibility of the tests, the salt was air-dried, after which the residual water content was approximately 16 wt.%. Detailed characterization of the air-dried salt revealed it to consist of different hydration states of sodium carbonate (Na_2CO_3), with thermonatrite ($Na_2CO_3.H_2O$) being the most dominant. Additionally, trona ($Na_2CO_3.NaHCO_3.2H_2O$) occurred in addition to small quantities of natron ($Na_2CO_3.10H_2O$) and gaylussite ($Na_2Ca(CO_3)_2.5H_2O$).

5.1.2 Pretreatment of salt residue

As initial experiments revealed that direct immobilization of the salt was ineffective due to the strongly hygroscopic nature of sodium carbonate, a pretreatment was necessary. As sodium carbonate is highly soluble, a double displacement reaction to form the insoluble calcite ($CaCO_3$) was proposed to be an effective way to improve the compatibility with the cementitious and alkali-activated matrices. A number of possible reagents exist, such as $CaCl_2$, $Ca(NO_3)_2$ and $Ca(OH)_2$. The former two were found to be ineffective as they either introduce new complications to the waste form (chloride attack in case of $CaCl_2$), or negatively impact the properties of the waste form (in the case of $Ca(NO_3)_2$). $Ca(OH)_2$ was therefore chosen as a reagent, with an additional benefit that the reaction (shown below) produces NaOH, which acts as an activator for the precursor of the alkali-activated matrices.

$$Ca(OH)_2 + Na_2CO_3.xH_2O \rightarrow CaCO_3 \downarrow + 2NaOH + xH_2O$$

The pretreatment was tested in two ways. Firstly, $Ca(OH)_2$ and the salt residue were both mixed together in water for three days (P1). Secondly, the salt residue was slowly added to a $Ca(OH)_2$ suspension over the course of three weeks (P2), to allow a more gradual reaction between both components, to prevent an overly Na-rich environment due to the low solubility of $Ca(OH)_2$.

5.1.3 Preparation of waste forms

After pretreatment, the resulting sludges were incorporated into either an alkali-activated or blended cementitious matrix. Waste loadings, expressed as the weight percentage of air-dried salt residue relative to the total mass of the waste form, varied from 10 to 20 wt.% in case of the alkali-activated matrices and 10 to 14 wt.% for the cementitious matrix. The fresh waste forms were cured in humid conditions (100% RH, room temperature) for 28 days to ensure that the waste form can withstand high humidities.

Table 15. Details of the recipes used for the immobilization of the molten salt residue. Abbreviations are as follows: BFS = blast furnace slag; MK = metakaolin; LF = limestone filler; L = limestone; LS = limestone sand; SF = silica fume; SCM = supplementary cementitious material.

Recipe	Activator/SCMs	Precursor/Binder	Waste Loading (wt%)
AAS	$Na_2O.2SiO_2$	BFS	10 – 20
CEM	BFS, LF, L, LS, SF	OPC (CEM I)	10 – 14

The waste forms were characterized by X-ray diffraction. Thermodynamic modelling was performed using HP Geochemistry.

5.2 Results

Both the alkali-activated slag and blended cementitious waste forms showed good mechanical properties after 28 days curing, with the compressive strength of AAS at 42 and 37 MPa (for 10 and 20 wt.% waste loading) and 15 MPa for the CEM waste forms (for both 10 and 14 wt.% waste loading). The samples also did not show any signs of bleeding or efflorescence, proving their good resistance to high humidity environments. Mineralogical characterization of the waste forms (**Figure *71***) revealed that, in both cases, all the sodium carbonate species had reacted away. Instead of everything transforming into calcite, an important crystallization of gaylussite was also observed. The crystallization of gaylussite was found to be more prominent relative to the amount of calcite formed in case of pretreatment P1, in which $Ca(OH)_2$ and the salt residue were directly mixed.

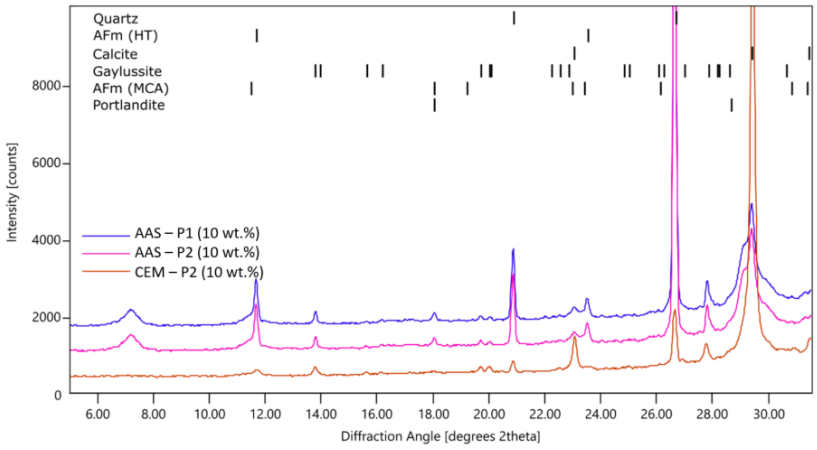

Figure 71. XRD analysis of the waste forms containing 10 wt.% of salt residue. P1 and P2 indicate the type of pretreatment.

To understand the mechanism behind the formation of gaylussite, thermodynamic modelling was performed. In a simulation of pretreatment P1, it was found that, in the case only a small amount of $Ca(OH)_2$ (or portlandite) is in solution, gaylussite will be the preferred phase to precipitate due to the sodium rich nature of the solution. As more Ca comes into solution, calcite will be more stable. By

contrast, a simulation of pretreatment P2 revealed that gaylussite should never be stable, as the gradual addition of salt to a Ca-rich suspension ensures the stability of calcite.

The observation of gaylussite in the P2 waste forms can attributed to the fact that, after pretreatment, the sludges are mixed with other phases, i.e. the binder, activator, SCMs, … which can affect the stability gaylussite. In the case of the AAS waste form, the addition of $Na_2O.2SiO_2$ as an activator ensures that the system contains sufficient sodium for gaylussite to be thermodynamically stable. In the case of the CEM waste form, no additional source of sodium is added, so the continued presence of gaylussite can best be understood as that of a metastable phase, which will on the long term react with the available $Ca(OH)_2$ to form additional calcite crystals.

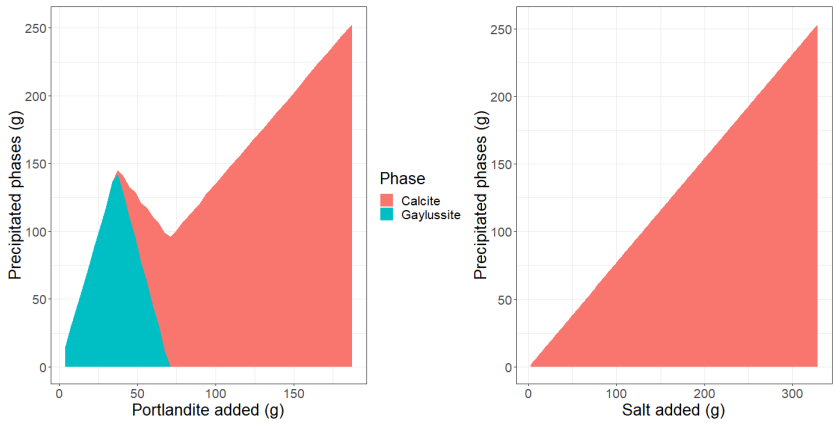

Figure 72. Thermodynamic simulation of the precipitation of calcite and gaylussite during the pretreatment. The diagram on the left simulates pretreatment P1, while the one on the right simulates pretreatment P2.

5.3 Way forward

This study has shown that it is possible to design both cementitious and alkali-activated matrices which are able to retain a highly hygroscopic sodium carbonate salt after pretreatment. The waste forms showed good mechanical properties which are unaffected by changes in temperature or humidity. The pretreatment was effective in eliminating all hygroscopic sodium carbonate from the system, although an intermediary Na-Ca carbonate phase, gaylussite, was still present. Through thermodynamic modelling, its presence can best be explained by the low solubility of $Ca(OH)_2$ artificially creating a high-sodium rich environment in which gaylussite is more stable than calcite, combined with the additional contribution of Na from the sodium disilicate used as an activator in the AAS waste form.

Now a set of stable waste forms has been attained, durability tests are being performed, which include carbonation resistance experiments, leaching experiments and alkali-silica reaction experiments. Preliminary results of the carbonation tests have shown that the structure of the waste forms is not significantly impacted by exposure to CO_2. Leaching of the alkali-activated waste forms in a basic solution for 3 months has shown that leaching is low for most elements with the exception of Na, which shows a high initial runoff in the first days of leaching, which is unsurprising due to the Na-rich nature of both the salt residue and the activating solution used in the preparation of the waste form.

6 VTT, University of Helsinki contributions

VTT has focused immobilization testing on gasification ash product (D6.1), specifically that produced from ion exchange resin. These resins are taken as a representative material for solid organic low and intermediate level waste (LILW) in Finland, and their gasification is primarily for the purposes of volume reduction prior to immobilization. While immobilization has been performed primarily on such ash, a limited set of samples were also produced with un-gasified resin for comparison. Likewise, while immobilization matrices have been primarily geopolymer-based binders due to their better performance as reported in EU-THERAMIN, a limited set of samples were also produced with ordinary Portland cement (SR sementti, Finnsementti) for comparison. Geopolymer precursor materials consisted of three types of metakaolin of varying reactivity (Metastar, Argical, and MK40), one of which is identical to that previously used in EU-THERAMIN (Metastar). Geopolymer activator consisted of a 10 M mixture of sodium silicate and potassium hydroxide solutions, equivalent to that used in EU-THERAMIN. Gasification ashes consisted of two types, with and without iron added to the un-gasified resin (8% by weight), both of which were doped with Cs, Eu, and Ce tracers for study in leaching experiments. Resulting ashes were included in amounts of 15% and 50% by weight (precursor replacement) in Argical-based geopolymers, while un-gasified resins were included at the 15% level. A limited set of samples were also produced with Cs, Eu, and Ce tracers added in the mixing water during geopolymer immobilization, rather than in the ash, using a “blank” ash produced in a similar gasification process from similar but un-doped resin. Lastly, samples with 15% inclusion of gasified operational waste (very low level organic mixed waste) were produced; these were discarded, due to the metallic aluminum content (and associated gas generation) making the waste product material unsuitable for immobilization in alkaline binder systems.

6.1 Results and discussion

Geopolymers with differing types of metakaolin were optimized to have similar workability, such that waste loading would not unduly change their consistency. Mixture proportions were adjusted such that the liquid-to-solid ratio (w/s, Figure 73) varied depending on precursor type, to attain a diameter of 125 mm during spread testing. These paste proportions were then used to create mortars using standard sand (1:2 paste:sand), for provision to leaching and post-mortem characterization tests carried out by both VTT and University of Helsinki.

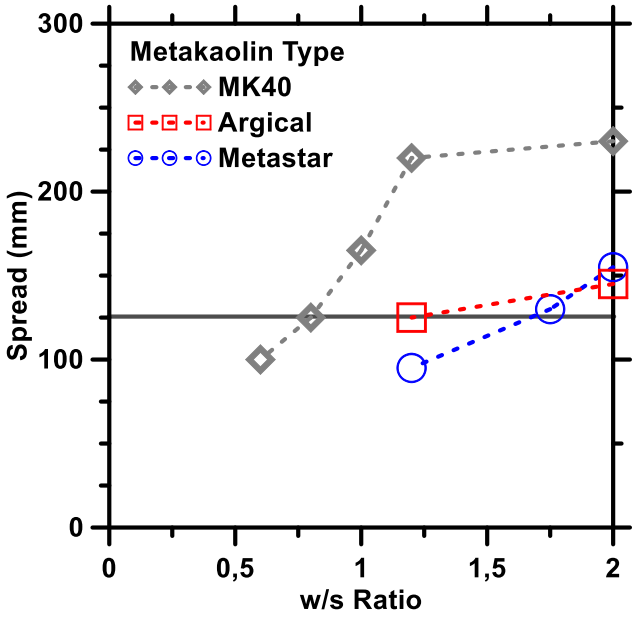

Figure 73. Spread tests of the three types of metakaolin-based geopolymers for varying liquid-to-solid ratios (w/s), illustrating how mixture proportions were selected.

6.1.1 Effect of waste loading on wasteform stability

Mechanical testing (compressive strength, Figure 74) was used as a first indicator of wasteform stability. A series of geopolymers were made using representative gasification ash (no tracers), and it was determined that loading up to 50% (by weight) was feasible while still maintaining adequate strength. For comparison, inclusion of Cs, Eu, and Ce tracers at a concentration of 1000 ppm in the mixing liquid (not doped into the ash itself) appeared to produce a further moderate reduction in strength. This provides an initial indication of the potential of these elements (and radionuclide analogs) to induce structural changes to the geopolymer matrix.

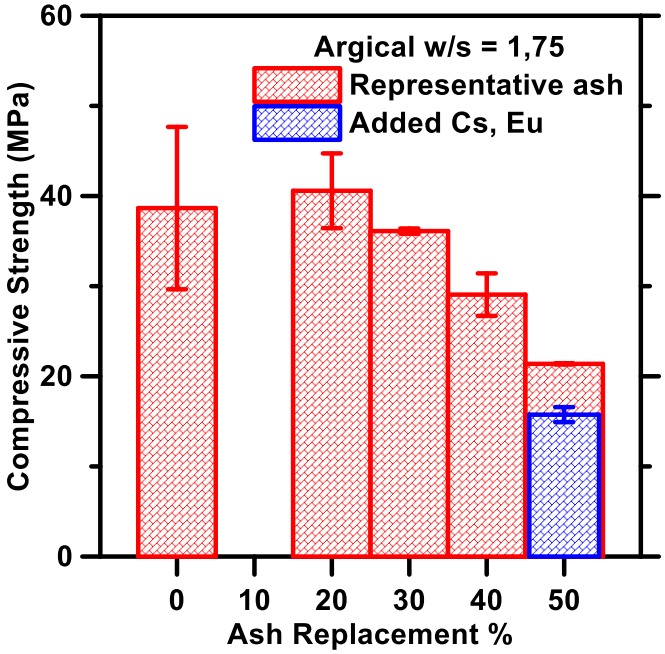

Figure 74. Compressive strength results as a function of ash waste loading.

For the un-gasified resin, reported in EU-THERAMIN to be limited to 15% inclusion, a comparison was also made between various waste types (Table 17). It can clearly be seen that for gasified wastes geopolymer matrixes exhibit superior binding capacity to cements, even in the case of gasified operational waste (high porosity due to gas production from intermixed metallic aluminum). For the un-gasified resin however, there is a strong dependence on the moisture content of the material. Lower compressive strength in the case of cement for resin conditioned to 50% relative humidity suggests absorption of water and consequent reduction in degree of hydration, while a similar trend for the resin conditioned to 95% relative humidity in geopolymers suggests water release and dilution of the activator solution (i.e., hindering activation). This highlights that with appropriate conditioning of resin moisture, there may be opportunities for improving wasteform performance even without gasification, and in fact for cement-based matrices this appears to be the best performing formulation (by compressive strength), although long-term durability in this case likely still presents risks.

Table 16. Compressive strength values (MPa) for various wastes compared between the cement and geopolymer mortars at 15% replacement of binder (by weight).

	Gasification ash (representative)	Resin (50% RH)	Resin (95% RH)	Gasified operational waste
Cement-based mortar	16,52	8,77	32,25	12,52
Geopolymer-based mortar	39,83	28,98	8,36	20,02

6.2 Conclusions and future work

Using compressive strength as an initial indication, cement and geopolymer formulations were demonstrated to maintain adequate mechanical stability for immobilization of both gasified and un-gasified ion-exchange resin. Additionally, results provide an initial indication that significant changes in geopolymer structure may be induced by low concentrations of tracer elements (during activation), potentially relating to alterations that will be observed during leaching. The beneficial influence of relative humidity conditioning on un-gasified waste immobilization was also shown to be a potential alternative to gasification for improved performance in cement-based matrices. Samples have been provided to connected work in physico-chemical characterization before and after leaching, which will be presented in more detail in deliverable report D6.6. Final report on Physico – chemical characterisation, to be published in summer 2024.

7 CEA Contribution: Conditioning of ashes from the thermal treatment by molten glass coating

The objective of this task is to demonstrate the immobilization of the ashes coming from the IRIS process [28] by Molten glass coating.

The process consisted of the implementation of a coating technique using molten glass to get an effective binder, resistant and allowing high waste loadings, to obtain a monolithic waste form (laboratory scale samples).

Characterisations of the reconditioned waste have been achieved by the determination of the microstructure at different scales. The waste loading was also a key point targeted to reach the optimum level versus the quality of the encapsulated material.

7.1 Description of the process

The process consists of doing a complete coating of the ashes at low temperature (< 900°C) using a specific glass formulation in order to encapsulate the ashes inside the glass. The idea here is to use low temperature melting glass, in order to avoid the volatilization of radionuclides and to get a monolithic form.

A specific glass frit having a very low melting temperature is selected (< 900°C). Various morphologies of the glass adjuvant and the ashes, and various mix ratios (from 20 to 80) have been tested to assess the best way of shaping (Figure 75).

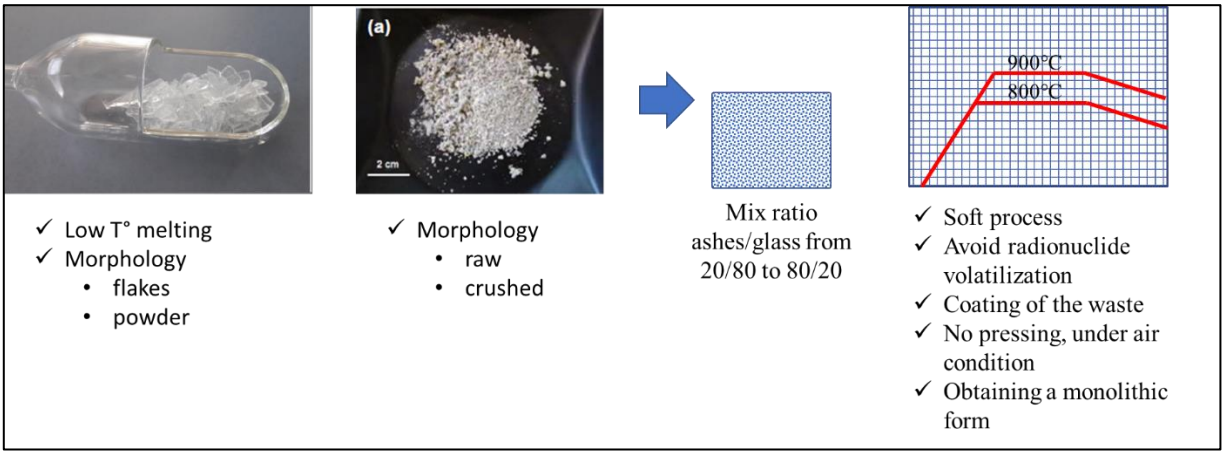

Figure 75 Description of the encapsulation process

The selected glass frit is a very simple composition made of silica, boron and sodium. One composition has been chosen in relation with its viscosity behavior as a function of temperature. The target is to use a glass that is able to soften at low temperature, namely around 800 degrees (Figure 76).

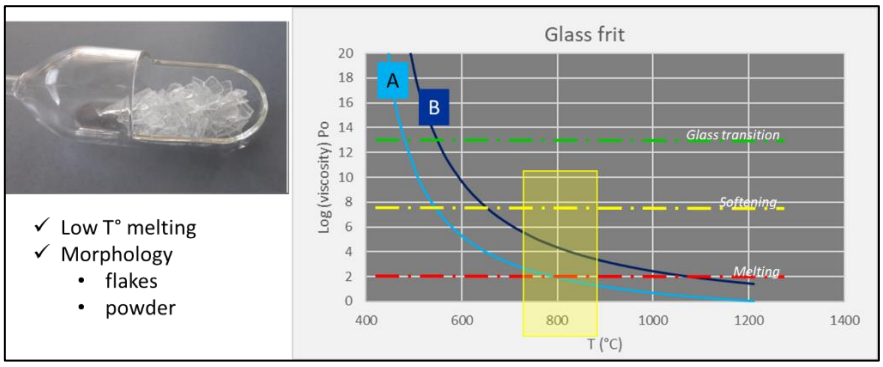

Figure 76 Viscosity variation of selected glass frit with temperature

7.2 Molten glass coating tests

Screening tests by varying the ratio of waste to glass have been achieved. The aim is to select the best material morphology and treatment temperature.

Visually, the best results in terms of homogeneity are reached with crushed glass and ash weight load up to 40%. Above 40% of load, the ashes are not well coated and so they won't be retained by the matrix

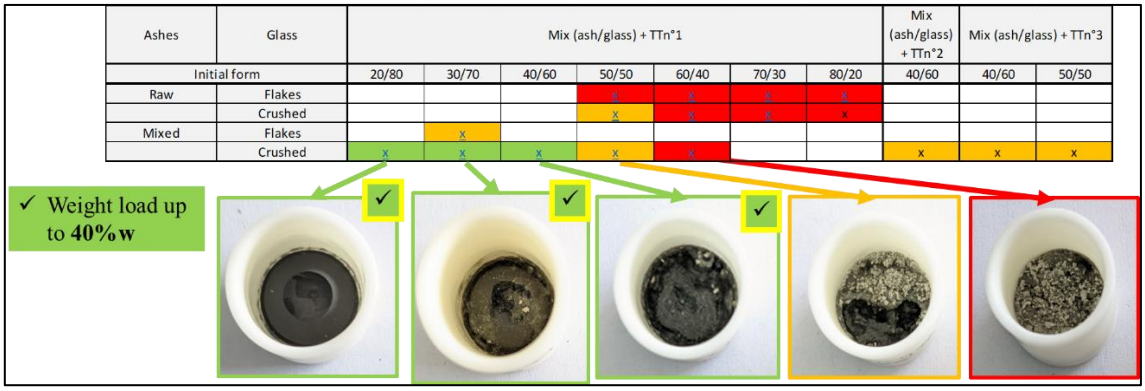

Ashes	Glass	Mix (ash/glass) + TTn°1							Mix (ash/glass) + TTn°2	Mix (ash/glass) + TTn°3	
Initial form		20/80	30/70	40/60	50/50	60/40	70/30	80/20	40/60	40/60	50/50
Raw	Flakes				x	x	x	x			
	Crushed				x	x	x	x			
Mixed	Flakes		x								
	Crushed	x	x	x	x	x			x	x	x

Figure 77 Molten glass screening tests

7.3 SEM characterizations

Glass microstructure observations of the encapsulated waste have been achieved.

In the 40% load sample, we observe some millimetric bubbles included into the glassy matrix. Many crystals are imbedded inside these bubbles and also distributed everywhere inside the glassy matrix (Figure 78).

The matrix is mainly composed of silicon, sodium, aluminium and Ca.

The crystals are mainly made of P, Na and Ca.

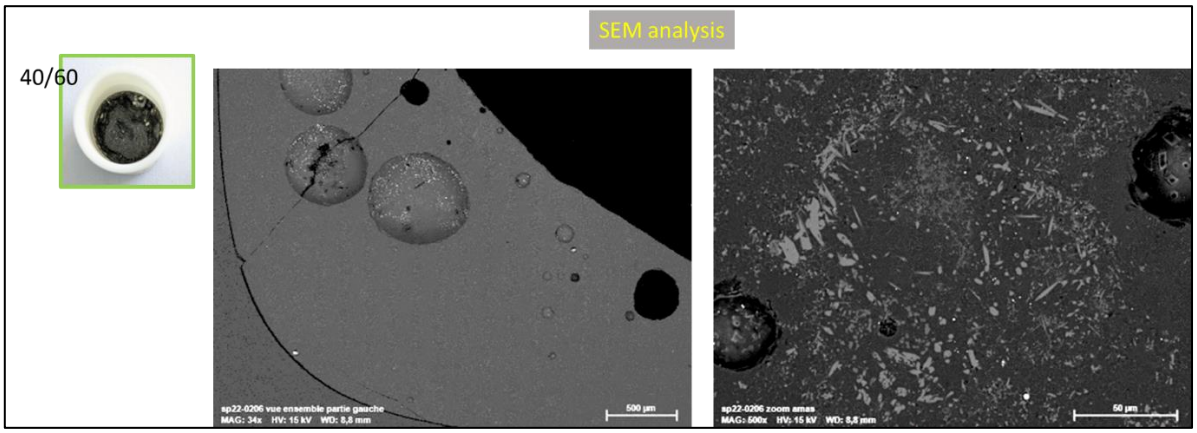

Figure 78 SEM observation of the 40% load molten glass

Less bubbles are observed in the 30% load and the crystalline phases are more regularly distributed inside the glass matrix (Figure 79). No crystals are observed inside the bubbles.

The glass matrix is also composed of silicium, sodium, aluminium and Ca

The crystals are mainly made of P, Na and Ca.

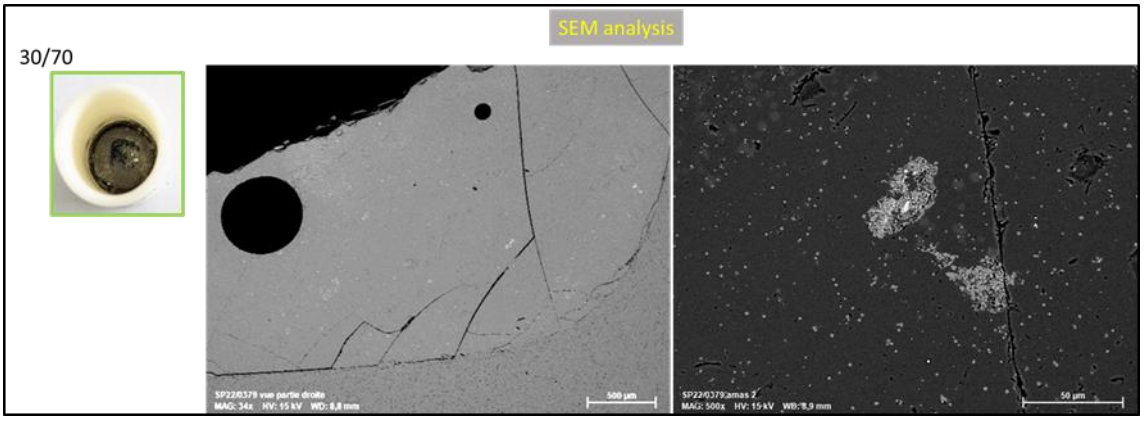

Figure 79 SEM observation of the 30% load molten glass

The 30% loaded molten glass coating appears to be the optimum in terms of waste encapsulation by the glass.

This material has been chosen for the leaching test evaluations.

8 University of Sheffield Contribution

These data are collected from presentations of virtual and face-to-face meetings.

8.1 Conditioning of Ashes from IRIS

Figure 80: From left to right: Iris ashes, Empty HIP can, Packed Can with 16 g ash with a hydraulic press

- No treatment for the ashes received from CEA
- Trial test for viability determination
- **X-ray diffraction:**
    - Very crystalline
    - Lots of overlapping features
    - Identified phases not certain
- As received ash:
    - Anorthite (CaAl2Si2O8)
    - Diopside (MgCaSi2O6)
    - Willemite? (Zn2SiO4)
- HIP material:
    - Anorthite (CaAl2Si2O8)
    - Diopside (MgCaSi2O6)
    - Spinel (‘MgAl2O4’ – AB2X4)
    - Zn, Fe, Cr substitutes likely

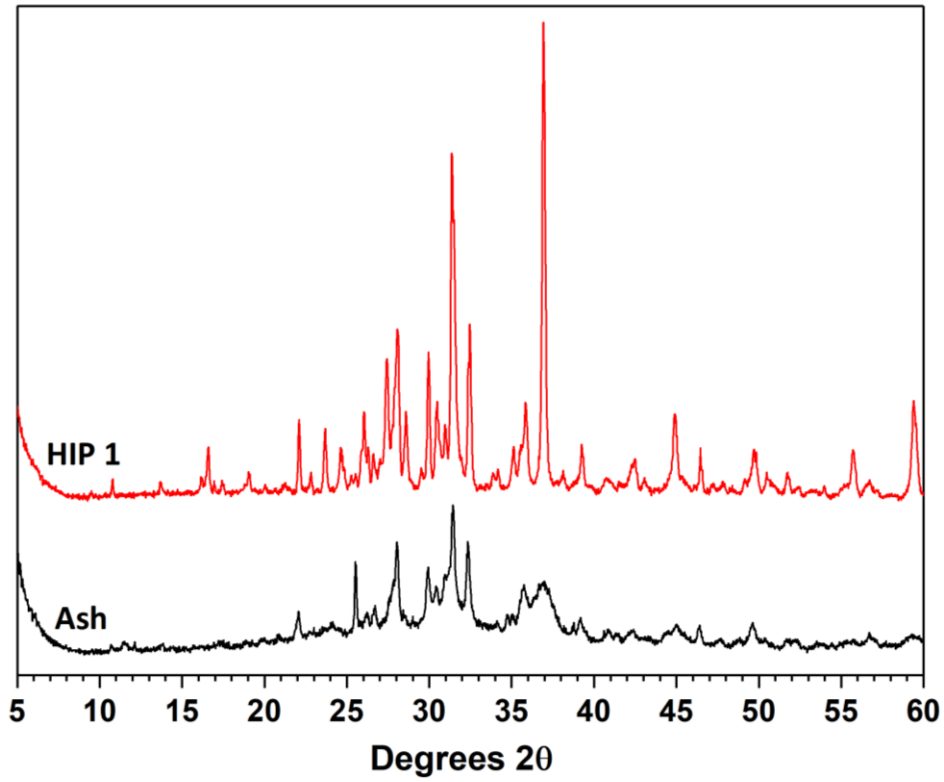

Figure 81: XRD pattern of IRIS ash as-received & HIP material. No phases indexed, too many overlaps to be sure

8.2 SEM of IRIS ashes

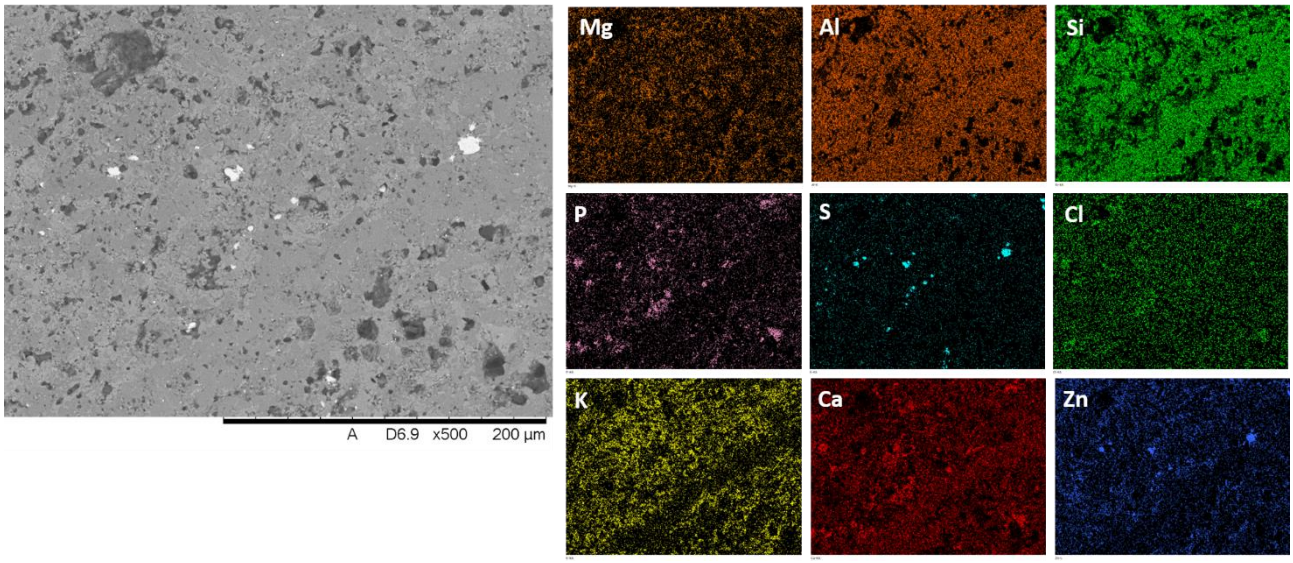

Figure 82: Scanning electron microscopy (SEM) micrograph & EDX maps (500x).

- Inhomogeneous product
- Clear separation
- Zn-S hot-spots
- Ca-P-Cl regions?
- However:
    - Fused product
    - Solid
    - Porosity

8.3 High-isostatic pressure

8.3.1 IRIS Ashes

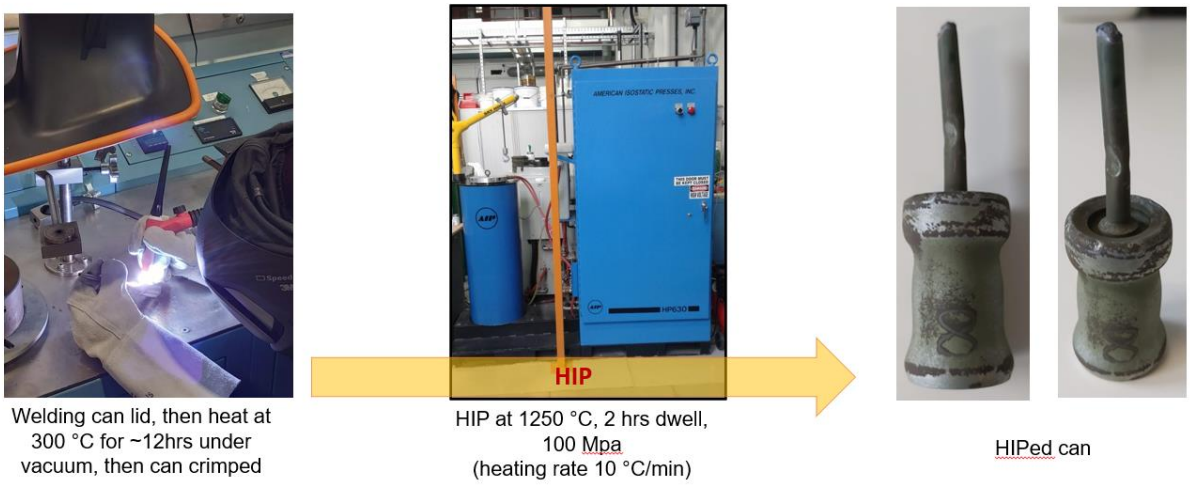

Figure 83: The process of HIPing.

- X-ray diffraction
  - Outside face:
    - Zincochromite ($ZnCr_2O_4$) / Magnetite (Fe_3O_4)
    - Haematite (Fe_2O_3)
  - Bulk material
    - Spinel ($ZnAl_2O_4$ / $MgAl_2O_4$ likely)
    - Chlorapatite ($Ca_5(PO_4)_3Cl$)

Figure 84: The inside of HIP Can ready for analysis.

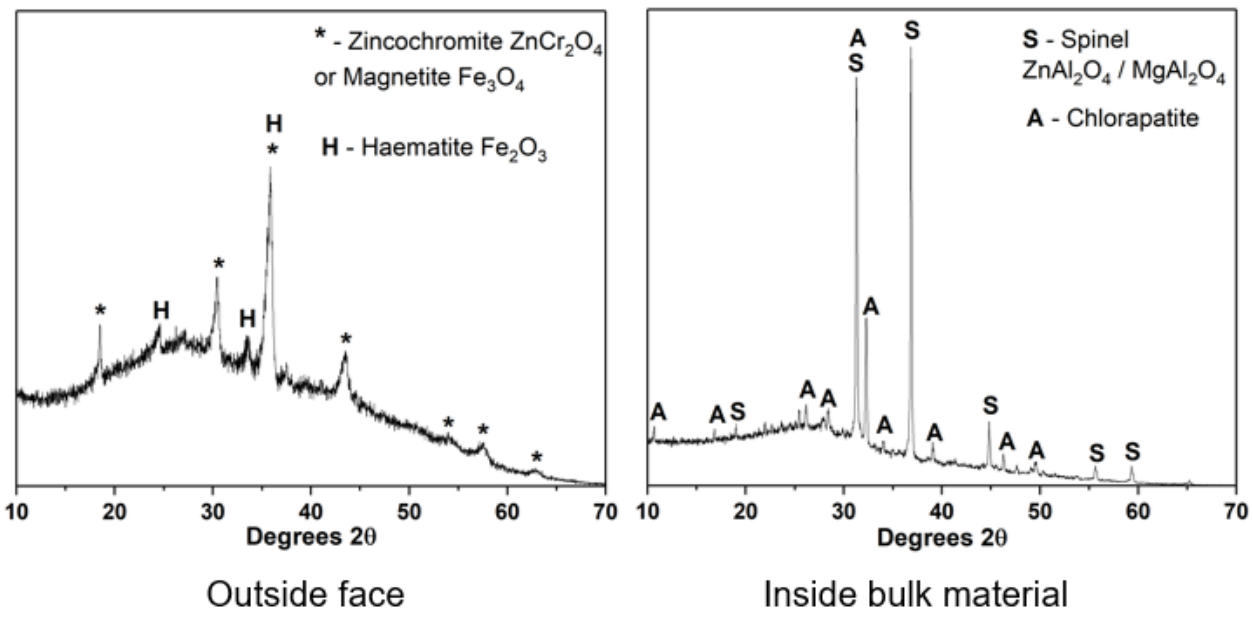

Figure 85: The XRD analysis of prepared mix

HIP Trials:

- 1 – Direct ashes, no pre-treatment (100% ash)
- 2 – Ground ashes + sodium tetraborate (95% ash, 5% $Na_2B_4O_7$)
- 3 – Ground ashes + sodium aluminate (95% ash, 5% $NaAlO_2$)
- 4 – Ground ashes (100% ash)

Summary of IRIS ash HIP trials

- 1250 °C, 100 MPa, 2 hr dwell
- All formed solid, densified products
- Required addition of $Na_2B_4O_7$ to form a true glass-crystalline product
- However, all except direct HIP of ashes formed lower porosity solid monoliths
- $Na_2B_4O_7$, $NaAlO_2$ and ground ash samples all taken forward for dissolution testing in WP6.6

	HIP 1 (direct)	HIP 2 ($Na_2B_4O_7$)	HIP 3 ($NaAlO_2$)	HIP 4 (ground)
Leucite ($KAlSi_2O_6$)	X		X	X
Anorthite ($CaAl_2Si_2O_8$)	X		X (reduced)	X
Diopside ($MgCaSi_2O_6$)	X		X (reduced)	X
Chlorapatite ($Ca_5(PO_4)_3Cl$)	X	X	X	X
Spinel (AB_2O_4)*	X	X	X	X
* Likely zincochromite $ZnCr_2O_4$, gahnite $ZnAl_2O_4$, spinel $MgAl_2O_4$				

Figure 86: Table of XRD analysis of different HIP experiments.

Figure 87: The picture of different HIP samples.

8.3.2 KIPT ashes

Waste

- Wood ash from incineration of contaminated wood (Chernobyl)
- Simulant non-active ash used

Treatment route:

- Incorporation within a geopolymer
- Cement is then crushed, and pressed into a pellet
- Sintering / Hot Press / Hot Isostatic Pressing
- Incorporation of CaF_2 to form stable fluorapatite $Ca_5(PO_4)_3F$

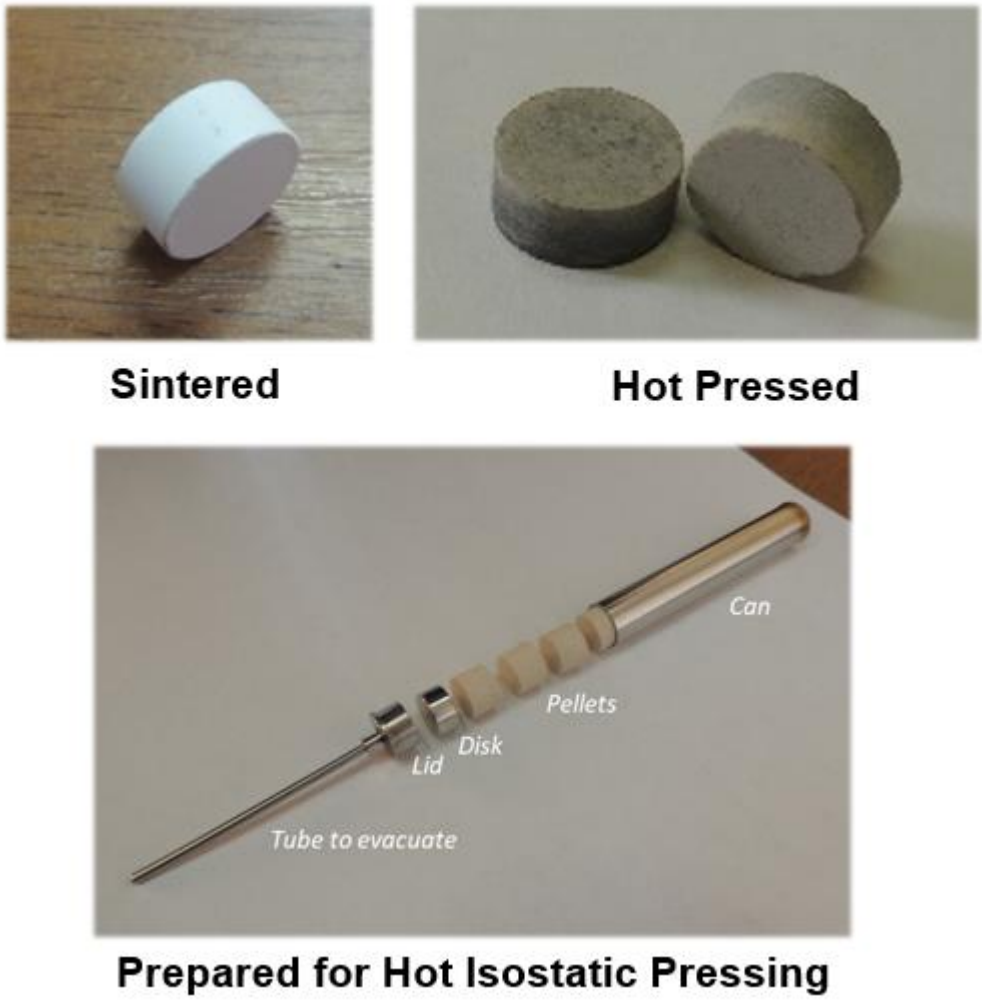

Figure 88:KIPT ashes ready for HIP.

Attempted HIP of capsules

- Research at KIPT interrupted due to war.
- Already prepared canisters were shipped to USFD to use our HIP.
- Powders used for the canister preparation & already HIPed canisters provided too.
- Metakaolin + ash canisters
- HIPed at 1100 °C, 200 MPa, 2hr dwell
- HIP cycle worked, however no canister densification
- Suspected pinhole in the welds?
- Working with KIPT on the next steps

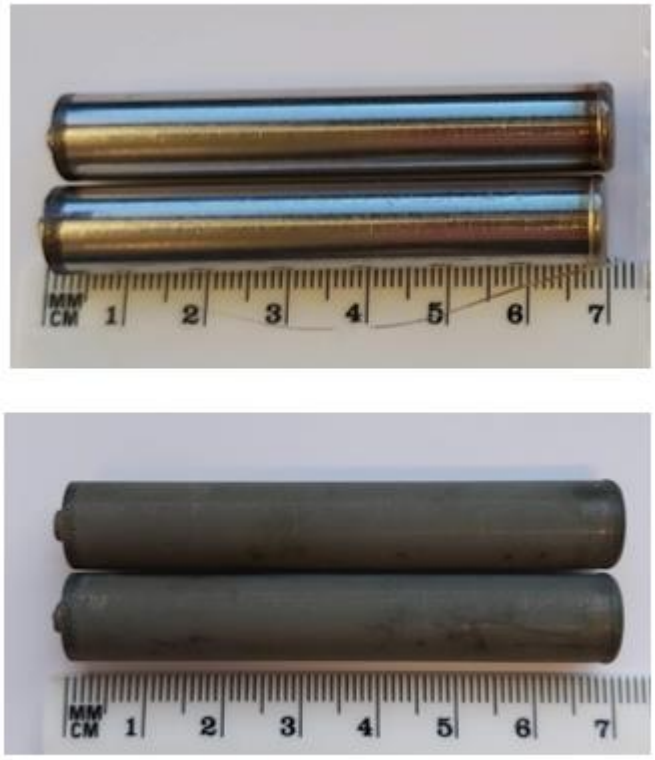

Figure 89: HIP capsules with KIPT ashes.

9 SIIEG Contributions

9.1 Experimental part

9.1.1 Analysis of new technologies

The first study related to the direct immobilisation of waste is in the article [29]; the process of immobilisation of radioactive waste containing Cs radionuclides in various kinds of so-called geopolymer matrices, including a metakaolin-based geopolymer matrix is described. The authors used this matrix to immobilise secondary radioactive waste generated at the Hanford nuclear power plant. As a result of the analysis of the possibilities to treat the waste of these types, the technology of SORW solidification in a geopolymeric matrix was considered. Such technologies are based on the chemical reaction of polycondensation of non-organic components containing SiO_2 and Al_2O_3, products of which are solid compounds with waste enclosed in them.

Direct conditioning of radioactive waste has been proven effective by using alkali-activated materials (AAM) and, in particular, geopolymers (GP) [30 - 32], which limits chemical interactions between waste and binder. Such technologies are based on a chemical reaction of polycondensation of non-organic components containing SiO_2 and Al_2O_3, products of which is the solid compound with waste enclosed in it. Geopolymerization is geosynthesis that involves naturally occurring silico-aluminates. Any source of silica and alumina, such as metakaolin (MK) and blast furnace slag (BFS), is the typical raw material for preparing geopolymer composites. They are readily dissolved in an alkaline solution like sodium/potassium hydroxide and sodium/potassium silicate, which are a source of geopolymer precursors and thus lend themselves to geopolymerization. Nowadays, geopolymers are typically synthesised at ambient temperatures by alkali hydroxide- or silicate-activation of reactive aluminosilicate powders. The authors [33,34] summarised the polymerisation process occurs via the following steps:

- Alkaline attack on the aluminosilicate source released silicate and aluminate species into the solution. In the case of the metakaolin system, 5- and 6-coordinated Al is converted into 4-coordinated aluminate species upon dissolution.
- Transportation of newly formed small dissolved species and the silicates initially supplied as activating solutions occur via a water-assisted mechanism, enabling them to interact. Such interactions result in the formation of aluminosilicate oligomers.
- Precipitation of dissolved species into an amorphous gel is then triggered once the silicate solution is destabilisation by the presence of dissolved aluminate in a sufficiently high concentration. This dissolution and gelation coincide and may be influenced by mechanical disruption (shearing or ultrasonication) and additional particle surfaces (aggregates and/or other added oxides), which may provide nucleation sites.
- Geopolymer gel with an amorphous, cross-linked, three-dimensional structure (often called a geopolymeric gel binder phase) grows until the reacting slurry solidifies. The time taken for this is greatly influenced by the mix design and curing temperature, along with the presence or absence of contaminants. Depending on the mix design and the curing temperature, the setting can be achieved almost instantaneously or over a duration of several days.
- The alkali-activated, cementitious materials are amorphous, making them an ideal substitute for Portland cement in various applications. Alkali-activated geopolymers have demonstrated desirable mechanical properties such as high flexure strength, toughness, and good resistance to acid corrosion. It must be noted that there is no universal composition of matrix – a formula for the immobilisation of RSOW is needed to adapt the formulation for specific waste.

9.2 Process feasibility

Direct solidification is commonly used to treat spent IERs due to simple operation and equipment and has been widely accepted cementation using Ordinary Portland Cement (OPC). An alternative solution to solidifying RSOW is the solidification in the OPC (II) matrix. Removal of organic

matter IERs by thermal gasification results in significant volume reduction demonstrated successfully in the THERAMIN project [34]. Cementation, traditionally used for encapsulation, is a conventional method to bind the gasified resin ash. TECDOC of IAEA reported that geopolymers were used to solidify radioactive wastes at Dukovany NPP [35]. The last time, many works indicated that alkali-activated geopolymer binders might be suitable matrices for encapsulating and stabilising ash. The potential to combine gasification as thermal treatment and various inorganic binders as encapsulation matrices was tested in the VTT. A comparison was made between the OPC matrix and the geopolymer matrix based on alkali-activated BFS and MK. An evaluation was performed using inactive caesium tracer as caesium (^{137}Cs, ^{134}Cs) is the primary source of radioactivity in IER within the first 200-300 years. This work aims to evaluate the application of geopolymerization to ash after gasification of the IER and the problems associated with the specificities of the ash.

9.2.1 Thermal treatment of ion exchangers

The State Institution “Institute of Environmental Geochemistry” NASU (IEG) research group have worked with partners for several years to develop a hybrid process of gasification of IER with after-ash incineration by plasma torch and gas cleaning technologies for different applications. [36]. The IEG set innovative equipment for effective deep thermal treatment of waste containing organic substances and shows that the first must be into a gasification step at a temperature of 600 °C to remove the significant organic gaseous compounds and then plasma torches incineration (1600°C) till complete mineral ash. The remaining radioactive ashes must be transferred to treated waste. The significant gasification problem is the completeness of thermal treatment, which allows the removal of organic substances from IER without releasing large amounts of radionuclides. The ion exchange resin combustion method is optimised by determining the temperature of the gasification process for the gradual conversion of mobile and volatile Cs species into inorganic and thermally stable compounds. Incineration of significant volumes of spent ion-exchange resins can be problematic, also taking into account the uncertainty of the behaviour of radionuclides depending on the temperature and duration of gasification. In Figure 90, the sequence of destruction of spherical particles of the cation IER during heat treatment is given. When heated, the particles of an IER crack from them, separating scales, and they decrease in size. In the future, cracking continues while the scales begin to burn out. At sufficiently high temperatures, particles of a spherical shape can be preserved in the samples. The presence of such particles in the samples significantly reduces the ultimate compressive strength of the geopolymer matrix. Reducing their number in the samples of compounds is an urgent problem and requires a higher temperature after the first gasification.

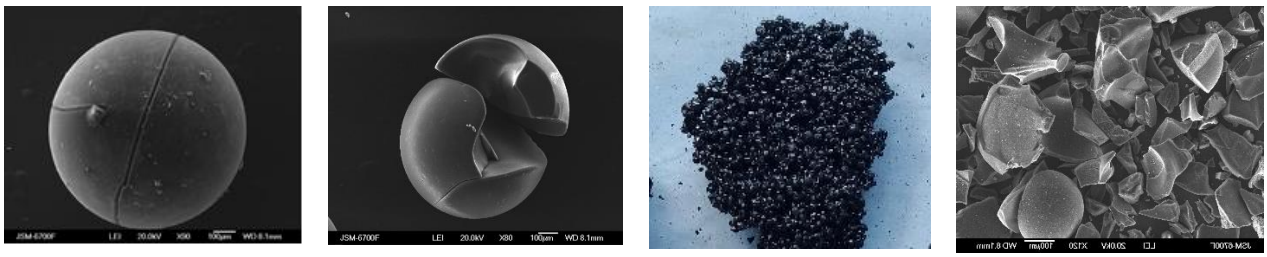

Figure 90: Destruction of IER under gasification

By temperature of about 900 °C mass sample decreases and remains at 13% of the initial, Figure 91. Repeated the study showed that complete decomposition (99%) can occur at a temperature of more the 1000 °C (Figure 92). After gasification, the ash was homogenised and mixed with the geopolymer.

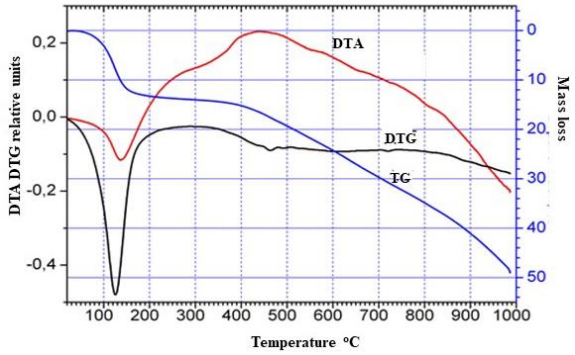

Figure 91: DTA analysis of samples of IER of the burnout

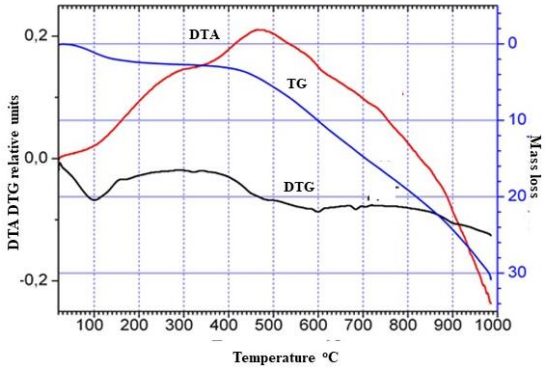

Figure 92: DTA of samples ash after the burnout of IER.

The cationic IER is characterised by releasing more significant quantities of degradation product, mainly SO_2. In the article Matsuda, the lower mass reduction of the cationic IER to the stabilisation processes of the residual matrix associated with the formation of sulfur structures [37].

9.2.2 Raw materials

Two primary alkali-activated materials (AAM) types can be distinguished depending on the amount of Ca in the raw materials. C-(N)-A-S-H type gels have formed in Ca-rich systems through hydration mechanisms similar to the formation of C-A-S-H in Portland types of cement [38]. The N-A-S-(H) type gels have formed in Ca-poor systems through polycondensation reactions, also called geopolymerization [39]. It is noted that water is part of C-A-S-H structures (through hydration reactions). Conversely, water is only required as a dissolution medium for N-A-S-(H) tridimensional aluminosilicate networks and is released upon gel formation (i.e., after poly-condensation). These fundamental differences in raw materials, reactivity or structures are starting points to understanding the distinct behaviour of both systems. The addition of alumino-silicate minerals to kaolinite is necessary for the formation of a gel. A weak structure is formed if only kaolinite is used without other alumino-silicates. Therefore, the synergy between different aluminosilicates seems essential [40].

- Metakaolin (MK)

The work used metakaolin obtained from kaolinite (brand P-2) of the Hlukhovetsky deposit (Ukraine). The X-ray diffractogram of metakaolin is shown in Figure 93 . This is one of the kaolins with a high degree of structure perfection, where the crystallinity index is 1.4 - 1.6 (according to Hinckley). Table 17 shows the chemical composition of kaolinite. These kaolinites have a broad spectrum of dispersion from 10 m2/g to 60 m2/g, which is determined by the thickness of kaolinite particles from 70 nm to 7 nm; one should expect different behaviour in alkaline solutions, which explains the different results of studying the strength of compounds with metakaolin obtained, as it were, in identical conditions. It was established [41] that increasing the dispersion of metakaolin from 15.7 m2/g to 25.6 m2/g increases the strength of compounds from 55 to 74 MPa. According to the studies, a sufficient number of reactive phases is formed. Metakaolin was obtained by heating kaolin for 4 hours at a temperature of 800 °C.

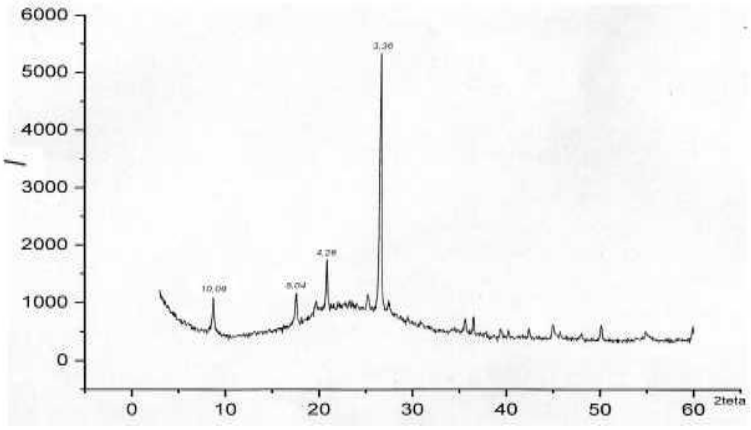

Figure 93: The X-ray diffractogram of metakaolin used in this study.

A small amount of mica and quartz were observed as impurities in metakaolin. The absence of kaolinite reflexes indicates that the transition from kaolin to metakaolin took place completely.

Table 17: Chemical composition of the metakaolin (oxide wt. %)

SiO_2	Al_2O_3	CaO	MgO	Fe_2O_3	MnO	Na_2O+K_2O	TiO_2
52.9	41.92	0.19	0.27	1.64	0.1	0.69	1.87

- Blast Furnace Slag (BFS)

The BFS is the raw material of the Mariupol metallurgical plant which has been used and practically no longer exists due to the current war. The mineral composition of the slag was determined on the X-ray diffractometer DRON - 3m (voltage 30 kW, 20 mA). The X-ray pattern of the slag is shown inFigure 94. The results of the X-ray phase analysis show that the slag is a complex multi-mineral substance.

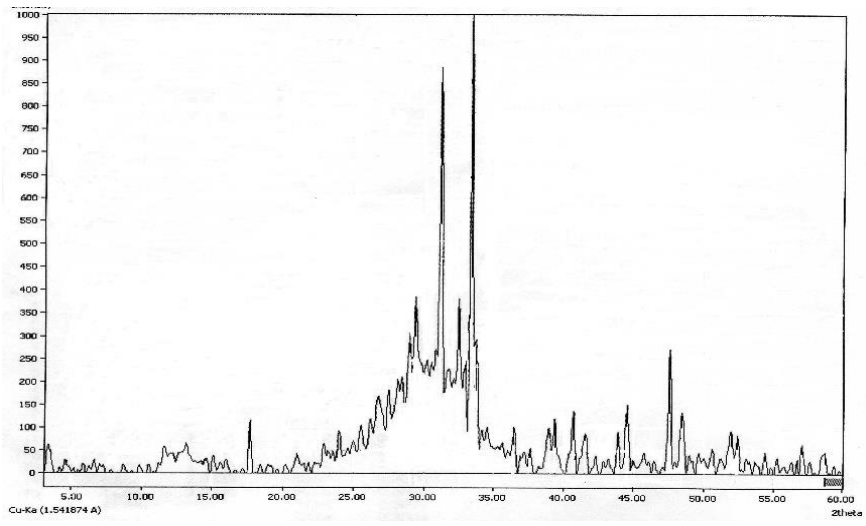

Figure 94: The XRD analysis of the slag Mariupol metallurgical plant.

Among the crystalline substances in the slag are established: Bredigite – $\alpha{\cdot}2CaO{\cdot}SiO_2$; Larnite – $\beta{\cdot}2CaO{\cdot}SiO_2$; Pseudowollastonite – $\alpha{\cdot}CaO{\cdot}SiO_2$; Rankinite –$3CaO{\cdot}2SiO_2$; Melilite (Gebelite) – $2CaO\ Al_2O_3{\cdot}SiO_2$; Hellenite – $2CaO\ SiO_2\ {\cdot}Al_2O_3$; Ackermanite – $CaO{\cdot}MgO{\cdot}2SiO_2$.

The BFS was dried, grounded and sieved (<125 μm). The slag was a fine-grained powder with a specific surface area of 288 m^2/kg, and the residue on a 0.08 sieve was 1.26%. Table 18 shows the following chemical composition of the BFS used in the work.

Table 18: Chemical composition of the furnace slag (oxide wt. %)

SiO_2	Al_2O_3	CaO	MgO	Fe_2O_3	MnO	SO_2	Na_2O+K_2O	TiO_2
36.53	7.92	42.94	9.47	0.24	0.1	0.54	1.29	0.47

The preliminary mechanical activation of the slag was carried out. It is important to note that the activation reaction rate depends on several factors, such as the particle size distribution and the mineral composition of the starting material. A positive result was obtained during the preliminary mechanical activation of the slag in the activator at 14,000 rpm. During activation, the size distribution of particles changes, and the dominant fraction is 65 μm, Figure 95.

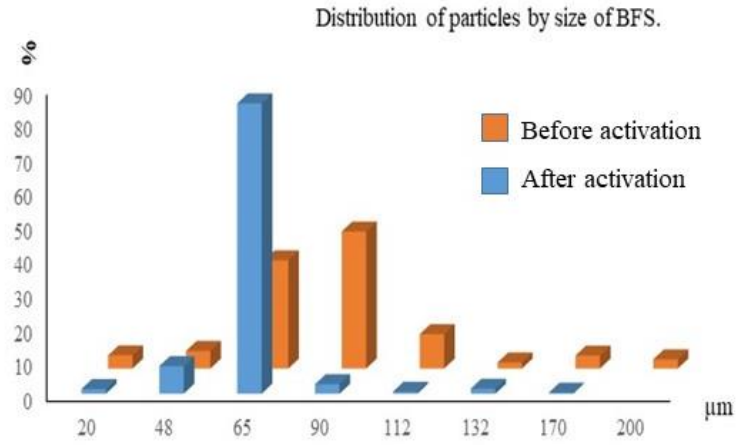

Figure 95: Distribution of particles by the size of BFS.

It should be expected that the selection of fractions < 100 μm, and even better < 80 μm, from the slag, will contributes to increasing the strength of the samples. If there is an opportunity to choose, then preference should be given to alkaline slags, which are established by methods of chemical analysis. It can be basic, neutral or acidic. The formula determines the basicity (MO) of slag:

$$MO = \frac{CaO + MgO}{SiO_2 + Al_2O_3}$$; oxides are taken in %.

Basic slags have MO >1, neutral - 1, and acidic < 1. The composition of slags includes crystalline substances (minerals) and amorphous aluminosilicate glassy substances. Its content in slag can exceed 50% by mass. According to the results of the chemical analysis, the slag is classified as basicity MO = 1.36. The composition of the slag also includes an amorphous phase, the amount of which is not determined.

The crystalline phases of slag do not take part in the creation of geopolymers but perform the functions of matrix fillers. A geopolymer binder of the required quality is formed at a specific ratio between Si and Al, Na (K) and Al, established based on gross chemical analyses of the components. The presence of phases, the composition of which is considered by chemical analyses, but the phases themselves do not take part in synthesising the geopolymer matrix, imposes the need for their quantitative consideration.

- Alkaline Activator Solution

Theoretically, alkali and alkali earth cations can be used as the alkali element in geopolymerisation reactions; however, most studies have focused on the effect of sodium (Na+) and potassium (K+) ions. The choice of alkali metal cation used during geopolymer synthesis depends on many factors,

the most important being the type of source materials and the foreseen application of the produced geopolymers. The size of the cation also affects the eventual crystal morphology: Na+, having a smaller size than K+, displays strong pair formation with smaller silicate oligomers (such as monomers). The larger size of K+ favours the formation of larger silicate oligomers with which Al(OH)4- prefers to bind. Therefore, more geopolymer precursors exist in KOH solutions, resulting in a better setting and stronger compressive strength than geopolymers synthesised in NaOH solutions.

Activating alkali hydroxide solutions were prepared by adding NaOH to water and heat, then Na_2OSiO_2xH2O with constant stirring until completely dissolved for a solution with potassium hydroxide. The solutions were prepared before mixing with sodium/potassium silicate. The alkaline activator solution: KOH, water and K_2SiO_3 or NaOH solution water and Na_2SiO_3 of appropriate molar ratios and cooling to 20°C were used for the geopolymerisation process.

9.2.3 Preparation of geopolymer formulations

The MK/BFS geopolymer pastes were prepared with different Al:Si:Na/K: H_2O ratios. Using KOH as an activator led to higher compressive strength than NaOH. The optimal amounts of water, activator, MK, and BFS have been determined based on the literature study and experimentally. Geopolymer samples were produced: alkaline activation solutions were prepared by mixing appropriate quantities of sodium silicate solution, K/Na hydroxide pellets, deionised water and stirring to reach homogeneity. The solution was mixed with powder components MK/BFS and added water until a 14-16 cm spreading cone was formed. The mixing operation was performed continuously at room temperature (600-800 rpm for 5-10 min). The geopolymer binder was measured on viscosity after mixing according to ASTM C1749 [42] and set time based on EN 196-3 [43]. The setting time of geopolymer pastes should not be less than the duration of the technological cycle - the time from the beginning to the end of compounds mixing and pouring into moulds.

The high degree of variability in the physical properties and chemical composition of the BFS/MK used in producing alkali-activated binders is a significant problem in conditioning ash. The geopolymer grouts to cast in cubes moulds (5x5x5 cm sides) and left in the moulds until the end of hardening. After the top layer was compacted, the moulds were vibrated to remove air bubbles for better compaction of the grouts. The negative effect of vibration compaction is the release of the liquid phase on the surface of the compound. The time of the end of hardening was determined by the Vicat Needle, the cone of the device, which was filled at the same time as the forms. Each batch had 3 to 5 samples. After mixing components, the mixture was put into moulds for a grout set, which lasted from 40 minutes to 155 minutes or more. General view of the sample in Figure 96 and Figure 97.

Figure 96: Geoptolymer matrix samples (cubes moulds of the 5 x5x5 cm side)

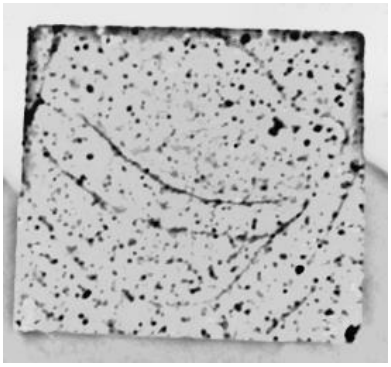

Figure 97 Geopolymer compound with ash IER (WP6-54).

Figure 98 Geopolymer matrix with crack.

Compressive strength measurements evaluated matrices after curing on an electromechanical press (ZD 10/90) according to EN 13791 [44]. The definition of compressive strength was carried out on the 7th and 28th days after manufacturing. The blank sample matrices had a limit compressive strength of more than 51 MPa with a porosity of about 0.5%. With such low porosity, samples dry up slowly. When gradient distribution water in samples may occur, they crack, Figure 98. To prevent this, a modified slag-alkaline binder was added metakaolin, which increased porosity up to 15% and reduced limit compressive strength up to 19.3 MPa. The composition of such samples is shown in Table 19.

Table 19: Composition of samples of compounds with different mechanisms of geopolymerization

Test №	Composition, %				
	BFS	Metakaolin	Liquid glass	NaOH	Water
WP6-9	68.5	-	15.8	5.5	10.3
WP6-12	-	46.2	11.8	4.0	37.9

Slag needs the most minor water to form a pasty state, and metakaolin needs the most.Table 20 shows the properties of the above samples.

Table 20: Properties of geopolymer samples with different mechanisms of geopolymerisation

Test №	Si/Al	(Na+K)/Al	Set time	Density, g/cm^3	Strength limit, MPa
WP6-9	1.55	0.4	120	>1.98	26.4
WP6-12	1.6	0.43	>150	1.44	14.2

Geopolymers showed a high compressive strength at 28 days of curing. The sample of BFS geopolymers WP6-9 shows the highest density and strength up to 26.4 MPa and 14.2 MPa for metakaolin geopolymer sample WP6-12. To improve the strength limit, the goal is to do optimisation of the recipe to obtain high strengths for BFS-based geopolymers. When the sample dries, its size decreases. If, due to uneven drying, the sample's surface dries faster than the deep (inner) layers, then cracks form in it. Cracks did not form during slow drying. The effect of combining slag with metakaolin in different ratios was studied on samples. After hardening, the samples were removed from the moulds, weighed and placed in desiccators in an atmosphere of saturated water vapour at room temperature. After seven days, drying of the samples at room temperature began.

To obtain reference geopolymers with good performance and appropriate matrix for immobilising ash, both BFS and MK precursors investigated whether C-A-S-H or N-A-S-H is more beneficial in waste encapsulation. The water-to-binder ratios (w/b) were also examined, and the results showed that the higher w/b of 0.6 to 0.8 can provide suitable MK-based geopolymers. Herein, alkali NaOH and Na-Silicate have been used as the alkaline solution for both precursors. Comparative studies were conducted on monocomponent samples in which the basis for the geopolymer was slag or metakaolin. The composition of such samples is shown in Table 19.

9.2.4 Results and Discussion

Due to the dependence of the ash on processing IER waste, one of the main goals concerning the ash characterisation was to select those factors responsible for the compressive strength. For this purpose, the original ash sample has been fractionated by sieving. Measurement of the compressive strength after drying to constant weight showed that with an increase in the amount of added ash fraction < 0.2 mm, in the amount of 16.6%, the strength was 10.5 MPa, and at increased to 29.6%, the strength decreased to 4.7 MPa. In the geopolymer matrix sample, when the ash fraction <0.6 mm was used in the composition, the strength limit was 0.9 MPa.

Table 21: Composition of binder, %

Sample composition	WP6-26	WP6-54	WP6-55	WP6-56
BFS	68.5	34.4	22.7	45.3
Metakaolin	-	1.3	0.85	1.7
Liquid glass	5.5	7.9	5.2	10.4
Hydroxide potassium	15.8	3.1	2.0	4.1
Water	10.3	19	23.9	16.0
IER ash	-	45.9	22.6	22.7

Thus, it was found that the most challenging issue when solidifying ash after thermal processing of IER is ash homogeneity in composition. From physical and mechanical properties, ash depends primarily on strength indicator compounds.

Table 22: Properties of samples.

Properties	WP6-26	WP6-54	WP6-55	WP6-56
Density, g/cm^3	2.3		2.26	
Porosity, %	0.5	14.0		
Setting time, min	180	190	160	180
Compressive strength, MPa	51	4.4	9.6	10.9
Degree gasification of IER	-	0.81	0.87	0.81
Fraction ash	-	<0.3	<0.3	<0.3

Before the measurements, the ash samples were ground in an agate mortar. The microstructure and morphology of the ash fractions have been investigated on SEM (JSM-6490LV). As was indicated

above, the presence of the sample's compounds of spherical particles significantly reduces their limited compressive strength (Figure 99), so decreasing the quantities in a sample of particles is a current problem. On the other hand, thermal processing IER to high values requires additional energy costs that may be impractical. The work has studied compounds obtained by solidification IER ash burned to 81% and 87%. Selected degree firing 80÷90% proceeding shows that when the IER in the samples amounts spherical particles many decreases, Figure 100.

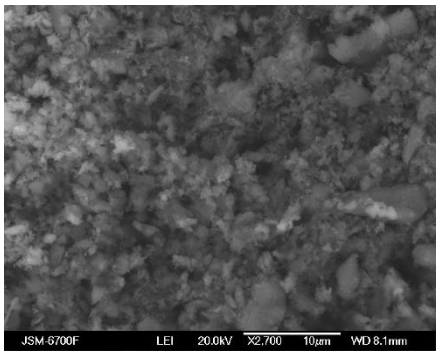

Figure 99: Ash of IER after thermal processing at 600 °C

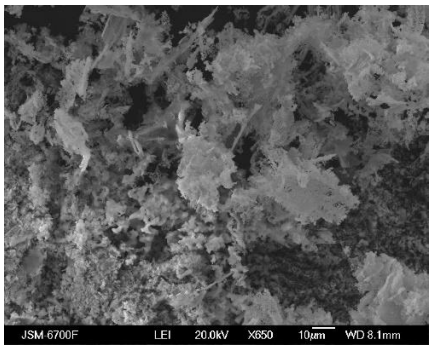

Figure 100: Ash of IER after thermal processing at 800 °C

Anyway, the strength of such specimens is extremely low, the same related significant dimensions particles ash. When selecting fractions by size 0.3mm, results improved, although when studying distribution, particle size observed the presence of large fractions,Figure 101.

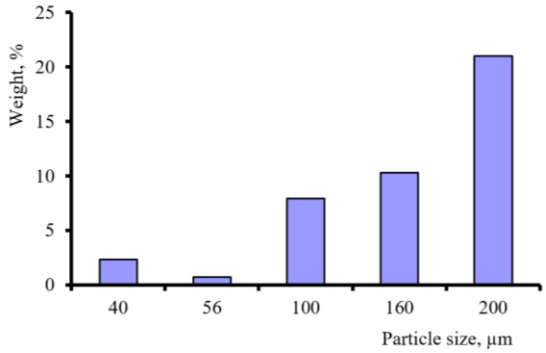

Figure 101: Size distribution in the fraction < 0.3 mm particles ash after burning 87% of the IER

Table 21Table 22shows that the best strength was the sample WP 6-56, which used the ash fraction <0.3 mm, a degree of gasification of 0.81. The amount of ash in the compound was 22.7%, and the amount of liquid glass increased to 19.4%.

The porosity of the samples has measured by saturating them with kerosene; the lowest values were obtained for these samples - about 0.5%. The Geopolymer metakaolin matrix showed significantly higher porous, up to 18%, than the BFS matrix, leading to higher transport properties, which could affect the durability of the geopolymer. As it turned out when combining two geopolymerization mechanisms, increasing the amount of metakaolin in the samples slightly reduces their compressive strength, but such samples do not crack during drying. Thus, previous studies have shown that BFS in the composition of the samples increases their strength, while metakaolin reduces the strength of the samples.

9.3 Experimental part (CEMI-52,5 R and CEMII/A-LL 42,5 R)

9.3.1 Raw materials

For the cementation of ash with Portland cement two commercial binders (CEMI-52,5R) and alkali-activated cement (CEMII/A-LL 42,5-R) were used for the experiments. The CEMI (OPC) specific surface was >350 m^2/kg with the content of tricalcium aluminate (C_3A) of no more than 8 % by mass, and CEMII varied within the 330-350 m^2/kg range. The most commonly used alkali-activated cements are the alkali-activated slag cement. One of the drawbacks of this cement is the small contents of Al_2O_3 in their composition. Ground granulated blast furnace slag was used as aluminosilicate components. Their chemical compositions are shown in Table 23. The comparatively low content of the glass phase in slag (56 %) was following [45] and can be explained by the high basicity modulus of slag (Mb = 1.1). The soluble actuation prompts the disintegration of Ca^{2+} particles, which improves a micro structuring wealthy in steady and high hydrate Calcium silicate (C S H) stages. Under soluble situations, the C S H gel varies in the Sodium Calcium Si H gel stage, which presents excellent toughness to matrices when presented to Carbon dioxide-rich cases, which was examined by Kumar et al.[46]

Table 23: Chemical composition (wt.%)

Cement material	SiO_2	Al_2O_3	Fe_2O_3	Na_2O+K_2O	CaO	MgO	SO_3
CEMI-52,5R (OPC-500)	21.80	5.30	4.90	-	65.90	1.10	0.99
CEMII/A-LL 42,5-R	36.2	12.8	0.3	-	46.4	3.6	0.6
Slag (GGBFS)	36.53	7.92	0.24	1.29	42.94	9.47	0.54

9.4 Process feasibility

As an alkaline activator in the cement, sodium silicate was a solution with silicate modulus Ms=2.87 and ρ=1300 kg/m3. The results of the experiments are given in Table 24 and Table 25.

Table 24: Composition of compounds, %

No.	CEMII/A-LL-42,5R	Sand	IER (cation)	Waste (ash)	Water
WP6-62	33.3	48.4	-	-	18.3
WP6-63	44.6	-	24.5	-	30.9
WP6-64	41.7	-	-	31.5	26.9

When OPC cement was mixed with water and sand, samples with a compressive strength of 9.2 MPa were obtained (sample WP-62, Figure 102). When replacing sand with ash from the burning of cations, an increase in the volume of compounds was observed as a result of the formation of bubbles (sample WP6-64, Figure 103 and Figure 104).

Figure 102: Sample WP6-62

Figure 103: Sample WP6-64

Figure 104: Sample WP6-64 after of compressive strength

The test on the compound with ash showed low compressive strength (2.3 MPa), low density of the samples (1.22 g/cm3), sample WP6-63, Figure 105.

Table 25: Properties of compounds on Portland cement

No.	Spreading cone, cm	Setting time, min	Compressive strength, MPa	Density, g/cm^3	Porosity, %
WP6-62	12	< 300	9.2	1.96	14
WP6-63	14	> 360	2.3	1.22	24
WP6-64	13	> 1 2 0	2.0	0.98	40

Figure 105: Sample WP6-63

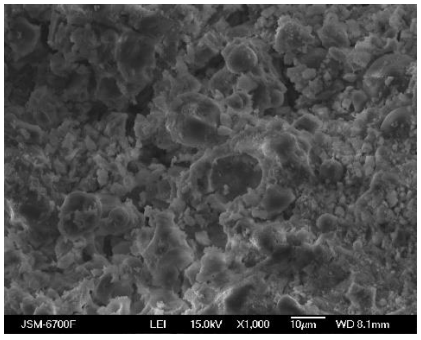

Figure 106: The SEM images of the sample WP6-63

Subsequent experiments were carried out using Portland cement of the second brand CEMI, and the composition was the same as in previous experiments, Table 26. Samples were obtained in which an increase in volume due to the formation of bubbles was also observed. Thus, it was found that the cement brand does not affect the formation of bubbles; that is, they arise due to the interaction of cationic ash with an alkaline medium, characteristic of an aqueous suspension of Portland cement. Observations showed that bubbles appear during the first 40-50 minutes. Considering this, after combining all the components, the mixture was stirred for 2-3 minutes every 15 minutes. After each mixing, the number of bubbles decreased. In total, five times stirs were performed. An interval of 15 minutes was necessary for the removed gases. The moulded samples WP6-69 are shown in Figure 107.

Table 26: Composition of compounds, %

№	CEMI	Ash	Doping Cs, Sr, Ce	Water
WP6-69	41.7	23.6	-	26.9
WP6-74	40.1	30.1	-	29.8
WP6-75	30.5	29.5	0.7	29.5

The ash remaining from the burning of cations with a loss of 80% of their mass has at least a two-phase composition, Figure 108 and Figure 109. The first phase is carbon, which is observed during the grinding of ash for subsequent sieving through a 0.2 mm sieve, since after heat treatment, the samples contain many aggregates formed as a result of sintering. Since many sulfide compounds are in the ash of cation exchangers, they enter into chemical reactions with cement with gas emissions.

The second phase is the underburning of destroyed globules of cations. He forms a gas upon interaction with calcium hydroxide, and whole globules of cations do not react with Portland cement (sample WP6-63). Considering this as an option, preliminary treatment of cationic ash with alkalis, possibly at an elevated temperature, can be considered.

Figure 107: Sample WP6-69

Figure 108: Ash from the burning of cations

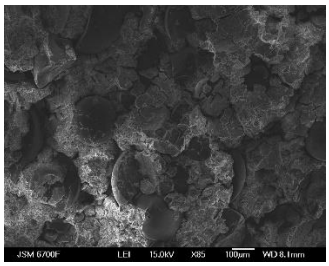

Figure 109: The SEM images underburning of destroyed globules of cations

The modified slag-alkaline CEMI cement with increased liquid glass was used to create a matrix into which the waste is embedded. Compression tests of the hardened matrices after ash conditioning the spent ion exchange resins were evaluated according to the ASTM C109/C109M standard. Compressive strength tests were performed using a laboratory press 28 days after casting for cement-slag matrices. The results are showsn in Table 27.

Table 27: Properties of compounds on slag-alkaline CEMI cement

№	BFS content, %	Waste fraction of ash, mm	Properties of compounds					Waste content, %
			Density g/cm^3	Compressive strength limit, MPa	Spreading cone, cm	Porosity %	Setting time, min.	
WP6-69	6.4	< 0.2	1.33	7.7	14	22	<300	23.6
WP6-74	7.2	< 0.2	1.49	5.8	17	22	<150	30.1
WP6-75	7.6	< 0.2	1.5	14.7	13	19	<150	30.1

Curing conditions were 28 days of continuous saved at t= 20ºC and RH= 99%. Determination of strength was done on samples cube size 50x50x50 mm. Two days later, the specimens were taken from the moulds and placed for further hardening at t = 22ºC and RH 100%. Regularities of formation of pore structure of the matrices were found to depend on slag contents and type of alkaline component. In general, the increase in slag contents is associated with higher contents of the alkaline component, resulting in lower volumes of open pores and higher volumes of conditionally closed pores.

Carbonation vulnerability

The cement matrices were assessed for their vulnerability to carbonation (Figure 110). The test was carried out using an elevated CO_2 concentration of 3-5%; the test duration was 90 days [47]. Analysing the results obtained for matrices at w/c = 0.50, it can be seen that samples with cement characterise OPC with the highest carbonation depth. A significant decrease in the carbonation depth is associated with the cement components' activity, mainly ground granulated blast furnace slag for CEMII/A-LL-42,5R. Additional products formed later from the reaction between cement hydration products and active mineral additives settle in the pores of hardening cement slurry. The change of the anionic part of the alkaline component from carbonate to silicate improved the water absorption and porosity of the reference matrices.

Figure 110: Carbonation of samples WP6-69.

The quality of cement matrices depends in part on formulation, mixing, emplacement, and execution. The long-term performance depends significantly on the quality of the emplaced cement-based material, which relates to the previously noted considerations.

REFERENCES

[1] https://pubchem.ncbi.nlm.nih.gov/compound/Sodium-Carbonate#section=pH (cited 3.8.2023)

[2] https://www.cluz.cz/en/metakaolin-and-geopolymer (cited 17.8.2023)

[3] Černá, A., Galek, V., Pražák, P., & Hadrava, J. (2022). Direct Conditioning Of Molten Salt Arising From The Thermal Treatment Of Solid Organic Waste. 31st International Conference Nuclear Energy for New Europe.

[4] B. V. Rangan, Fly Ash-Based Geopolymer Concrete Fly Ash-Based Geopolymer Concrete. Geopolymer Cement and Concrete, 7982, 68–106, 2014.

[5] A. Albidah, M. Alghannam, H. Abbas, T. Almusallam, & Y. Al-Salloum, Characteristics of metakaolin-based geopolymer concrete for different mix design parameters. Journal of Materials Research and Technology, 10, 84–98, 2021.

[6] K. K. Poloju, K. Srinivasu, Impact of GGBS and strength ratio on mechanical properties of geopolymer concrete under ambient curing and oven curing. Materials Today: Proceedings, 42, 962–968, 2020.

[7] Davidovits, J. (2018). “Geopolymers based on natural and synthetic metakaolin a critical review,” in Ceramic engineering and science proceedings, 16, 201–214.

[8] Geddes, D. A., Ke, X., Bernal, S. A., Hayes, M., and Provis, J. L. (2018). “Metakaolin-based geopolymers for nuclear waste encapsulation”. in: Calcined clays for sustainable concrete. RILEM Bookseries. 16. 183–188.

[9] Santi, A., Mossini, E., Magugliani, G., Galluccio, F., Macerata, E., Lotti, P., Gatta, G. D., Vadivel, D., Dondi, D., Cori, D., Nonnet, H., & Mariani, M. (2022). Design of sustainable geopolymeric matrices for encapsulation of treated radioactive solid organic waste. Frontiers in Materials, 9. https://doi.org/10.3389/fmats.2022.1005864

[10] M.C. Alonso, F. Puertas, Garcia-Lodeiro I., P. Perez-Cortes, Immobilization of the treated wastes by geopolymer or cement-based materials encapsulation, in: PREDIS Proceedings of April Workshop 2022, Espoo, Finland., 2022.

[11] M. Palacios, S. Gismera, M.M. Alonso, J.B. d’Espinose de Lacaillerie, B. Lothenbach, A. Favier, C. Brumaud, F. Puertas, Early reactivity of sodium silicate-activated slag pastes and its impact on rheological properties, Cem Concr Res. 140 (2021) 106302. https://doi.org/https://doi.org/10.1016/j.cemconres.2020.106302.

[12] P. Perez-Cortes, I. Garcia-Lodeiro, F. Puertas, M.C. Alonso, “Effect of incorporating a molten salt waste from nuclear power plants on the properties of geopolymers and Portland cement wasteforms,” Cem Concr Compos. 142 (2023) 105210. https://doi.org/https://doi.org/10.1016/j.cemconcomp.2023.105210.

[13] ENRESA, Criterios de Aceptación de Unidades de Almacenamiento. Referencia 031-ES-IN-0002 rev. 1. Julio 2008., (2008).

[14] K. Kanehashi, Structural roles of calcium in alkaline and alkaline-earth aluminosilicate glasses by solid-state 43Ca, 17O and 27Al NMR, Solid State Nucl Magn Reson. 84 (2017) 158–163. https://doi.org/https://doi.org/10.1016/j.ssnmr.2017.03.001.

[15] A. Buchwald, H.D. Zellmann, C. Kaps, Condensation of aluminosilicate gels—model system for geopolymer binders, J Non Cryst Solids. 357 (2011) 1376–1382. https://doi.org/https://doi.org/10.1016/j.jnoncrysol.2010.12.036.

[16] M. Palacios, F. Puertas, Effect of shrinkage-reducing admixtures on the properties of alkali-activated slag mortars and pastes, Cem Concr Res. 37 (2007) 691–702. https://doi.org/https://doi.org/10.1016/j.cemconres.2006.11.021.

[17] Data consultation – Any Compound, Https://Thermoddem.Brgm.Fr/Data/Mineraux.Php?Title=gaylussite (Accessed 17 December 2022). (n.d.).

[18] J. Figg, A.E. Moore, W.A. Gutteridge, On the occurence of the mineral trona (Na2CO3.NaHCO3.2H2O) in concrete deterioration products., Cem Concr Res. 6 (1976) 691–696. https://doi.org/https://doi.org/10.1016/0008-8846(76)90033-8.

[19] J. Wang, et al. “Treatment and disposal of spent radioactive ion-exchange resins produced in the nuclear industry”. In: Progress in Nuclear Energy 78 (2015), pp. 47-55. doi: https://doi.org/10.1016/j.pnucene.2014.08.003

[20] A. Santi, et al. “Design of sustainable geopolymeric matrices for encapsulation of treated radioactive solid organic waste”. In: Frontiers in Materials 9 (2022), pp. 1-17. doi: https://doi.org/10.3389/fmats.2022.1005864

[21] B. I. El-Eswed, et al. “Stabilization/solidification of heavy metals in kaolin/zeolite based geopolymers”. In: International Journal of Mineral Processing 137 (2015), pp. 34-42. doi: https://doi.org/10.1016/j.minpro.2015.03.002

[22] P. Cappelletti, et al. “Immobilization of Cs and Sr in aluminosilicate matrices derived from natural zeolites”. In: Journal of Nuclear Materials 414 (2011), pp. 451-457. doi: https://doi.org/10.1016/j.jnucmat.2011.05.032

[23] A. Dyer, et al. “Ion-exchange in chabazite”. In: Microporous and Mesoporous Materials 22 (1998), pp. 135-150. doi: https://doi.org/10.1016/S1387-1811(98)00069-9

[24] W. Baek, et al. “Cation exchange of cesium and cation selectivity of natural zeolites: Chabazite, stilbite, and heulandite”. In: Microporous and Mesoporous Materials 264 (2018), pp. 159-166. doi: https://doi.org/10.1016/j.micromeso.2018.01.025

[25] ISIN - National Inspectorate for Nuclear Safety and Radiation Protection, GUIDA TECNICA N. 33 Criteri di Sicurezza Nucleare e Radioprotezione Per La Gestione Dei Rifiuti Radioattivi (“TECHNICAL GUIDE No. 33 Nuclear safety and Radiation Protection Criteria For RadioactiveWaste management”, Document written in Italian), 2023

[26] M. Oksa, E. Holt, EU-project PREDIS: Pre-disposal management of radioactive waste, 2023. https://predis-h2020.eu/. (2023).

[27] A. Akin, J. Dymačková, P. Pražák, R. Trtílek, P. Kovařík, E. Sulejmanov, Molten Salt Oxidation of Ion Exchange and Oils in Carbonate Salts and Evaporator Residue–16531, WM Symposia, Inc., PO Box 27646, 85285-7646 Tempe, AZ (United States), 2016.

[28] H Nonnet and al. D6.1 PREDIS Deliverable “Summary report: Description of the thermal processes used for the thermal treatment of the RSOW and the physical properties and chemical composition of the resulting treated wastes”

[29] W. Gong W. Lutze, IL. Pegg. DuraLith Alkali-Aluminosilicate Geopolymer Waste Testing for Hanford secondary Waste. May 2011 VSL-10R2140-1 PNNL-20565

[30] Shi et al. Recent progress in low-carbon binders Cem Con Res. (122) 227-250, 2019

[31] T. Vehmas, et al., Geopolymerisation of gasified ion-exchange resins, mechanical properties and short-term leaching studies, IOP Conf. Ser.: Mater. Sci. Eng. 818 012007, 2020

[32] J.L. Provis, J.S.J. van Deventer, Geopolymers: Structure, Processing, Properties and Industrial Applications, 2009

[33] J.L. Provis, S.A. Bernal, Geopolymers and related alkali-activated materials, Annu. Rev. Mater. Res. 44 (1) (2014) 299–327

[34] M.Nieminen, et al., Gasification-based thermal treatment of Low and Intermediate Level Waste containing organic matter IOP Conf. Ser.: Mater. Sci. Eng. 818 012007, 2020

[35] INTERNATIONAL ATOMIC ENERGY AGENCY, The Behaviours of Cementitious Materials in Long Term Storage and Disposal of Radioactive Waste. IAEA TECDOC No. 1701.

[36] B. Zlobenko, Yu. Fedorenko, A. Rozko, Attractive solutions for the encapsulation of ashes after thermal treatment of ion-exchange resins, Int. conference DECOM’23, IAEA, 2023.

[37] M. Matsuda et al., Decomposition of Ion Exchange Resins by Pyrolysis, Vol. 75, Issue 2, 1986

[38] F. Puertas, M. Palacios, H. Manzano, J.S. Dolado, A. Rico, J. Rodríguez, A model for the C-A-S-H gel formed in alkali-activated slag cements, J. Eur. Ceram. Soc. 31 (12) (Oct. 2011) 2043–2056, 2011.

[39] V. F. F. Barbosa, K.J.D. MacKenzie, C. Thaumaturgo, Synthesis and characterisation of materials based on inorganic polymers of alumina and silica: sodium polysialate polymers, Int. J. Inorg. Mater. 2 (4) (Sep. 2000) 309–317,

[40] N. Sedira, Castro-Gomes J., Kastiukas G., Zhou X., Vargas A. A review on mineral waste for chemical-activated binders: mineralogical and chemical characteristics / Mining Science. 2017. Vol. 24. P. 29-58.

[41] A. Buchwald, Hilbig H., Kaps C. Alkali- activated metakaolin-slag blands-performance and structure in dependence on their composition // Mater Science. – 2007. 42(9). P3024-3032

[42] ASTM C191 Standard Test Methods for Time of Setting of Hydraulic Cement by Vicat Needle

[43] EN 196-3, Part 3: Determination of setting time and soundness. BSEN196-3:1995

[44] EN 13791 - Assessment of in-situ compressive strength in structures and precast concrete components

[45] National standard of Ukraine DSTU B V.2.7-181:2009 Alkaline cements. Specification

[46] Kumar Panigrahi et al. Durability characteristics of geopolymer concrete - Progress and perspectives J. of Building Engineering, v59, n. 1, 2022

[47] CEN/TS 12390-12:2010. Testing Hardened Concrete—Part 12: Determination of The Potential Carbonation Resistance of Concrete: Accelerated Carbonation Method; British Standards Institution: London, UK, 2010.